

Two-patch herbivore/vegetation models with density-dependent migration



Mohamed Abdalaziz Abdalla Bakheet

Department of Mathematics & Applied Mathematics

University of Cape Town

Supervisor: Dr. Henri Laurie

Thesis Presented for the Degree of

DOCTOR OF PHILOSOPHY

in the Department of Mathematics & Applied Mathematics

UNIVERSITY OF CAPE TOWN

November 20, 2013

The copyright of this thesis vests in the author. No quotation from it or information derived from it is to be published without full acknowledgement of the source. The thesis is to be used for private study or non-commercial research purposes only.

Published by the University of Cape Town (UCT) in terms of the non-exclusive license granted to UCT by the author.

Declaration

By submitting this thesis electronically, I declare that the entirety of the work contained therein is my own, original work, that I am the owner of the copy- right thereof (unless to the extent explicitly otherwise stated) and that I have not previously in its entirety or in part submitted it for obtaining any qualifi- cation.

Mohamed Bakheet

Date

Copyright ©2013 University of Cape Town
All rights reserved.

Abstract

In this thesis we constructed two mathematical models for herbivore/vegetation interactions in environment of two patches, using the metaphysiological approach and a density-dependent migrations. In the first model we considered the case when the environment is constant, and we constructed a system of four perturbed ordinary differential equations describing the dynamics when only herbivores allowed to move between the two patches searching for food. The model contain two different time-scales, fast for migrations and slow for the other demographic changes in the system. We used the geometric singular perturbation theory in order to reduce the dimension of the system. Using the continuation software AUTO we provided bifurcation diagrams for the reduced systems and we also provided some numerical illustrations to show the dynamics of the system for different migrations propensities. We analyzed the bifurcation diagrams using Morse decompositions and Conley index theory, to confirm their correctness.

We constructed a second mathematical model, by considering that the vegetation growth depends on seasonal rainfall and the soil moisture. We provided some numerical simulations to illustrate several variates of dynamics for different migration speed and, when the migration propensities and the vegetation quality are change.

Dedication

To my mother
To my family & friends.

Acknowledgements

I would like to express my sincere gratitude to my supervisor Dr. Henri Laurie, for his guidance, inspiration and invaluable support, he continually encouraged me. Hence, this work would not have been done without his guidance and valuable suggestions. I would like express my deep gratitude to Dr. David Richardson for his valuable suggestions. I am particularly grateful for the assistance given by Professor Konstantin Mischaikow. I wish to thank my friend Dr. Mohamed Omar for his support. I also extend my thanks to the staff of the Department of Mathematics & Applied Mathematics, University of Cape Town. My special thanks are extended to the people at the DIMACS center for their support and for giving me the opportunity to visit the center and do part of this study. The pleasant atmosphere at DIMACS has been much appreciated. I would like also to thank Alneelain university for the funding that made my study possible.

Contents

Contents	v
List of Figures	viii
List of Tables	xv
1 General introduction	1
1.1 Introduction	1
1.2 Aims and scope of the thesis	8
1.3 Thesis outlines	9
2 Two-patch herbivore/vegetation model	11
2.1 Model background	11
2.1.1 General overview of the metaphysiological models	11
2.1.2 Owen-Smith’s metaphysiological model	12
2.2 Description of the two-patch model	16
2.2.1 Density-dependent migration	16
2.2.2 Two-patch model in a constant environment	17
3 A brief introduction to the Geometric Singular Perturbation Theory	19
3.1 Introduction	19
3.2 Manifolds	21
3.2.1 Invariant sets and invariant manifolds	22
3.2.2 Stable and unstable manifolds	22
3.2.3 Normally hyperbolic manifolds	23
3.2.4 Center manifold theorem	23
3.3 Fenichel’s first theorem	25
3.4 Reduction theorem	25

3.5	Summary	26
4	Analysis of the two-patch model using the geometric singular perturbation method	28
4.1	Dynamics near the manifold \mathcal{M}_0	32
4.2	The dynamics of the two-patch model for small $\varepsilon > 0$	39
4.3	Numerical results for the reduced systems	43
4.3.1	Bifurcations of the reduced systems	43
4.3.1.1	The bifurcation diagrams for the reduced system of $\varepsilon = 0$	44
4.3.1.2	The bifurcation diagrams for the reduced system when $\varepsilon > 0$	48
4.4	Conclusions	54
5	Analyzing the bifurcation diagrams using Conley index and Morse decomposition theory	58
5.1	Introduction	58
5.2	Methods	65
5.2.1	Isolating invariant sets	66
5.2.2	Morse decompositions	67
5.2.3	Chain maps and graded modules braid	70
5.2.4	Conley index theory	74
5.2.5	Connection matrices	78
5.3	Conclusions	85
6	Two-patch model in a seasonal environment	87
6.1	Introduction	87
6.2	Soil moisture model background	88
6.3	Model formulations	88
6.3.1	Soil moisture	89
6.3.1.1	Rainfall	89
6.3.1.2	Infiltration	89
6.3.1.3	Evaporation	91
6.3.1.4	Transpiration	92
6.3.2	Vegetation growth	92
6.3.2.1	Green vegetation biomass	92
6.3.2.2	The changes in dry vegetation biomass	93
6.4	The seasonal two-patch model	93

CONTENTS

6.5	Numerical simulations	98
6.6	Conclusions	110
7	Concluding remarks	112
	Bibliography	116
	Appendix A. Stability of the reduced two-patch model on \mathcal{M}_0	125
	Appendix B. Soil moisture equations	134

List of Figures

2.1	Schematic outline a general metaphysiological model. The loss in the resource biomass is due to consumer intake. The loss in the consumer biomass is due to the metabolism and physiological attrition.	12
2.2	Diagram of the two-patch model. The loss in vegetation biomass in each patch is due to the herbivores intake. The loss in herbivore biomass in each patch is due to mortality, metabolism and emigration to the other patch. Herbivore leaves patch 1 and patch 2 at the rates m_1 and m_2 , respectively.	15
4.1	Simulations for the two-patch model (4.1) (the (a) figure), and the reduced model on the manifold \mathcal{M}_0 (4.10) (the (b) figure). The numerical solutions were obtained using MATLAB solver <i>ode15s</i> , where both solutions started from the same initial conditions. For the parameter values in Table 4.1, the patterns demonstrated in the Figures 4.1(a) and 4.1(b) show that both vegetation biomasses oscillate at same level. The herbivore biomasses on the two patches also show an oscillatory behavior. In Figure 4.1(a) we summed the herbivore biomass on the both patches. This Figure shows that the behavior of the dynamics for the two-patch model (4.1) for small $\varepsilon = 0.01$ is the same as the dynamics for the reduced model (4.10). The minimum values for v_1 and v_2 are 0.0039 and 0.0342 respectively, while their maximum values are 0.4918, 0.8644 and 1.3446 respectively. The initial points were $v_1 = 0.4$, $v_2 = 0.55$ and $H = 0.8$	34
4.2	Numerical simulations for the two-patch model (4.1) (Figure 4.2(a)) and the reduced system (4.10) on the manifold \mathcal{M}_0 (Figure 4.2(b)). In these runs $\alpha_1 = 3.75$, $\alpha_2 = 2.5$, and the other parameters are shown in Table 4.1. The patterns show that the vegetation biomasses and herbivore biomasses oscillate and after short period of time they reach their stable equilibria. The initial points were $v_1 = 0.65$, $v_2 = 0.2$ and $H = 0.8$	34

4.3 The nullclines of the reduced system (4.10) in v_1 and v_2 coordinates. In 4.3(a) $\alpha_1 = 5.0$ and $\alpha_2 = 9.5$. In 4.3(b) $\alpha_1 = 15.0$ and $\alpha_2 = 3.5$. The nullclines cross over at a single positive fixed points. 37

4.4 The nullclines for the system (4.10). The nullclines on the both figures intersect at two positive points. In 4.4(a) $\alpha_1 = 3.75$ and $\alpha_2 = 4.5$. In 4.4(b) $\alpha_1 = 3.75$ and $\alpha_2 = 10.5$ 38

4.5 Numerical simulations shows the dynamics of the two-patch model (4.1) (Figure 4.5(a)) and the reduced system on the manifold \mathcal{M}_ε (4.20) (Figure 4.5(b)). In these figures, the patterns show that the vegetation biomasses on both patches oscillate. The total herbivore biomasses on the two patches also showed an oscillatory behavior. We used the parameter values showed in Table 4.1, with $A_1 = 50$, $A_2 = 100$, $\varepsilon = 0.01$ and $\alpha_2 = 1.50$. In the figures v_1 oscillates between 0.0143 and 0.9621, v_2 oscillates between 0.0025 and 0.8898, and H oscillates between 0.0358 and 1.5403. The initial points were $v_1 = 0.6$, $v_2 = 0.35$ and $H = 0.5$ 41

4.6 Simulations for the two-patch model (4.1) (Figure 4.6(a)), and the reduced system on the manifold \mathcal{M}_ε (4.20) (Figure 4.6(b)). In this figure we used the parameter values showed in Table 4.1 with $\varepsilon = 0.01$ and $\alpha_1 = \alpha_2 = 4$. The initial points were $v_1 = 0.45$, $v_2 = 0.5$ and $H = 0.6$ 42

4.7 Phase plane for the reduced two-patch model (4.10) when $\alpha_2 = 2.5$. In this figure we started the solutions from four different points indicated by small squares, and it shows that all the solutions will tend to a single stable fixed point in the phase plane. 45

4.8 Bifurcation diagrams for the reduced two-patch model (4.10). It ranges over the parameter space of α_2 and plots the fixed points, fold points, Hopf bifurcation points, and periodic orbits of the system at these values. The figures on the left show only the fixed points, fold points, and Hopf bifurcation points (indicated by squares). The solid lines correspond to stable fixed points, and dashed lines indicate unstable fixed points. The figures on the right, show the periodic orbits that bifurcate from the Hopf points. The dashed lines in periodic orbits indicate unstable periodic solutions, while the solid lines indicate stable periodic orbits. 46

4.9 Simulation for the reduced two-patch model (4.10), for $\alpha_2 = 1.5$, showing a single stable limit cycle. The other parameters used are shown in Table 4.1. The initial points were indicated by small squares. 47

4.10 Simulation for the reduced two-patch model (4.10), for $\alpha_2 = 3$, and for the other parameters shown in Table 4.1. The output shows that a single stable fixed point appears in the system. 47

4.11 Phase plane corresponding to $\alpha_2 = 5.29636$ and the other parameters shown in Table 4.1. The outputs show that the solutions will either tend to a single stable fixed point, or a single stable limit cycle in the phase plane. 47

4.12 Phase plane corresponding to $\alpha_2 \geq 11$, and the other parameters shown in Table 4.1. The outputs show that all the solutions will be attracted to a single stable limit cycle in the phase plane. The behavior of the system after this point will remain the same. 48

4.13 Bifurcation diagrams for the reduced two-patch model (4.20) for $\varepsilon = 0.001$. The figures on the left show the fixed points, fold points, and Hopf bifurcation points (four points indicated by small squares). In the figures to the left, the solid lines correspond to stable fixed points, and the dashed lines indicate unstable fixed points. The figures on the right show the families of periodic orbits that bifurcate from the Hopf points. The dashed lines in periodic orbits indicate instability, while the solid lines indicate stability. 50

4.14 Simulation for the reduced system (4.20) for $\varepsilon = 0.001$, $\alpha_2 = 1.25$ and for the parameter values showed in Table 4.1. In this run, the solutions were started near the unstable fixed point and from two arbitrary points in the phase plane. The output shows that all the solutions will be attracted to a single stable limit cycle. 51

4.15 Simulations for the reduced system (4.20) for $\varepsilon = 0.001$, $\alpha_2 = 2.98$ and for the other parameter values shown in Table 4.1. The solutions were started near the unstable fixed point and two arbitrary points near the stable equilibrium. The output shows that a single stable fixed point attract all the solutions. 51

4.16 Simulation for the reduced system (4.20) for $\varepsilon = 0.001$, $\alpha_2 = 3.7$ and for the other parameter values shown in Table 4.1. The solutions were started near the two unstable fixed points and near the unstable periodic orbit. The output shows that one of the points will be attracted to stable fixed point, and the other points will be attracted to a single stable periodic orbit in the phase space. 51

4.17 Simulation for the reduced system (4.20) for $\varepsilon > 0$ for $\varepsilon = 0.001$, $\alpha_2 = 7.3$ and for the other parameter values shown in Table 4.1. We started the solutions from three different arbitrary points. The outputs show that all the solutions would be attracted to the stable periodic orbit in the phase plane. 52

4.18 Bifurcation diagrams for the reduced two-patch model (4.10) when $K_1 = 200$, $K_2 = 150$, $\alpha_1 = 4.5$, and the other parameters shown in Table 4.1. 54

4.19 Bifurcation diagrams for the reduced two-patch model (4.10) when $K_1 = 250$, $K_2 = 150$, $\rho_1 = 0.002$, $\rho_2 = 0.001$, $\alpha_1 = 4.5$, and the other parameters shown in Table 4.1. 55

5.1 Bifurcation diagram illustrates the reduced two-patch model when $\varepsilon = 0$, where α_2 considered as a bifurcation parameter. In this figure $\alpha_1 = 4.5$ and the other parameter values are given in Table 4.1. Solid lines correspond to stable fixed points and stable periodic orbits, dashed lines correspond to unstable fixed points and unstable periodic orbits. Hopf bifurcations are indicated by squares. All bifurcations are labeled. 59

5.2 Phase plane corresponding to $\alpha_2 = 1.5$ in the bifurcation diagram 5.1. The solutions started near the unstable equilibrium point that is indicated by small square, and the long time dynamics show that the solution will be attracted to stable limit cycle in the phase plane. 60

5.3 Phase plane corresponding to $\alpha_2 = 2.07143$ from the bifurcation diagram 5.1. In this case the system has only a single stable fixed point in the phase space. The solutions were started from three arbitrary initial points indicated by squares. A unique stable fixed point attract all the solutions. 60

5.4 Phase plane corresponding to $\alpha_2 = 3.42$ from the bifurcation diagram 5.1. In this case only a single stable fixed point appear in the system. The solutions were started from three different initial points indicated by small squares. The figures show that all the solutions will be attracted to a single stable fixed point in the phase space. 61

5.5 Phase plane corresponding to $\alpha_2 = 3.73$ from the bifurcation diagram 5.1. The system in this case has two fixed points, a stable fixed point and an unstable fixed point. In this run the solutions were started near the unstable fixed point and from two other arbitrary points indicated by squares. The unique stable fixed point attract all the solutions. 61

5.6 Phase plane corresponding to $\alpha_2 = 4.2251$. The system in this case has four stationary solutions, two stable fixed points, an unstable fixed point and an unstable periodic orbit. The initial solutions were indicated by small squares, where they started near the unstable fixed point and from a point on the unstable periodic orbit. Both solutions attracted to one of the stable fixed point in the phase space. 62

5.7 Phase plane corresponding to $\alpha_2 = 5.75$ from the bifurcation diagram 5.1. In this case the system has six stationary solutions, two stable fixed points, a stable periodic orbit, an unstable fixed point, and two unstable periodic orbits. The solutions were started near the unstable fixed point and from two other points near the unstable periodic orbits. The output shows that the point near the unstable fixed point will be attracted to one of the stable fixed points, while the points near the unstable periodic orbits will be attracted to the stable periodic orbit in the system. 62

5.8 Phase plane corresponding to $\alpha_2 = 8.85714$ from the bifurcation diagram 5.1. The system in this case also contains six stationary solutions, two stable fixed points, a stable periodic orbit, an unstable fixed point, and two unstable periodic orbits. In these figures the initial solutions were started near the unstable stationary solutions and they are indicated by small squares. The output shows that all the solutions will be attracted to the stable periodic orbit. 63

5.9 Phase plane corresponding to $\alpha_2 = 10.2143$ from the bifurcation diagram 5.1. In this case the system has five stationary solutions, a stable fixed point, two unstable fixed points, a stable periodic orbit, and an unstable periodic orbit. The solutions were started near the two unstable fixed points and from a point near the unstable periodic orbit. The output shows that all these solutions will be attracted to the single stable periodic orbit in the system. 63

5.10 Phase plane corresponding to $\alpha_2 = 10.8929$ from the bifurcation diagram 5.1. The system in this case has four stationary solutions, three unstable fixed points, and a single stable periodic orbit. We started the solution from three points (indicated by small squares) near the unstable fixed points. The output shows that the solutions will be attracted to the single stable periodic orbit in the system. 64

5.11 Phase plane corresponding to $\alpha_2 = 12$ from the bifurcation diagram 5.1. The system in this case contains two stationary solutions, an unstable fixed point and a stable periodic orbit. The solution were started from a point (indicated by small square) near the unstable fixed point. The stable periodic orbit attract the solution. 64

5.12 N : an isolating neighborhood of S 66

5.13 The Morse sets that obtained from the bifurcation diagram 5.1. Morse sets in this figure are labeled from M_{μ_1} to $M_{\mu_{10}}$ and each set consist of the stationary points that results from the intersection between the curves and the vertical lines. 69

6.1 Schematic outline the seasonal model. The soil layers partitioned into two layers and the deep drainage. The water from rainfall infiltrate to the first layer, where the run-off and evaporate only remove water from this layer. Transpiration remove water from both layers. The vegetation roots reach the two top layers A and B . Vegetation biomass partitioned to green vegetation and dry vegetation. Herbivores consume from both types. 90

6.2 Diagram outline the two-patch model in a seasonal environment. The soil moisture sub model described with more detail in (6.1). 95

6.3 A sample of random daily rainfall showing the rainfall amount during the days of the raining season. 101

6.4 Numerical simulations for the seasonal two-patch model (6.13) when there are no migrations between the patches $\alpha_1 = \alpha_2 = 0$. The parameter values used are shown in Table 6.2 and Table 6.3. (a) patch 1 (b) patch 2. The initial points were $v_{g_1} + v_{d_1} = 0.46, v_{g_2} + v_{d_2} = 0.43, h_1 = 0.175, h_2 = 0.2667$ and $H = 0.42$ 102

6.5 Numerical simulation for the seasonal model (6.13) when we used a constant daily rainfall (the mean value of the generated data in Figure 6.3. The parameter values used are shown in Table 6.2 and Table 6.3. The initial values were $v_{g_1} = 0.6, v_{g_2} = 0.4, v_{d_1} = 0.333, v_{d_2} = 0.225, h_1 = 0.2667, h_2 = 0.0.3$ and $H = 0.42$ 103

6.6 Numerical simulations for the seasonal two-patch model (6.13), showing the dynamics on patch 1. The parameter values used are shown in Table 6.2 and Table 6.3. In these simulations, the figures in the left column correspond to the solutions when $\varepsilon = 0.01$, where the figures in the right column correspond to $\varepsilon = 0.1$. In all these figures we used $\alpha_1 \leq \alpha_2$. The figures in each row associated with different values of α_1 and α_2 . Figures (a) and (b) correspond to $\alpha_1 = 0.3$ and $\alpha_2 = 0.4$. Figures (c) and (d) correspond to $\alpha_1 = \alpha_2 = 0.5$, while the figures (e) and (f) correspond to $\alpha_1 = 0.4$ and $\alpha_2 = 0.7$. The initial values were $v_{g_1} + v_{d_1} = 0.45$ and $H = 0.42$ 104

6.7 The dynamics on patch 2 for the seasonal two-patch model (6.13) when $\varepsilon = 0.01$ (the figures in the left column), and when $\varepsilon = 0.1$ (the figures in the right column). Figures (a) and (b) correspond to $\alpha_1 = 0.3$ and $\alpha_2 = 0.4$, while figures (c) and (d) correspond to $\alpha_1 = \alpha_2 = 0.5$, and figures (e) and (f) correspond to $\alpha_1 = 0.4$ and $\alpha_2 = 0.7$. The initial values were $v_{g_2} + v_{d_2} = 0.45$ and $H = 0.42$ 105

- 6.8 Numerical simulations for the seasonal two-patch model (6.13) show the dynamics on patch 1. The parameter values used are shown in Table 6.2 and Table 6.3. The figures in the left column correspond to $\varepsilon = 0.01$, and the figures in the right column correspond to $\varepsilon = 0.1$. In all figures we set $\alpha_1 \geq \alpha_2$. Figures (a) and (b) correspond to $\alpha_1 = 0.8, \alpha_2 = 0.5$. In (c) and (d), $\alpha_1 = \alpha_2 = 0.7$, and in figures (e) and (f) $\alpha_1 = 0.6$ and $\alpha_2 = 0.4$. The initial values were $v_{g_1} + v_{d_1} = 0.45$ and $H = 0.42$. 106
- 6.9 The dynamics on patch 2 for the seasonal two-patch model (6.13) when $\alpha_1 = 0.8$ and $\alpha_2 = 0.5$ (the figures in the first row), $\alpha_1 = \alpha_2 = 0.7$ (the figures in the second row) and when $\alpha_1 = 0.6$ and $\alpha_2 = 0.4$ (the figures in the third row). The figures in the left column correspond to $\varepsilon = 0.01$, where the figure on the right column correspond to $\varepsilon = 0.1$. The initial values were $v_{g_2} + v_{d_2} = 0.45$ and $H = 0.42$ 107
- 6.10 Numerical simulations show different behavior by the seasonal two-patch model (6.13), when we used $\beta_1 = \beta_2 = 10$, and the other parameters are shown in Tables 6.2 and 6.3. The dynamics on patch 1 is shown by the figures in the left column, and the figures in the right column show the dynamics on patch 2. We started the solutions from different initial points, and we set $\alpha_1 \leq \alpha_2$ in all these figures. When $\alpha_1 = \alpha_2 = 0.0$, the output is shown in the figures (a) and (b). In (c) and (d) we used $\alpha_1 = 0.3$ and $\alpha_2 = 0.4$ and in (e) and (f) $\alpha_1 = 0.4$ and $\alpha_2 = 0.7$. From top to bottom, the initial values were $(v_{g_1} + v_{d_1} = 0.25, v_{g_2} + v_{d_2} = 0.43, H = 0.85)$, $(v_{g_1} + v_{d_1} = 0.25, v_{g_2} + v_{d_2} = 0.43, H = 0.41)$ and $(v_{g_1} + v_{d_1} = 0.25, v_{g_2} + v_{d_2} = 0.43, H = 0.38)$, respectively. 108
- 6.11 In these simulations we set $\alpha_1 \geq \alpha_2$. The dynamics on patch 1 is shown in the figures in the left column, where the figures in the right column show the dynamics on patch 2. In these figures we used $\beta_1 = \beta_2 = 10$, and the other parameters are given in Tables 6.2 and 6.3. In (a) and (b) $\alpha_1 = 0.8$ and $\alpha_2 = 0.5$, in (c) and (d) $\alpha_1 = \alpha_2 = 0.7$ and in (e) and (f) we used $\alpha_1 = 0.6$ and $\alpha_2 = 0.4$. The initial values used in the plots in this figure were the same, $(v_{g_1} + v_{d_1} = 0.25, v_{g_2} + v_{d_2} = 0.43, H = 0.38)$, $(v_{g_1} + v_{d_1} = 0.25, v_{g_2} + v_{d_2} = 0.43, H = 0.38)$ 109

List of Tables

2.1	Units of variables, parameters and typical parameter values of Owen Smith’s meta-physiological model (Owen-Smith [2004]).	14
4.1	Parameters of the non-dimensionalized model (2.5). The second column gives the non-dimensionalized group of variables of the parameter in the first column. The third column gives the value used in this thesis. Note that these values are counted for all parameters except α_2	35
4.2	Table showing the equilibrium points for the reduced two-patch model (4.10) and their corresponding eigenvalues. These values were obtained numerically using the parameter values shown in Table 4.1, and the values for α_1 and α_2 correspond with their values in Figure 4.3 and 4.4. The calculations were carried out in Appendix A.	38
4.3	The bifurcation points and turning points from the bifurcation diagram 4.8, for the reduced two-patch model (4.10). In this table we labeled each point with the same label that appears on the bifurcation diagram 4.8.	45
4.4	The bifurcation points, turning points and their labels as they appear in the bifurcation diagram 4.13 for the reduce a two-patch model (4.20).	49
5.1	Table shows the values of the unstable stationary solutions for certain values of α_2 , from the bifurcation diagram 5.1. In this table we labeled each unstable stationary solution with either u_i (for unstable fixed points) or R_i (for unstable cycles).	59
6.1	Description of the variables in the seasonal two-patch model. The parameters are taken from (Richardson and Hahn [2007]).	96
6.2	Parameters value (Richardson and Hahn [2007])	96
6.3	Table represents the parameters value and the description of the non-dimensionalized seasonal two-patch model (6.13).	97

Chapter 1

General introduction

1.1 Introduction

Modelling ecological systems implies dealing with a large number of variables. These systems are complex, where the complexity may result from the internal structure of populations, individual behavior, physiology, etc. (Auger et al. [2012]). Several modelling approaches have been used to model such systems. The individual-based simulation models (IBMs) is one of these modelling approaches, in which the location of individual animals is monitored as they move in the landscape (Levin and Pacala [1997]; Lomnicki [1999]; Volker [1999]). Another modelling approach is the structured metapopulation models, where the special structure can be the local population size, or the spatial structure of the landscape (Caswell and Etter [1993]; Gyllenberg and Silvestrov [1994]; Hanski [1994a,b]; Hanski et al. [1996]; Ovaskainen and Hanski [2001]).

Many ecological phenomena are sensitive to spatial heterogeneity (Pickett and Cadenasso [1995]; Turner [1989]), in which the heterogeneity can be the landscape structure such as habitat patches. Animal migrations affect the dynamics of local populations in spatially structured systems, while the dispersal of the animals among different patches may be affected by spatial properties such as patch size, distance between patches, etc.(Allen [1987]; Andújar and Perry [1993]; Cronin [2003]; Fahrig and Merriam [1985]; Fahrig and Paloheimo [1988]; Gyllenberg et al. [1993]; Hanski [1991]; Hanski and Simberloff [1997]; Hastings [1977, 1982]; Levin [1974]; Metz and Gyllenberg [2001]).

Mathematical models addressing the dynamics of population in patchy environments and the dispersal among different patches have become important in theoretical and empirical studies concerning the relationship among population dynamics, animal movement, and landscape structure. The literature on the theoretical models that attempt to describe such systems is vast. Several authors modeled the population dynamics in patchy environments as a metapopulation linked through

the dispersal between patches (Hanski and Gilpin [1991]; Hastings and Wolin [1989]), by assuming that the environment is composed of a set of two or more separated patches, connected via species migrations, using simple nonlinear differential equations (Abrams et al. [2007]; Holt [1985]; Kareiva et al. [1990]; Roy et al. [2008]; So et al. [2001]). In the following we have reviewed some selected recent works on these aspects. We briefly start by reviewing some models in which the time scale that animal needs to disperse between different patches have the same order as the time scale for the other local dynamics (interpatch interactions).

Holt (Holt [1987]) formulated mathematical models for a predator-prey in two patches, using system of ordinary differential equations, to explore the population coexistence. He argued that predators are likely to aggregate in patches where prey densities are relatively high, and prey in turn seeks for patches that provide refuges. He discussed the influence of this migration behavior on the interactions between alternative prey species in the system. In his study he showed that, because of an aggregative predator response, one prey species can exclude another from refuge patch. He also showed that, if there is an intraspecific competition for refuges in the system, then similar prey species will compete for refuges. In the case of exclusive and overlapping refuges, he concluded that, among the individuals outside exclusive refuges and that seeking a shared refuges, the intraspecific interference occurs.

Kuang and Takeuchi (Kuang and Takeuchi [1994]) studied a predator-prey model in a two-patch system, in which only prey can disperse between the patches. They formulated a system of three ordinary differential equations governing the dynamics, for the purpose of studying the uniform persistence of the system, and the existence of locally and globally stable positive equilibria. Through stability analysis, they proved that the system has a at least a positive equilibrium, which is globally asymptotically stable for certain conditions. Moreover, they showed that the stability of the predator-prey system may change by changing the amount of migrations in both patches. They concluded that for small migration rates the equilibrium is globally asymptotically stable, furthermore a Hopf bifurcation takes place when the stability changes from stable to unstable.

Karivan (Krivan [1997]) studied a predator-prey models in a two-patch environment to examine the influence of individual optimal behavior (optimal behavior means that animals maximize their fitness, measured through the instantaneous net reproductive rate) on the persistence and the stability of a Lotka-Volterra continuous model, following the idea behind the ideal free distribution (Fretwell and Lucas [1970]). In his study, he examined two cases of the model: First, when only predators are free to migrate between patches and second, when both predators and prey can migrate between patches. His results showed that the system under the ideal free distribution has closed orbits and the equilibrium is a center. He concluded that the optimal behavior of animals

leads to the persistence of predator-prey systems. Moreover, he proved that the system is not persistent when only predators are free to move randomly between patches. Furthermore, when both species are free to move between patches, the random system persistent.

Cui ([Cui \[2002\]](#)) considered a two-patch predator-prey model in a periodic environment, in which only prey can disperse between the source patch and the refuge patch, using a system of nonautonomous ordinary differential equations. His study gives insight into the effects of the dispersals on the permanence and the existence of ultimate bounds for the populations on the system. Through analysis, he established conditions based on the dispersal rates for the existence of lower and upper bounds for the prey and predator populations, and for the permanency of the system.

Feng and Hinson ([Feng and Hinson \[2005\]](#)) explored the dynamics of a predator-prey model in a two patch environment, in which only predators are allowed to move between the two patches. Mathematical analysis showed that the system admits nine equilibria and, under certain conditions, these equilibrium points are positive. Furthermore, they determined conditions for which the equilibria are unstable, stable, and globally asymptotically stable.

Later, Feng and others ([Feng et al. \[2011\]](#)) explored the dynamics of the same model, when both prey and predators are free to migrate, in which the predator migration rate is a prey density dependent. Using three different types of Holling functional responses, they explored the stability of the positive equilibria and the existence of lower and upper bounds for the populations. They determined conditions for which the prey and predator populations have ultimate bounds. Through stability analysis, they proved that the system has three equilibrium points. Moreover, the origin is unstable equilibrium point, and under certain conditions the two other equilibrium points are globally stable.

Quaglia and others ([Giulia et al. \[2012\]](#)) studied a model for predator and prey in a system of two patches. They considered two cases for migrations: First, when both prey and predator are free to migrate between the patches, and the second, when only one of the two populations is allowed to migrate between patches. They found that, when both species are allowed to migrate, the system admits only three equilibria, while in the case of one directional migrations, the system has four equilibria. Through stability analysis, they showed that the origin is unconditionally unstable, and under certain conditions the other three equilibria are stable.

When only predators are free to migrate, they found that the system has seven equilibrium points, in which the origin is unconditionally unstable. Through stability analysis, they determined conditions for which the other equilibrium points are stable. In the case when only prey are allowed to migrate, they found that the system has five equilibrium points, where the origin again is unconditionally unstable, and under certain conditions, the other equilibrium points are stable.

1. INTRODUCTION

In ecological systems, the variation and the affects of some parameters may take place at time scales that are different from the time scales of the other processes in the system. For example, when the dispersal of animals between different patches is assumed to be delayed, i.e. migrated animals will take long time to reach other patches and hence, the changes in the population (density) on the patches where animals departed from will be immediate, while the changes in the population (density) on the other patches will be delayed by the animals transfer time. For such cases, some authors used delayed differential equations to model systems that include more than one time-scale. In the following we listed some selected recent articles.

Xu ([Xu and Chen \[2000\]](#)) studied a time delayed two-patch ratio-dependent predator-prey model. In their model, they assumed that only prey are allowed to disperse between the two patches, and they further assumed a time delay due to gestation in predators population, using a Michaelis-Menten functional response type. Through mathematical analysis, they established conditions for the uniform persistence of the system. Moreover, they determined conditions on the time delay for the existence of unique positive equilibrium, and for the locally and globally asymptotic stability of the system.

Neubert and others ([Neubert et al. \[2002\]](#)) considered a time delayed Lotka-Volterra predator-prey model in multi-patch system. They formulated the model as integrodifferential equations that describe the dynamics in the local patches, where both prey and predators can disperse between the patches, to study the effects of time delays that produced by dispersals, in the stability of the system. In the case of single patch, and when only one species is allowed to disperse in the system, they concluded that the nontrivial equilibrium is locally asymptotically stable for any finite travel-time distribution. They further showed that, when all migrations have the same duration then the equilibrium remains locally asymptotically stable. In the case of two patches, they concluded that, when only predators disperse in the system, the equilibrium is stabilized for any finite travel-time distribution. In the case of discrete-delays, and when the travel-time distribution is a delta function, the stability of the equilibrium is undetermined. In the case of multiple patches, and when all the patches are coupled to each other in the system in exactly the same way, they concluded that, for a distributed delay, the results are the same as in the single-patch case.

Xu and others ([Xu et al. \[2004\]](#)) studied a delayed Lotka-Volterra type predator-prey model in a periodic two-patch environment. They used a system of three delayed ordinary differential equations, to study the effects of dispersion, periodicity of the environment and time delays on the system stability. In their model, they assumed two time delays in the system due to gestation, and due to the negative feedback of predator crowding. They further assumed that only prey are free to disperse between the two patches. Through the mathematical analysis, they determined conditions

for the uniform persistence of the system. Moreover, using "Gaines and Mawhins continuation theorem" they showed that there exists at least a positive periodic solution for the system. Furthermore, they determined conditions for which the positive periodic solution is unique and globally asymptotic stable.

Changjin and others ([Changjin et al. \[2010\]](#)) studied a class of delayed predator-prey model in a two patches environment, in which only prey are allowed to move between the two patches. They considered two time delays in the system due to gestation, and due to the negative feedback of predator crowding, to investigate the stability, and local Hopf bifurcation. Through the mathematical analysis, they provided conditions for the existence of a unique positive equilibrium, furthermore they showed that, under certain conditions this equilibrium is asymptotically stable, moreover, they showed that the system undergoes a Hopf bifurcation at the equilibrium. They further determined the direction, stability, and period of the periodic solutions that bifurcate from the Hopf point.

Instead of using time delays to model migrations, number of authors assumed that the dispersal of animals between different patches occur much faster in time, than the other local (interpatch) interactions. The models in these cases involve at least two different time-scales, namely slow and fast time-scales. This kind of model is known as slow-fast systems. A number of mathematical methods based on perturbation techniques have been used to study slow-fast systems. The aggregation of variables method (AGG) and the geometric singular perturbation theory (GSP) are two of these methods, which have been recently used and applied to mathematical biology. The geometric singular perturbation method (GSP) will be discussed in more detail Chapter 3.

The aggregation of variables method (AGG) was introduced in ecology by Iwasa and others ([Iwasa et al. \[1987\]](#)). From a mathematical point of view, this method takes the advantage of the existence of different time-scales and reduces the dimension of systems to systems containing a smaller number of variables governing the global dynamics ([Auger and Poggiale \[1996\]](#); [Auger et al. \[2000a, 2008a, 2012\]](#)).

There is an immense literature on the applications of the aggregation of variables (AGG) method in biology. In the following, we have reviewed a few selected recent articles.

Auger and Poggiale ([Auger and Poggiale \[1996\]](#)) studied a model for a single species lives in two different patches, to examine the effects of different density dependent migration on the stability of the system. They used two different time-scales in their model, fast for migration and slow for demographic changes. Using the aggregation of variables method, they reduced the dimension of the model. They studied the emergence of global properties on the resulting aggregated system. Through mathematical analysis, they showed the the existence of positive equilibria and the coex-

istence between the species. They concluded that, for some parameters values the occurrence of a Hopf bifurcation is possible.

Poggiale ([Poggiale \[1998\]](#)) considered a two-patch predator-prey model to study the effects of spatial heterogeneity on prey and predator communities. The model consist of a system of four ordinary differential equations describing the inter-patch and intra-patch, where two different time scales were used. Prey migration rates from the predation patch to its refuge patch are assumed to be prey density dependent or predator density dependent. They used the aggregation of variable method to reduce the dimension of the systems. From the reduced models for different functional responses they observed emergence of global properties at the macro-level.

Bernstein and others ([Bernstein et al. \[1999\]](#)) studied a three-patch predator-prey model, to analyze the influence of the ideal free distribution (IFD) on the stability of predator-prey systems. They applied the aggregation of variables method to reduce the system dimension. When the migration is fast, they showed that the predators migration has no effects on the overall stability of the system. They also showed that the spatial heterogeneity can play role on the system stability if the growth rates of the prey populations in the three patches are different. Furthermore, they showed that under the ideal free distribution, the stability of the system is independent of predator migration. For lower emigration speed, they showed that for a certain conditions the spatial heterogeneity and migration play minor role on the system stability.

In ([Auger and de la Parra \[2000\]](#); [Auger et al. \[2000a\]](#)), Auger and others reviewed some recent work on the aggregation of variables method for continuous and discrete time models. They presented different models in population dynamics that contain different time-scales in which the AGG method can be applied. They presented some models of species distributed among a system of separated patches connected through fast migrations to show how the AGG method can be used to reduce multi time-scale systems to obtain less dimensional systems, that are mathematically handled to examine the existence of positive equilibria, permanency, persistence, systems stability, Hopf bifurcations, periodic solutions, etc.

Mchich and others ([Mchich et al. \[2005\]](#)), studied two predator-prey models in a two distinct patches connected through fast migrations, to explore the effects of density-dependent migrations on the stability of the systems. They assumed that predators and prey both present on the resource patch, while on the refuge patch only prey are present. In the first model, they assumed that the prey migrate from the refuge patch to the resource patch at a constant migration rates, while their migration rate from the resource patch is predator density dependent. The stability analysis of the aggregate model showed that the system has two positive equilibrium, where the center is a saddle node equilibrium, and the other equilibrium is stable.

1. INTRODUCTION

In the second model, they assumed that prey migration rate from the refuge patch towards the resource patch is proportional to the total density of prey. Through stability analysis for the reduced system, they showed that the system has a unique positive equilibrium point. Furthermore, the stability of the equilibrium depends on the bifurcation parameter, in which it is stable when the parameter is greater than zero, unstable when the parameter is less than zero, and center when the parameter equals zero.

In (Mchich et al. [2007]), Mchich and others studied a Lotka-Volterra predator-prey model in a patchy environment to explore the effects of the density dependent migrations on the stability of the system. They constructed a system of four ordinary differential equations, describing the interactions between the species on the local patches, in which the migration occurs faster in time. They further assumed that both predators and prey are allowed to migrate in the system, where the predators migration rate is constant, while the migration rate of prey is predator density dependent. Using the aggregation of variables method, they obtained reduced system containing only two differential equations.

Through the stability analysis for the aggregated system, they showed that the system has two equilibrium points. They further showed that when the bifurcation parameter crosses zero, a Hopf bifurcation occurs. Furthermore, they proved that when the bifurcation parameter is zero, then the dynamics is a center. They concluded that, in the absence of migrations, periodic solutions may occur in the system. Moreover, when the two patches were connected, their results show that the system is not persistent and for a given value of parameters periodic solutions occur in the system. These result leads to differences in the qualitative dynamics of the single patch and of the coupled two-patch system.

In (El Abdllaoui et al. [2007]) Abdllaoui and others considered a two-patch predator-prey model, using a system of four ordinary differential equations, to examine the effects of density-dependent migrations on the stability of the system. In their model, they assumed that prey and predators can migrate between the patches, in which the migration occurs faster in time comparing to the other local processes. They further assumed that the migration rate for prey is a predator density dependent and, in turn, predators migrate toward patches that have a high density of prey. They used the aggregation of variables method to reduce the dimension of the system to a system of two ordinary differential equations.

Through the mathematical analysis for the reduced model, they first proved that all the solutions are bounded. Furthermore, they showed that the system has three equilibrium points, the trivial equilibrium, the predator free equilibrium, and possibly the coexistence of all species equilibrium, where the trivial equilibrium is a saddle point, and for certain values of the bifurcation parameter,

1. AIMS AND SCOPS OF THE RESEARCH

the predator free equilibrium is stable. Numerical bifurcation analysis for the reduced system and for the full system, showed the existence of Hopf bifurcations. Moreover, for small ϵ , both diagrams for the aggregated system and for the full system in one parameter family are consistent.

Marva and others (Marvá et al. [2012]), studied the dynamics of a spatially distributed periodic multi strain SIS epidemic model. In their study they considered the case when the population distributed among different patches, where the susceptible and the infected individuals can migrate between the patches, with a periodic migration rates. They assumed that the migrations occur much faster than the epidemics process. The existence of two different time scales in the model allowed them to use the aggregation of variables method to obtain reduced systems.

Through mathematical analysis of the reduced system, they showed that the global asymptotic stability of the disease free equilibrium depends on the global reproduction numbers. Furthermore, they provided conditions on the global reproductive numbers, for which a single-strain periodic solution is uniformly globally asymptotically stable. They deduced that the epidemic will be eradicated if the global reproductive number is less than 1. They further examined the effects of fast migrations on the epidemic behavior. In the case of homogeneous environment, in which the epidemic behaves exactly the same at every patch, their study concluded that fast migrations ensure the eradication of the epidemic.

1.2 Aims and scope of the thesis

Although there are number of models considered the effects of spatial heterogeneity and density dependent migrations on the stability of multi-patch systems, but combining the effects of animal dispersals, local population dynamics (inter-patch) and seasonal variations of the environment, in multi-patch systems has not been considered.

In this thesis we aim to study the dynamics of herbivore/vegetation interactions in two-patch systems. Two basic mathematical models for a single herbivore species living in two separated heterogeneous patches of vegetation, were developed in this thesis. In the first model, we aimed to study the interactions in a constant environment, in which all the parameters were assumed to be constant. In the second model we considered the case when the vegetation growth depends on the rainfall and the soil moisture availability.

The proposed models are different from what have been mentioned in the literature above, in terms of local inter-patch dynamics, and the rule of migrations. For the local dynamics on each isolated patch (inter-patch), we will follow the metaphysiological modelling approach using Owen-Smith's model (Owen-Smith [2004]). In our study, only herbivores are allowed to migrate between

the two-patches, in which their migrations are assumed to be depending on the amount of vegetation biomass and the vegetation quality on the local patches. Moreover, the migrations are assumed to occur faster in time than the other local processes in the system, where the animals expansion will be limited by the local patch area.

Most chapters in this thesis focus on the analysis of the constant environment model, constructed in Chapter 2. The description of the seasonal two patch model is discussed in more detail in Chapter 6, with the aid of some simulation results.

1.3 Thesis outlines

The thesis is organized in the following way: In Chapter 2 we focus on the construction of the two-patch model in a constant environment. The chapter starts by giving a short background about the metaphysiological models and the Owen-Smith model (Owen-Smith [2004]). Using density-dependent migrations we construct a system of four perturbed ordinary differential equations that describe the dynamics of the herbivores/vegetation in a heterogeneous, constant two-patch environment, where only herbivores are allowed to move between the two patches. In that model the time scale for migrations is assumed to be faster than the time scale of the other local demographic changes.

Chapter 3 represents some fundamental concepts from the dynamical systems and from the geometric singular perturbation theory. In that chapter we provide some definitions and theorems, that are necessary in the study of the singular perturbed two-patch model of Chapter 2. The main objects in the geometric singular perturbation theory are the manifolds. We presented definitions for invariant manifolds, normally hyperbolic manifolds, stable and unstable manifolds and the center manifold theorem.

Chapter 4 is devoted to the mathematical analysis of the two-patch model in a constant environment, using the geometric singular perturbation theory (GSP). The chapter starts with some preliminary result which is necessary for the mathematical analysis. In that chapter, we use the geometric singular perturbation theory to obtain a lower dimensional systems. We provide some numerical simulations for different initial conditions and for different migration parameters. Using the continuation software AUTO07p, we obtain bifurcation diagrams for the reduced systems for different migration parameters.

Chapter 5 focuses on the analysis of the bifurcation diagrams of the reduced systems, using the Morse decompositions and the Conley index theory. The bifurcation diagrams provided in Chapter 4 have shown insignificant outcomes (from the biological point of view). That is, when the

1. THESIS OUTLINES

propensity parameter α_2 takes certain values, the diagrams have no limit cycles. To make sure that these results are correct (from the mathematical point of view), we use the Morse decompositions and the Conley index theory. We start that chapter by giving some theoretical background from algebraic topology. We explain how Morse decompositions are formed. By assigning Conley index to each Morse set, we are able to find connection matrices between the elements of each Morse set. Using the connection matrices that we have obtained, we calculate transition matrices to see if there are continuations between the Morse sets, to justify the resulting bifurcation diagrams of Chapter 4.

In Chapter 6, we extend the two-patch model of Chapter 2, to include the effects of seasonal environment, by assuming that the vegetation growth depends on a daily rainfall and on the amount of the soil moisture. We use simplified assumptions based on the model by Richardson and Hahn ([Richardson and Hahn \[2007\]](#)) to model the soil moisture and the seasonal growth rate. In that model, each patch is assumed to have two horizontal layers, reached by the vegetation roots. In that chapter, the vegetation biomass is divided into green biomass and dry biomass, where herbivores consume from both types. We provide some numerical simulations using different values for the migration propensity parameters and with different initial conditions, to describe the dynamics of the seasonal two-patch model.

In Chapter 7, we conclude the thesis and we give some insight to the possible future work.

Chapter 2

Two-patch herbivore/vegetation model

In this chapter we describe a two-patch herbivore/vegetation model based on Owen-Smith's metaphysiological model (Owen-Smith [2004]). Our main goal is to explore the dynamics of a single herbivore species living in a two heterogeneous separated patches of vegetation connected by a density-dependent herbivore migrations. We introduce heterogeneity in the model by assuming a spatial heterogeneity in the patches, and by assuming that the vegetation biomass is different in each patch. By examining different herbivore migrations, we will be able to study the effects of density-dependent migrations on the stability of the system. Furthermore, by considering environmental effects such as a seasonal rainfall, we can examine the system when there is one or more seasonal parameter affected by a seasonal rainfall. The seasonal two-patch model will be discussed in more detail in Chapter 6.

2.1 Model background

2.1.1 General overview of the metaphysiological models

The demographic approach have been the dominant paradigm in population modeling, in which the population numbers considered as the central variable (Getz and Owen-Smith [1999]). In the demographic approach, the change in the total number of individuals in a fixed space is due to births and immigration, and the loss rate is due to deaths and emigration (Nisbet and Gurney [1982]). An alternative approach is the metaphysiological modeling. This approach was introduced by Wayne Getz in (Getz [1991, 1993, 1994]). The metaphysiological approach models the population as a single meta-organism via its biomass density in which the rate of change is governed by resource extraction and conversion, and the rate of biomass losses relative to physiological attrition and mortality losses (Owen-Smith [2002b]; Ramos-Jiliberto et al. [2002]). The general structure of the

2. OWEN-SMITH'S METAPHYSIOLOGICAL MODEL

metaphysiological model for a system with one producer species and one consumer species is given by the following:

$$\begin{aligned}\frac{dX}{Xdt} &= R(X) - I(X, Y) \\ \frac{dY}{Ydt} &= G(X, Y) - M_P(Y) - M_\mu(Y, Z)\end{aligned}$$

where X is the resource biomass, Y is the consumer biomass, $R(X)$ is the resource production function, $I(X, Y)$ is the relative rate of the resource biomass losses (consumer intakes), $G(X, Y)$ is relative growth rate of consumer which is the conversion into consumer biomass from the consumed biomass, $M_P(Y)$ is relative rate of loss in consumer biomass through metabolism, and $M_\mu(X, Y)$ is the relative rate of biomass loss through mortality due to predation.

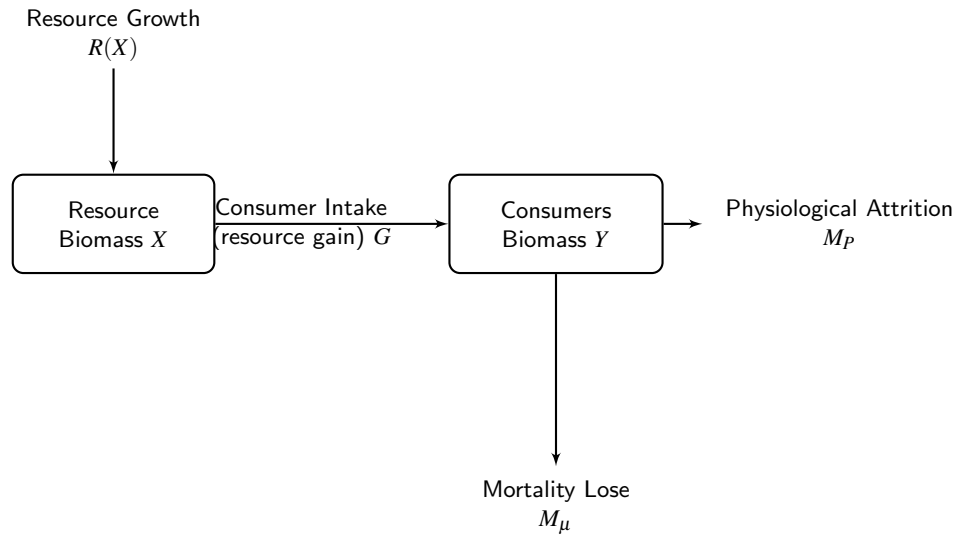


Figure 2.1: Schematic outline a general metaphysiological model. The loss in the resource biomass is due to consumer intake. The loss in the consumer biomass is due to the metabolism and physiological attrition.

2.1.2 Owen-Smith's metaphysiological model

Owen-Smith (Owen-Smith [2004]) modeled the vegetation and herbivore dynamics through their biomass changes using a metaphysiological approach by incorporating variability in vegetation growth, vegetation quality and quantity, and the adaptive responses of herbivores. In his model, Owen-Smith considered the consumer to be a large herbivore, while the resource is some component of vegetation. In the vegetation equation he assumed that the rate of loss in vegetation biomass

2. OWEN-SMITH'S METAPHYSIOLOGICAL MODEL

is a Holling type-II functional response, with a logistic vegetation growth. Furthermore, he partitioned the vegetation resource into two components, the above ground biomass which is available for herbivore, and the underground biomass (ungrazable grass) where this component is not available for consumption. For the herbivore biomass change, Owen-Smith assumed the growth rate to be the conversion from consumed vegetation biomass into herbivore biomass. In his model, the losses in herbivore biomass are assumed to be through metabolic loss and through mortality losses, where he assumed that the mortality loss is inversely dependent on resource gains. Furthermore, he assumed that the mortality has two additive components: the mortality due to senescence and the mortality due to diminishing food. Owen-Smith's model is given by the following system of ordinary differential equations:

$$\frac{dV}{dt} = rV \left(1 - \frac{V}{K} \right) - \frac{i_m(V - v_u)}{b_i + V - v_u} H, \quad (2.1a)$$

$$\frac{dH}{dt} = \left[\frac{c i_m(V - v_u)}{b_g + V - v_u} - m_p - q_0 - q_s - \frac{q m_p(b_g + V - v_u)}{c i_m(V - v_u)} \right] H, \quad (2.1b)$$

where V is the vegetation density, H is the herbivore density, r_V is the maximum vegetation intrinsic growth rate, K is the vegetation carrying capacity, i_m is the herbivore intake rate, b_g is the half-saturation rate for conversion, b_i is the half-saturation rate for eating, v_u is the ungrazable amount (vegetation reserve), c is the rate of conversion from consumed vegetation biomass into herbivore biomass, m_p is the relative rate of physiological attrition in herbivores biomass, q_s mass loss rate of herbivores due to senescence, q_0 and q determine the mortality due to starvation with diminishing food gains G , where

$$G = \frac{c i_m(V - v_u)}{b_g + V - v_u}.$$

To introduce the effects of seasonality, Owen-Smith examined two different seasonal patterns that affect the vegetation growth. Moreover, he divided the season into two equal periods (of length of six months each), namely the wet season and the dry season. He assumed that the vegetation grow through the wet season and ceases through the dry season. Alternatively, recognizing that the rainfall occurs stochastically, he allowed the vegetation to grow in the weeks when the rainfall had occurred, counterbalanced by zero growth during the weeks when there was no rainfall, with the probability of rainfall varying seasonally according to some patterns (Owen-Smith [2002a]).

In the following section we describe a two-patch herbivore/vegetation model in a constant environment. The model is based on Owen-Smith's model (2.1), which describes the interaction

2. DESCRIPTION OF THE MODEL

Symbol	Description	Unit	Value
V	Vegetation biomass	g m^{-1}	
H	Herbivore biomass	g m^{-1}	
K_1	Patch-1 vegetation carrying capacity	g m^{-1}	300
K_2	Patch-2 vegetation carrying capacity	g m^{-1}	200
r	Maximum vegetation relative growth rate	week^{-1}	0.2
i_m	Maximum herbivore intake rate	week^{-1}	0.175
b_i	Half-saturation rate for consumption	g m^{-1}	25
b_g	Half-saturation rate for conversion	g m^{-1}	75
v_u	Ungrazable amount of vegetation	g m^{-1}	10
c	Conversion rate from vegetation biomass into herbivore biomass	–	0.75
m_p	Relative rate of physiological attrition in herbivore biomass	week^{-1}	0.1
q_s	Mortality due to senescence	year^{-1}	0.07
q_0	Herbivore mortality due to starvation	year^{-1}	1.25
q	Herbivore mortality due to starvation	year^{-1}	1.5

Table 2.1: Units of variables, parameters and typical parameter values of Owen Smith’s metaphysiological model ([Owen-Smith \[2004\]](#)).

between herbivore and vegetation in a two-patch environment coupled with migration, where only herbivore are allowed to move between the two patches searching for food. The case when the vegetation growth rate is influenced by a seasonal environment will be discussed in more detail in Chapter 6.

2. DESCRIPTION OF THE MODEL

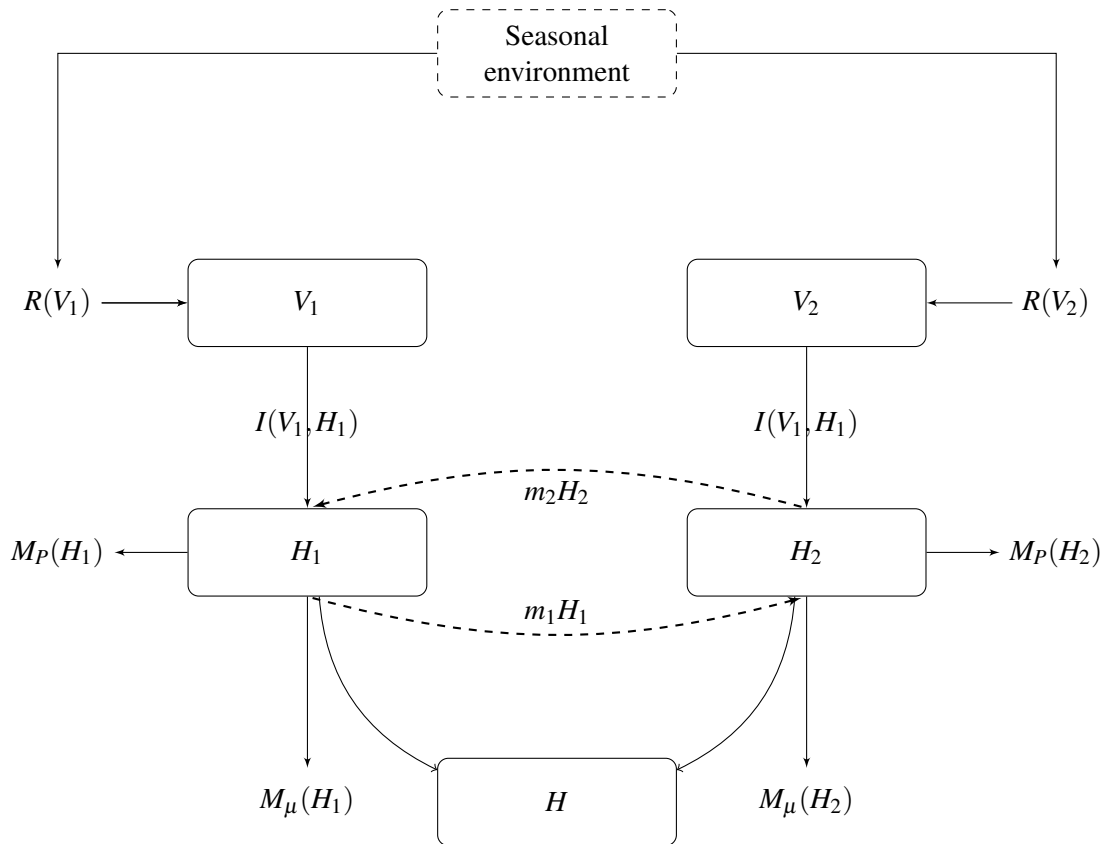


Figure 2.2: Diagram of the two-patch model. The loss in vegetation biomass in each patch is due to the herbivores intake. The loss in herbivore biomass in each patch is due to mortality, metabolism and emigration to the other patch. Herbivore leaves patch 1 and patch 2 at the rates m_1 and m_2 , respectively.

2.2 Description of the two-patch model

Assume that there are two separated patches of vegetation V_1 and V_2 different in size, and assume that a single herbivore population lives on the both patches. The subpopulation dynamics is due to the interactions between the herbivores and the vegetation. When a patch of vegetation does not satisfy the nutrient requirements of the herbivores (i.e. vegetation quantity is too low), herbivores transfer to the other patch. No mortality considered due to the migration process. Therefore, the changes in herbivore density observed on each patch is due to the migrations and the inre-patch changes (i.e. growth and loss in the local populations biomasses). We assume that the migration process occurs faster in time than the other demographic changes, i.e. the changes in herbivore and vegetation biomasses through growth and loss require a much larger time-scale than the changes in herbivore biomasses through migration. Therefore, we will use two different time-scales.

2.2.1 Density-dependent migration

In patchy environments, spatial connections can have important consequences on the global dynamics of the systems (Auger et al. [2000b]; Hassell et al. [1991]). In many habitats the density of animals is limited by the shortage of food resources, or by the patches area where food is located.

Herbivore migration may depend on the availability of suitable vegetation resources present on the patch, it may also depends on the increase in the local herbivores biomass in the patch. In both cases, the migration depends on the local densities. Density-dependent migrations can be positively density-dependent migration, i.e. the probability that an individual leaves the patch increases with the local population size increases, or it may be negatively density-dependent migration, i.e. the probability of herbivore leaving the patch decreases with the increasing on the local herbivore density (Saether et al. [1999]). It is of great interest to consider the herbivore migrations in spatially structured environments to see how the total herbivore density influences the dynamics of the system.

In our two-patch model, we assume that the herbivore migration depends on the vegetation availability in the local patch. When the vegetation biomass in any patch becomes low, herbivore moves to the other patch, while the patch area will be a factor limiting herbivores expansion. Assume that there are no mortality due to the migration. Furthermore, consider the following properties:

- (i) if the vegetation density present in a patch is low, herbivores move from this patch,
- (ii) if the vegetation density present in a patch is high, herbivores remain on the patch,

2. TWO-PATCH MODEL IN A CONSTANT ENVIRONMENT

(iii) the expansion of herbivores in each patch depends on the patch area, and the total herbivore biomass in the local patch i is given by $A_i H_i$,

where A_i denotes the area of patch i .

Density-dependent migration with the above properties can be given by the following:

$$m_i = \frac{\alpha_i A_i H_i}{1 + \bar{\beta}_i V_i}$$

where $\alpha_i, i = 1, 2$ is the propensity to leave patch i , and $\bar{\beta}_i, i = 1, 2$ is positive parameter.

With the above properties, we assume the changes in herbivore densities on each patch due to migration to be the following:

$$\frac{d}{dt} \begin{bmatrix} A_1 H_1 \\ A_2 H_2 \end{bmatrix} = \begin{bmatrix} f_1(V_1, V_2) A_1 H_1 \\ f_2(V_1, V_2) A_2 H_2 \end{bmatrix} + \begin{bmatrix} -m_1 & m_2 \\ m_1 & -m_2 \end{bmatrix} \begin{bmatrix} A_1 H_1 \\ A_2 H_2 \end{bmatrix}, \quad (2.2)$$

where the functions f_1 and f_2 represent the local population changes on patch-1 and patch-2 respectively.

Hence the biomass change due to migration is given by

$$\text{Migration in} - \text{Migration out} = \frac{\alpha_j A_j H_j}{1 + \bar{\beta}_j V_j} - \frac{\alpha_i A_i H_i}{1 + \bar{\beta}_i V_i}; \quad i, j = 1, 2, i \neq j.$$

As we assumed, migration process occurs faster in time than the local demographic changes on the subpopulations, hence we use two different time scales to distinguish between the two process, the fast time-scale is for migration, and the slow time-scale is for demographic changes.

2.2.2 Two-patch model in a constant environment

Using the above mentioned assumptions, our two-patch model describing the interactions between herbivore/vegetation in a two heterogeneous constant patchy environment with a density-dependent migration is given by the following system of ordinary differential equations:

$$\frac{dV_i}{dt} = rV_i \left(1 - \frac{V_i}{K_i} \right) - \frac{i_m(V_i - v_u)}{b_i + V_i - v_u} H_i, \quad (2.3)$$

$$\begin{aligned} \frac{dH_i}{dt} = & \left[\frac{c i_m(V_i - v_u)}{b_g + V_i - v_u} - m_p - q_0 - q_s - \frac{q m_p(b_g + V_i - v_u)}{c i_m(V_i - v_u)} \right] H_i \\ & + \mathcal{L} \left[\frac{\alpha_j A_j H_j}{(1 + \bar{\beta}_j V_j)} - \frac{\alpha_i A_i H_i}{(1 + \bar{\beta}_i V_i)} \right] / A_i; \quad i, j = 1, 2, i \neq j \end{aligned} \quad (2.4)$$

2. TWO-PATCH MODEL IN A CONSTANT ENVIRONMENT

where V_i, H_i are the vegetation and herbivore densities on patch i respectively, K_i is the vegetation carrying capacity of patch i , $\mathcal{L} \gg 1$ is a parameter used to distinguish between the slow time-scale and the fast time-scale, $\alpha_i, \bar{\beta}_i$ are the migration parameters, A_i is the area of patch i , and the other parameters are as they stated in (2.1).

Consider the following change of variables

$$(t, V_1, V_2, H_1, H_2) \mapsto (\tau, v_1, v_2, h_1, h_2) = \left(\frac{rt}{\varepsilon}, \frac{V_1}{K_1}, \frac{V_2}{K_2}, \frac{H_1}{K_1}, \frac{H_2}{K_2} \right)$$

where $\varepsilon = \frac{1}{\mathcal{L}}$.

Divide the both sides of (2.3) and (2.4) by \mathcal{L} and by applying the above change of variables, the two-patch model in a constant environment becomes the following:

$$\begin{aligned} \frac{dv_i}{d\tau} &= \varepsilon \left[v_i(1-v_i) - \frac{\eta_i(v_i - \rho_i)}{1 + \gamma_i(v_i - \rho_i)} h_i \right] \\ \frac{dh_i}{d\tau} &= \varepsilon \left[\frac{\xi_i(v_i - \rho_i)}{1 + \bar{\gamma}_i(v_i - \rho_i)} - \frac{\mu_i(1 + \bar{\gamma}_i(v_i - \rho_i))}{v_i - \rho_i} - \mu \right] h_i \\ &\quad + \frac{\alpha_j \zeta_j}{1 + \beta_j v_j} h_j - \frac{\alpha_i}{1 + \beta_i v_i} h_i \quad i, j = 1, 2; i \neq j \end{aligned} \quad (2.5)$$

where $\eta_i = \frac{i_m K_i}{r b_i}$, $\gamma_i = \frac{K_i}{b_i}$, $\xi_i = \frac{c i_m K_i}{r b_g}$, $\bar{\gamma}_i = \frac{K_i}{b_g}$, $\mu = (m_p + q_0 + q_s) / r$, $\mu_i = \frac{q m_p b_g}{c r i_m K_i}$, $\zeta_i = \frac{A_i K_i}{A_j K_j}$, $\beta_i = \bar{\beta}_i K_i$, and $\rho_i = \frac{v_u}{K_i}$.

Chapter 3

A brief introduction to the Geometric Singular Perturbation Theory

3.1 Introduction

The system described by the equations (2.5) includes two different time-scale and as we mentioned in Chapter 2, the complexity of this system arises from the existence of different time scales. The existence of different time scales gives us the advantage of using the method of geometric singular perturbation (GSP) to reduce the model complexity. The goal of using this method is to obtain an unperturbed two-patch model for small nonzero ε . The method will also allow us to reduce the dimension of the two-patch model (2.5) to systems with fewer variables at slow time-scale, and hence the new model will be easier to analyze. In this chapter we give a brief introduction to the theory of geometric singular perturbation. Before we introduce the GSP, we give some theoretical results for dynamical systems. First we will define the type of dynamics under the concern.

Consider the following singularly perturbed system:

$$\begin{aligned}\frac{dv}{d\tau} &= \varepsilon f(v, h, \varepsilon), \\ \frac{dh}{d\tau} &= \varepsilon S(v, h, \varepsilon) + F(v, h, \varepsilon),\end{aligned}\tag{3.1}$$

where $v \in \mathbb{R}^m$, $h \in \mathbb{R}^n$, $m, n > 1$, f, S , and F are sufficiently smooth functions, and $0 < \varepsilon \ll 1$. The singularity in (3.1) results from the small parameter ε .

Changing the time-scale by choosing $\tau = \frac{t}{\varepsilon}$, system (3.1) can transform into the following system:

$$\begin{aligned} \frac{dv}{dt} &= f(v, h, \varepsilon), & v &\in \mathbb{R}^m \\ \varepsilon \frac{dh}{dt} &= \varepsilon S(v, h, \varepsilon) + F(v, h, \varepsilon), & h &\in \mathbb{R}^n. \end{aligned} \quad (3.2)$$

Both systems (3.1) and (3.2) are equivalent as long as $\varepsilon \neq 0$. The time-scale represented by t is said to be the fast time-scale, whereas the time-scale τ is considered as the slow time-scale. In system (3.1), h corresponds to fast variable and v corresponds to slow variable, hence (3.1) is called the slow system and (3.2) is called the fast system.

There are several population models in the literature that include different time scales. Some of these models are associated with the population dynamics in patchy environments that are connected by strong (or fast) intra-patch interactions such as migrations. A number of mathematical methods based on perturbation techniques have been used to reduce the dimension of slow-fast systems such as (3.2) and (3.1), with clear separation in time-scales, to obtain systems with fewer variables governing the global dynamics. The aggregation of variables method have been reviewed with some recent works in Chapter 1. The geometric singular perturbation method was developed by Fenichel in (Fenichel [1979]). This method is used to reduce and to analyze systems involving multiple time-scales with clear separation in time-scales (Cronin and O'Malley [1998]). The method uses the slow-fast decompositions of central dynamical structures such as invariant manifolds to reduce the dimensions of dynamical systems, and also to investigate the existence of solutions with special structure such as homoclinic orbits (Hek [2010]).

Both methods, the aggregation of variables and the GSP, have evolved in many applications with biological background. For recent reviews, we refer to (Auger et al. [2000a, 2008a, 2012]; Chiorino et al. [1999]; Hek [2010]; Marva et al. [2012]; Poggiale et al. [2009]).

Before we define the method of geometric singular perturbation, we introduce some fundamentals and theoretical results from dynamical systems. We begin first with the definition of the flow, which is the class of objects we are about to study.

Consider the following nonlinear system of differential equations

$$\dot{x} = f(x); \quad x \in \mathbb{R}^n, \quad f : \mathbb{R}^n \longrightarrow \mathbb{R}^n. \quad (3.3)$$

Definition 3.1 (Perko [1993]). *Let E be an open subset of \mathbb{R}^n and let $f \in C^1(E)$. For $x_0 \in E$, let $\phi(t, x_0)$ be the solution of the initial value problem (3.3) on its maximal interval of existence $I(x_0)$.*

Then for $t \in I(x_0)$ the set of mappings $\phi_t : E \rightarrow E$ defined by

$$\phi_t(x_0) = \phi(t, x_0)$$

is called the flow of the dynamical system (3.3).

If $s + t \in I(X_0)$, then we have

$$\phi_{s+t}(x_0) = \phi_t(\phi_s(x_0)).$$

Definition 3.2. A point $x^* \in \mathbb{R}^n$ is called an equilibrium point of (3.3) if $f(x^*) = 0$.

The linearized system at x^* of the nonlinear system (3.3) is given by

$$\dot{x} = Ax; \quad x \in \mathbb{R}^n, \quad (3.4)$$

where $A = Df(x^*)$ is the Jacobian matrix evaluated at x^* .

In the following section we define the manifolds and the sets that remain invariant under the flow, and we also define some important manifolds such as the stable, unstable and the center manifolds.

3.2 Manifolds

Definition 3.3. Let $n \in \mathbb{N}$. An n -manifold or a manifold of dimension n is a metric space \mathcal{M} such that for every $x \in \mathcal{M}$ there is a neighborhood Γ of x homeomorphic to an open subset of \mathbb{R}^n .

Definition 3.4 (Perko [1993]). An n -dimensional differentiable manifold \mathcal{M} (or a manifold of class C^k) is a connected metric space with an open covering $\{\Gamma_\xi\}$ i.e.

$$\mathcal{M} = \bigcup_{\xi} \Gamma_\xi$$

such that

- (1) for any ξ in \mathcal{M} there exists an open neighborhood Γ_ξ homeomorphic to an open unit ball $B = \{x \in \mathbb{R}^n \mid |x| < 1\}$ in \mathbb{R}^n . i.e. for any ξ there exists a homeomorphism $h_\xi : \Gamma_\xi \rightarrow B$ of Γ onto B and
- (2) if $\Gamma_\xi \cap \Gamma_\mu \neq \emptyset$ and $h_\xi : \Gamma_\xi \rightarrow B, h_\mu : \Gamma_\mu \rightarrow B$ are homeomorphisms then $h_\xi(\Gamma_\xi \cap \Gamma_\mu)$ and $h_\mu(\Gamma_\xi \cap \Gamma_\mu)$ are subsets of \mathbb{R}^n and the map

$h_{\xi\mu} \equiv h_{\xi} \circ h_{\mu}^{-1} : h_{\mu}(\Gamma_{\xi} \cap \Gamma_{\mu}) \rightarrow h_{\xi}(\Gamma_{\xi} \cap \Gamma_{\mu})$ is differentiable (or of class C^k), and for all $x \in h_{\xi}(\Gamma_{\xi} \cap \Gamma_{\mu})$ the Jacobian determinant $\det Dh(x) \neq 0$.

The manifold \mathcal{M} is said to be analytic if the maps $h_{\xi\mu} \equiv h_{\xi} \circ h_{\mu}^{-1}$ are analytic.

3.2.1 Invariant sets and invariant manifolds

Definition 3.5 (Miess [2007]). A set \mathcal{M} is said to be an invariant set under the flow ϕ , if $\bigcup_{t \in \mathbb{R}} \phi(t, \mathcal{M}) = \mathcal{M}$.

The most common invariant manifolds are: Equilibrium points, periodic orbits, invariant tori, stable, unstable and center manifolds.

A set \mathcal{M} is said to be locally invariant if there exists a neighborhood Γ of \mathcal{M} such that no trajectory can leave \mathcal{M} without also leaving Γ .

Definition 3.6 (Wiggins [2003]). An invariant set $\mathcal{M} \in \mathbb{R}^n$ is said to be a C^k ($k \geq 1$) invariant manifold of (3.3) if \mathcal{M} has the structure of a C^k differentiable manifold.

When we study the structure of orbits near equilibria we come to some important invariant manifolds such as stable manifolds, unstable manifolds and center manifolds.

3.2.2 Stable and unstable manifolds

Definition 3.7 (Perko [1993]). Consider the nonlinear system (3.3) with its linearization (3.4). Suppose that the $n \times n$ matrix A has k negative distinct eigenvalues $\lambda_1, \dots, \lambda_k$ and $n - k$ distinct positive eigenvalues $\lambda_{k+1}, \dots, \lambda_n$. Let $\{V_1, \dots, V_n\}$ be a corresponding set of eigenvectors. Then the stable and unstable subspaces of the linear system (3.4), E^s and E^u , are the linear subspaces spanned by $\{V_1, \dots, V_k\}$ and $\{V_{k+1}, \dots, V_n\}$ respectively, i.e.

$$E^s = \text{Span}\{V_1, \dots, V_k\}$$

$$E^u = \text{Span}\{V_{k+1}, \dots, V_n\}$$

Theorem 3.1 (Stable and Unstable Manifold Theorem Perko [1993]).

Let E be an open subset of \mathbb{R}^n containing the origin, let $f \in C^1(E)$, and let ϕ_t be the flow of the nonlinear system (3.3). Suppose that $f(0) = 0$ and that $Df(0)$ has k eigenvalues with negative real part and $n - k$ eigenvalues with positive real part. Then there exists a k -dimensional differentiable manifold \mathcal{M}^s tangent to the stable subspace E^s of the linear system (3.4) at 0 such that for all

$t \geq 0, \phi_t(\mathcal{M}^s) \subset \mathcal{M}^s$ and for all $x_0 \in \mathcal{M}^s$

$$\lim_{t \rightarrow \infty} \phi_t(x_0) = 0,$$

and there exists an $(n - k)$ -dimensional differentiable manifold \mathcal{M}^u tangent to the unstable subspace E^u of the linear system (3.4) at 0 such that for all $t \geq 0, \phi_t(\mathcal{M}^u) \subset \mathcal{M}^u$ and for all $x_0 \in \mathcal{M}^u$

$$\lim_{t \rightarrow -\infty} \phi_t(x_0) = 0.$$

3.2.3 Normally hyperbolic manifolds

Definition 3.8 (Ma and Wang [2005]). Let $v \in C^r$, $r \geq 1$ and \mathcal{M} be an invariant manifold of v . \mathcal{M} is said to be hyperbolic if

- (1) \mathcal{M} is C^r manifold,
- (2) for each point $x_0 \in \mathcal{M}$, the Jacobian matrix $Dv_{N_{x_0}}(x_0)$ of the normal vector field $v_{N_{x_0}}$ of v is nondegenerate;
- (3) the real parts of all eigenvalues of $Dv_{N_{x_0}}(x_0)$ are nonzero.

An invariant manifold is said to be normally hyperbolic if every point on the manifold is hyperbolic K. R. T. Jones [1994].

3.2.4 Center manifold theorem

Definition 3.9 (Lynch [2009]). The center eigenspace, denoted by E^c , is defined by the eigenvectors corresponding to the eigenvalues with zero real part, and the center manifold, denoted by \mathcal{M}^c , is the invariant subspace which is tangent to the center eigenspace E^c .

Theorem 3.2 (Perko [1993]).

Let $f \in C^r(E)$, where E is an open subset of \mathbb{R}^n containing the origin and $r \geq 1$. Suppose that $f(0) = 0$ and $Df(0)$ has k eigenvalues with negative real part, j eigenvalues with positive real part and $m = n - k - j$ purely imaginary eigenvalues. Then there exists a center manifold \mathcal{M}^c of class C^r with dimension $(n - m - j)$ tangent to the center eigenspace E^c of the (3.4) at the origin.

Now we see how one can study the dynamics of systems using the center manifold theorem. Consider the following nonlinear system:

$$\begin{aligned} \dot{x} &= f(x, y) \\ \dot{y} &= g(x, y); \quad (x, y) \in \mathbb{R}^n \times \mathbb{R}^m. \end{aligned} \tag{3.5}$$

Suppose that a manifold in the phase space is presented by the graph of a function \mathcal{H} according to

$$y = \mathcal{H}(x).$$

The manifold is invariant under the flow of (3.5) if the vector field is tangent to the surface (Wiggins [2003]). Moreover, the tangency condition is given in the following

$$D\mathcal{H}(x)\dot{x} = \dot{y},$$

or

$$D\mathcal{H}(x)f(x, \mathcal{H}(x)) = g(x, \mathcal{H}(x)) \quad (3.6)$$

with the $\mathcal{H}(0) = 0$ and $D\mathcal{H}(0) = 0$ (Wiggins [2003]). In order to solve equation (3.6), one can expand the function \mathcal{H} in a power series (if \mathcal{H} is analytic).

Now using the above mentioned definitions and theorems we are in position to define the geometric singular perturbation theorem to study systems with two clear time scales such as (3.1) and (3.2).

When $\varepsilon = 0$ in (3.1) and (3.2), we obtain the following nonperturbed systems:

$$\begin{aligned} \frac{dv}{d\tau} &= 0, & v &\in \mathbb{R}^m \\ \frac{dh}{d\tau} &= F(v, h, 0), & h &\in \mathbb{R}^N \\ \frac{d\varepsilon}{d\tau} &= 0, \end{aligned} \quad (3.7)$$

and

$$\begin{aligned} \frac{dv}{dt} &= f(v, h, 0), & v &\in \mathbb{R}^m \\ 0 &= F(v, h, 0), & h &\in \mathbb{R}^N. \end{aligned} \quad (3.8)$$

The differential system (3.7) is called the reduced slow subsystem and the algebraic differential system (3.8) is called the reduced fast subsystem (Cronin and O'Malley [1998]; Fenichel [1979]; K. R. T. Jones [1994]). The systems (3.7) and (3.8) are two different approximations to (3.1). The set $\mathcal{M} = \{F(v, h, 0) = 0\}$ of the invariant manifolds of (3.8) is exactly the set of the equilibria of system (3.7). The flow of (3.7) is defined on \mathbb{R}^k , and since $\frac{dv}{d\tau} = 0; v \in \mathbb{R}^m$, then there will be a (m)-parameter family of solutions (v is almost constant at the fast time scale). Moreover, the flow of (3.7) on the N -dimensional set $\{F(v, h, 0) = 0\}$ is trivial. The geometric singular perturbation theory analyzes the dynamics of (3.1) for small nonzero ε by suitably combining the dynamics of

the two limits (3.7) and (3.8).

3.3 Fenichel's first theorem

Consider the unperturbed systems (3.7) and (3.8). Let $\mathcal{K} \subset \mathbb{R}^m$ be a compact domain. Assume that there is a function \mathcal{H}^0 defined by

$$\mathcal{H}^0 : \mathcal{K} \longrightarrow \mathbb{R}^N.$$

For $v \in \mathcal{K}$, assume that \mathcal{M}_0 is a N -dimensional manifold contained in the set of equilibria $\{f(u, v, 0) = 0\}$ defined as follows

$$\mathcal{M}_0 = \{(v, h, 0) \mid h = \mathcal{H}^0(v)\}. \quad (3.9)$$

The manifold \mathcal{M}_0 is normally hyperbolic if the Jacobian matrix

$$Df(v^*, h^*)$$

has exactly N eigenvalues with $\text{real}(\lambda) \neq 0$.

Assuming that the manifold \mathcal{M}_0 defined by (3.9) is normally hyperbolic, the following Fenichel's theorem states that for small nonzero ε there exist a slow manifold \mathcal{M}_ε , persists under small perturbation of the small nonzero ε to \mathcal{M}_0 .

Theorem 3.3 (Fenichel's Persistence Theorem, [K. R. T. Jones \[1994\]](#)).

Suppose $\mathcal{M}_0 \subset \{F(v, h, 0) = 0\}$ is compact, possibly with boundary, and normally hyperbolic. Then for $\varepsilon > 0$ and sufficiently small, there exists an invariant manifold \mathcal{M}_ε , $\mathcal{O}(\varepsilon)$ close and diffeomorphic to \mathcal{M}_0 , and locally invariant under the flow of the system (3.7).

Now, using the Fenichel's first Theorem 3.3, we see the possibility of reducing the system (3.7) to a system with fewer variables, by combining the dynamics given by (3.1) and (3.8) and restricting the flow to the slow manifold \mathcal{M}_ε .

3.4 Reduction theorem

Assume that $\mathcal{M}_0 \subset \{F(v, h, 0) = 0\}$, is normally hyperbolic such that

$$\mathcal{M}_0 = \{F(v, h, 0) \mid h = \mathcal{H}^0(v)\}.$$

Assume that \mathcal{H}^ε is a C^r function, for any $r < \infty$. The following theorem by Jones ([K. R. T. Jones \[1994\]](#)) restates the Fenichel's first theorem and gives the manifold \mathcal{M}_ε as a graph of function \mathcal{H}^ε .

Theorem 3.4 ([K. R. T. Jones \[1994\]](#)).

For a sufficiently small ε , there exists a function \mathcal{H}^ε , defined on a compact domain in \mathbb{R}^k , such that the graph

$$\mathcal{M}_\varepsilon = \left\{ (v, h, \varepsilon) \in \mathbb{R}^k \mid h = \mathcal{P}(v, \varepsilon) \right\}$$

is locally invariant under (3.1).

According to the [Theorem 3.4](#), we substitute the function \mathcal{H}^ε into [\(3.1\)](#), thus we obtain an equation for the variable v . Since v is almost constant at the fast time-scale in [\(3.7\)](#), then v can be considered as a parameter, therefore this equation will suffice to describe the flow on \mathcal{M}_ε . The flow on \mathcal{M}_ε is given by

$$\frac{dv}{dt} = f(v, \mathcal{P}(v, \varepsilon)), \quad v \in \mathbb{R}^m \tag{3.10}$$

When $\varepsilon = 0$ in [\(3.1\)](#), the flow on the slow manifold \mathcal{M}_0 is given by

$$\frac{dv}{dt} = f(v, \mathcal{P}(v), 0), \quad v \in \mathbb{R}^m \tag{3.11}$$

The manifold \mathcal{M}_ε is invariant if the following condition occurs

$$D\mathcal{P}(v, \varepsilon)F(v, \mathcal{P}(v, \varepsilon)) = f(v, \mathcal{P}(v, \varepsilon)). \tag{3.12}$$

To estimate the functions $\mathcal{P}(v, \varepsilon)$, different methods have been used in the literature (for instance see [Auger et al. \[2008b\]](#); [Hek \[2010\]](#); [Poggiale et al. \[2009\]](#)). Since \mathcal{P} is a C^r as a power series of ε as the following

$$\mathcal{P} = \mathcal{H}^0 + \varepsilon\mathcal{H}^1 + \varepsilon^2\mathcal{H}^2 + \dots$$

and we only need to determine the functions $\mathcal{H}^0, \mathcal{H}^1, \dots$.

3.5 Summary

We summarize the geometric singular perturbation method in the following steps:

- (1) By choosing a different time scale $\tau = t/\varepsilon$, we provide an equivalent slow-fast system [\(3.2\)](#) for the new time-scale.
- (2) Letting $\varepsilon \rightarrow 0$ in the both slow and fast systems [\(3.1\)](#) and [\(3.2\)](#), we find the two limits for

3. REDUCTION THEOREM

the system in the different time scales, and hence we obtain two unperturbed systems of differential equations and algebraic differential equations.

- (3) We linearize the fast dynamics around an arbitrary critical point of the slow manifold \mathcal{M}_0 , to verify its normal hyperbolicity.
- (4) If the manifold $\mathcal{M}_0 = \{(v, h) \in \mathbb{R}^k | h = \mathcal{H}^0(v)\}$ is normally hyperbolic, then we restrict the flow of (3.2) to the manifold \mathcal{M}_0 to obtain the dynamics for $\varepsilon = 0$.
- (5) We estimate the manifold $\mathcal{M}_\varepsilon = \{(v, h) \in \mathbb{R}^k | h = \mathcal{P}(v, \varepsilon)\}$ as a perturbed function of ε using the results from Theorem 3.4, such that the manifold \mathcal{M}_0 is the limit of \mathcal{M}_ε when $\varepsilon \rightarrow 0$. In order to obtain the reduced system for $\varepsilon > 0$ we restrict the flow of (3.2) to the manifold \mathcal{M}_ε .

Chapter 4

Analysis of the two-patch model using the geometric singular perturbation method

Recall the two-patch model (2.5)

$$\frac{dv_i}{d\tau} = \varepsilon \left[v_i(1 - v_i) - \frac{\eta_i(v_i - \rho_i)}{1 + \gamma_i(v_i - \rho_i)} h_i \right] \quad (4.1a)$$

$$\begin{aligned} \frac{dh_i}{d\tau} = \varepsilon \left[\frac{\xi_i(v_i - \rho_i)}{1 + \tilde{\gamma}_i(v_i - \rho_i)} - \frac{\mu_i(1 + \tilde{\gamma}_i(v_i - \rho_i))}{v_i - \rho_i} - \mu \right] h_i \\ + \frac{\alpha_j \zeta_j}{1 + \beta_j v_j} h_j - \frac{\alpha_i}{1 + \beta_i v_i} h_i \quad i, j = 1, 2; i \neq j \end{aligned} \quad (4.1b)$$

The descriptions of the model parameters are shown in Table 2.1 and Table 4.1.

The system (4.1) involves two clear different time scales, namely the fast time-scale τ and the slow time-scale t , where $t = \varepsilon\tau$ and $\varepsilon \ll 1$. This system is of the general form of the slow-fast system (3.1).

Throughout this chapter we will use the geometric singular perturbation method (GSP) presented in Chapter 3, to study the dynamics of the two-patch model (4.1). Using this method, we will obtain reduced systems for different orders of ε , that contain only three differential equations governing the global dynamics.

Denote the aggregated herbivore biomass in the both patches by H , hence

$$H = h_1 + h_2.$$

4. ANALYSIS OF THE TWO-PATCH MODEL

Using the total herbivore density H , system (4.1) can be rewritten in the following form

$$\frac{dv_1}{d\tau} = \varepsilon \left[v_1(1-v_1) - \frac{\eta_1(v_1-\rho_1)}{1+\gamma_1(v_1-\rho_1)} h_1 \right] \quad (4.2a)$$

$$\frac{dv_2}{d\tau} = \varepsilon \left[v_2(1-v_2) - \frac{\eta_2(v_2-\rho_2)}{1+\gamma_2(v_2-\rho_2)} (H-h_1) \right] \quad (4.2b)$$

$$\begin{aligned} \frac{dh_1}{d\tau} = \varepsilon h_1 & \left[\frac{\xi_1(v_1-\rho_1)}{1+\bar{\gamma}_1(v_1-\rho_1)} - \mu_1 \left(\frac{1+\bar{\gamma}_1(v_1-\rho_1)}{v_1-\rho_1} \right) - \mu \right] \\ & + \left[\frac{\alpha_2 \xi_2}{1+\beta_2 v_2} (H-h_1) - \frac{\alpha_1}{1+\beta_1 v_1} h_1 \right] \end{aligned} \quad (4.2c)$$

$$\begin{aligned} \frac{dH}{d\tau} = \varepsilon & \left[\left\{ \frac{\xi_2(v_2-\rho_2)}{1+\bar{\gamma}_2(v_2-\rho_2)} - \mu_2 \left(\frac{1+\bar{\gamma}_2(v_2-\rho_2)}{v_2-\rho_2} \right) - \mu \right\} H + \left\{ \frac{\xi_1(v_1-\rho_1)}{1+\bar{\gamma}_1(v_1-\rho_1)} \right. \right. \\ & \left. \left. - \frac{\xi_2(v_2-\rho_2)}{1+\bar{\gamma}_2(v_2-\rho_2)} - \mu_1 \left(\frac{1+\bar{\gamma}_1(v_1-\rho_1)}{v_1-\rho_1} \right) + \mu_2 \left(\frac{1+\bar{\gamma}_2(v_2-\rho_2)}{v_2-\rho_2} \right) \right\} h_1 \right]. \end{aligned} \quad (4.2d)$$

See Table 4.1 for the description of the parameters.

In system (4.2), the variables v_1, v_2 and H correspond to slow variables, whereas h_1 corresponds to fast variable.

For biological realism and for the mathematical analysis purposes, we prove the positive invariance of all the solutions of the system (4.2) that started with any positive initial conditions.

Consider the domain Ω as the following

$$\Omega = \{(v_1, v_2, h_1, H) \mid v_1 \geq 0, v_2 \geq 0, h_1 \geq 0, H \geq 0\}.$$

Let $V_0 = (v_1(0), v_2(0), h_1(0), H(0))$.

Lemma 4.1.

Assume that $V_0 \in \Omega$. Then, Ω is positively invariant with respect to the flow (4.2), for all $\tau \geq 0$.

Proof:

To prove that Ω is invariant with respect to (4.2), we only need to show that the right hand sides of system (4.2) remain positive if the corresponding variable is zero and the other variables are greater than or equal to zero. Then, from Proposition B.7 in Smith and Waltman [1995] we obtain that $v_1(t), v_2(t), h_1(t)$ and $H(t)$ are positive. To prove that the right hand sides of (4.2) is positive, in

4. ANALYSIS OF THE TWO-PATCH MODEL

each equation we substituted the corresponding variable by zero and we obtained

$$\frac{dv_1}{d\tau}|_{v_1=0} = \frac{\varepsilon \eta_1 \rho_1}{1 - \gamma_1 \rho_1} h_1, \quad (4.3a)$$

$$\frac{dv_2}{d\tau}|_{v_2=0} = \frac{\varepsilon \eta_2 \rho_2}{1 - \gamma_2 \rho_2} h_2, \quad (4.3b)$$

$$\frac{dh_1}{d\tau}|_{h_1=0} = \frac{\alpha_2 \zeta_2}{1 + \beta_2 v_2} H, \quad (4.3c)$$

$$\begin{aligned} \frac{dH}{d\tau}|_{H=0} = \varepsilon \left\{ \frac{\xi_1(v_1 - \rho_1)}{1 + \bar{\gamma}_1(v_1 - \rho_1)} + \frac{\mu_2(1 + \bar{\gamma}_2(v_2 - \rho_2))}{v_2 - \rho_2} \right. \\ \left. - \frac{\xi_2(v_2 - \rho_2)}{1 + \bar{\gamma}_2(v_2 - \rho_2)} - \frac{\mu_1(1 + \bar{\gamma}_1(v_1 - \rho_1))}{v_1 - \rho_1} \right\} h_1. \end{aligned} \quad (4.3d)$$

It is clear that Equation (4.3c) is positive, knowing that α_2 , ζ_2 and β_2 are all positive and $H \geq 0$, $v_2 \geq 0$. We have $\gamma_i = \frac{K_i}{b_i}$ and $\rho_i = \frac{v_u}{K_i}$ and then $\gamma_1 \rho_1 = \frac{v_u}{b_i} < 1$ (see Table 2.1 for parameters value). This means that Equations (4.3a) and (4.3b) are positive. In Equation (4.3d), $h_1 \geq 0$, $h_1 \geq 0$ and, $H = 0$ means that $h_1 + h_2 = 0$. This conclude that $h_1 = h_2 = 0$ and then (4.3(d)) is nonnegative ■

To apply the geometric singular perturbation method, we first put system (4.2) in the general form of the slow-fast systems (3.1) and (3.2), by rewriting (4.2) in the slow time scale t . Let $t = \varepsilon \tau$, then system (4.2) in the slow time-scale t is given by the following

$$\frac{dv_1}{dt} = v_1(1 - v_1) - \frac{\eta_1(v_1 - \rho_1)}{1 + \gamma_1(v_1 - \rho_1)} h_1 \quad (4.4a)$$

$$\frac{dv_2}{dt} = v_2(1 - v_2) - \frac{\eta_2(v_2 - \rho_2)}{1 + \gamma_2(v_2 - \rho_2)} (H - h_1) \quad (4.4b)$$

$$\begin{aligned} \varepsilon \frac{dh_1}{dt} = \varepsilon h_1 \left[\frac{\xi_1(v_1 - \rho_1)}{1 + \bar{\gamma}_1(v_1 - \rho_1)} - \mu_1 \left(\frac{1 + \bar{\gamma}_1(v_1 - \rho_1)}{v_1 - \rho_1} \right) - \mu \right] \\ + \left[\frac{\alpha_2 \zeta_2}{1 + \beta_2 v_2} (H - h_1) - \frac{\alpha_1}{1 + \beta_1 v_1} h_1 \right] \end{aligned} \quad (4.4c)$$

$$\begin{aligned} \frac{dH}{dt} = \left[\frac{\xi_2(v_2 - \rho_2)}{1 + \bar{\gamma}_2(v_2 - \rho_2)} - \mu_2 \left(\frac{1 + \bar{\gamma}_2(v_2 - \rho_2)}{v_2 - \rho_2} \right) - \mu \right] H \\ + \left[\frac{\xi_1(v_1 - \rho_1)}{1 + \bar{\gamma}_1(v_1 - \rho_1)} - \mu_1 \left(\frac{1 + \bar{\gamma}_1(v_1 - \rho_1)}{v_1 - \rho_1} \right) \right. \\ \left. - \frac{\xi_2(v_2 - \rho_2)}{1 + \bar{\gamma}_2(v_2 - \rho_2)} + \mu_2 \left(\frac{1 + \bar{\gamma}_2(v_2 - \rho_2)}{v_2 - \rho_2} \right) \right] h_1. \end{aligned} \quad (4.4d)$$

The two systems (4.2) and (4.4) are equivalent as long as $\varepsilon \neq 0$, while system (4.4) have a singular nature at $\varepsilon = 0$. The two limits for (4.4) and (4.2) when $\varepsilon = 0$ are given by the following two systems:

4. ANALYSIS OF THE TWO-PATCH MODEL

the slow system

$$\frac{dv_1}{dt} = v_1(1-v_1) - \frac{\eta_1(v_1 - \rho_1)}{1 + \gamma_1(v_1 - \rho_1)} h_1 \quad (4.5a)$$

$$\frac{dv_2}{dt} = v_2(1-v_2) - \frac{\eta_2(v_2 - \rho_2)}{1 + \gamma_2(v_2 - \rho_2)} (H - h_1) \quad (4.5b)$$

$$0 = \frac{\alpha_2 \zeta_2}{1 + \beta_2 v_2} (H - h_1) - \frac{\alpha_1}{1 + \beta_1 v_1} h_1 \quad (4.5c)$$

$$\begin{aligned} \frac{dH}{dt} = & \left[\frac{\xi_2(v_2 - \rho_2)}{1 + \tilde{\gamma}_2(v_2 - \rho_2)} - \mu_2 \left(\frac{1 + \tilde{\gamma}_2(v_2 - \rho_2)}{v_2 - \rho_2} \right) - \mu \right] H + \left[\frac{\xi_1(v_1 - \rho_1)}{1 + \tilde{\gamma}_1(v_1 - \rho_1)} \right. \\ & \left. - \frac{\xi_2(v_2 - \rho_2)}{1 + \tilde{\gamma}_2(v_2 - \rho_2)} - \mu_1 \left(\frac{1 + \tilde{\gamma}_1(v_1 - \rho_1)}{v_1 - \rho_1} \right) + \mu_2 \left(\frac{1 + \tilde{\gamma}_2(v_2 - \rho_2)}{v_2 - \rho_2} \right) \right] h_1 \end{aligned} \quad (4.5d)$$

and the fast system

$$\frac{dv_1}{d\tau} = 0 \quad (4.6a)$$

$$\frac{dv_2}{d\tau} = 0 \quad (4.6b)$$

$$\frac{dh_1}{d\tau} = \frac{\alpha_2 \zeta_2}{1 + \beta_2 v_2} (H - h_1) - \left(\frac{\alpha_1}{1 + \beta_1 v_1} \right) h_1 \quad (4.6c)$$

$$\frac{dH}{d\tau} = 0 \quad (4.6d)$$

$$\frac{d\varepsilon}{d\tau} = 0 \quad (4.6e)$$

The geometric singular perturbation theory can be applied to our two-patch model (4.4), and hence we can obtain reduced systems, if the equilibria of the fast system (4.6) are normally hyperbolic stable (i.e. all the eigenvalues of the Jacobian matrix are bounded away from the imaginary axis (Hek [2010])). The following Lemma proves that the fast dynamics (4.6) has a positive unique equilibrium, which is normally hyperbolic.

Lemma 4.2.

If $\varepsilon = 0$, then fast dynamics (4.2) has a unique normally hyperbolic manifold \mathcal{M}_0 . Furthermore, this manifold admits a one-dimensional normally hyperbolic stable manifold.

Proof:

To apply the results from the center manifold theorem, we add the equation for the center manifold $\frac{d\varepsilon}{d\tau} = 0$, to system (4.6). The nullclines for the fast system (4.6) are

$$\left\{ (v_1, v_2, h_1, H, 0) \in \Omega \mid \frac{\alpha_2 \zeta_2}{1 + \beta_2 v_2} (H - h_1) - \left(\frac{\alpha_1}{1 + \beta_1 v_1} \right) h_1 = 0 \right\}.$$

Denote the critical manifold of this equilibrium by the following

$$\mathcal{M}_0 = \left\{ (v_1, v_2, h_1, H, 0) \in \Omega \mid h_1^* = \frac{\alpha_2 \zeta_2 H}{1 + \beta_2 v_2} \Big/ \left(\frac{\alpha_1}{1 + \beta_1 v_1} + \frac{\alpha_2 \zeta_2}{1 + \beta_2 v_2} \right) \right\}.$$

The linearization of system (4.6) about the manifold \mathcal{M}_0 is given by the following matrix

$$D(f|_{h_1^*}) = \begin{pmatrix} 0 & 0 & 0 & 0 & 0 \\ 0 & 0 & 0 & 0 & 0 \\ \frac{h_1^* \alpha_1 \beta_1}{(1 + \beta_1 v_1)^2} & -\frac{\alpha_2 \zeta_2 \beta_2 (H - h_1^*)}{(1 + \beta_2 v_2)^2} & -\left(\frac{\alpha_1}{1 + \beta_1 v_1} + \frac{\alpha_2 \zeta_2}{1 + \beta_2 v_2} \right) & \frac{\alpha_2 \zeta_2}{1 + \beta_2 v_2} & 0 \\ 0 & 0 & 0 & 0 & 0 \\ 0 & 0 & 0 & 0 & 0 \end{pmatrix}.$$

The matrix $D(f|_{h_1^*})$ has four null eigenvalues and one nonzero negative eigenvalue

$$\lambda = -\left(\frac{\alpha_1}{1 + \beta_1 v_1} + \frac{\alpha_2 \zeta_2}{1 + \beta_2 v_2} \right).$$

From the definition (3.8), it follows that the manifold \mathcal{M}_0 is normally hyperbolic. Moreover, the manifold \mathcal{M}_0 has a one dimensional stable manifold.

From Lemma 4.2, all the conditions in Fenichel's Theorem 3.3 and in the reduction Theorem 3.4 are satisfied. Now one can apply Theorem 3.4 to restrict the flow of the two-patch model (4.2), on the normal hyperbolic manifold \mathcal{M}_0 , when $\varepsilon = 0$. For $0 < \varepsilon \ll 1$, Theorem 3.4 tells us that there exists a manifold \mathcal{M}_ε such that $\mathcal{M}_\varepsilon \rightarrow \mathcal{M}_0$ as $\varepsilon \rightarrow 0$. The flow of the two-patch model (4.2) can be restricted to the slow manifold \mathcal{M}_ε and, as the result we obtain system with less variables.

4.1 Dynamics near the manifold \mathcal{M}_0

According to the conditions for the reduction Theorem 3.4, the flow of the slow system (4.4) restricted to the normally hyperbolic manifold \mathcal{M}_0 , is given by the following

$$\frac{dv_1}{dt} = f_1(v_1, v_2, h_1^*, H) \tag{4.7a}$$

$$\frac{dv_2}{dt} = f_2(v_1, v_2, h_1^*, H) \tag{4.7b}$$

$$\frac{dH}{dt} = F(v_1, v_2, h_1^*, H), \tag{4.7c}$$

where f_1, f_2 and F are functions that represent the right hand side of the system (4.4), that correspond to the variables v_1, v_2 and H respectively, and evaluated at (v_1, v_2, h_1^*, H) .

Consider \mathcal{P}^0 to be a C^r function of v_1, v_2 and H defined by

$$\mathcal{P}^0(v_1, v_2, H) = \frac{m_2}{m_1 + m_2} H,$$

where

$$m_1 = \frac{\alpha_1}{1 + \beta_1 v_1} \quad m_2 = \frac{\alpha_2 \zeta_2}{1 + \beta_2 v_2}. \quad (4.8)$$

The manifold \mathcal{M}_0 can be expressed using \mathcal{P}^0 as follows

$$\mathcal{M}_0 = \{(v_1, v_2, h_1, H) \in \mathbb{R}_+^4 \mid h_1 = \mathcal{P}^0\}. \quad (4.9)$$

Substituting h_1^* by its value back in (4.7), we obtain the reduction of the two-patch model (4.4) to the manifold \mathcal{M}_0 , so that the reduced system is given by the following

$$\frac{dv_1}{dt} = v_1(1 - v_1) - \frac{\eta_1 m_2 (v_1 - \rho_1) H}{(1 + \gamma_1 (v_1 - \rho_1)) (m_1 + m_2)} \quad (4.10a)$$

$$\frac{dv_2}{dt} = v_2(1 - v_2) - \frac{\eta_2 m_1 (v_2 - \rho_2) H}{(1 + \gamma_1 (v_2 - \rho_2)) (m_1 + m_2)} \quad (4.10b)$$

$$\frac{dH}{dt} = \left(\frac{1}{(m_1 + m_2)} \left[\frac{\xi_1 m_2 (v_1 - \rho_1)}{1 + \tilde{\gamma}_1 (v_1 - \rho_1)} + \frac{\xi_2 m_1 (v_2 - \rho_2)}{1 + \tilde{\gamma}_2 (v_2 - \rho_2)} \right] - \mu \right) H, \quad (4.10c)$$

$$- \left[\frac{\mu_1 m_2 (1 + \tilde{\gamma}_1 (v_1 - \rho_1))}{v_1 - \rho_1} - \frac{\mu_2 m_1 (1 + \tilde{\gamma}_2 (v_2 - \rho_2))}{v_2 - \rho_2} \right] - \mu \Big) H, \quad (4.10d)$$

where m_1, m_2 are given by (4.8).

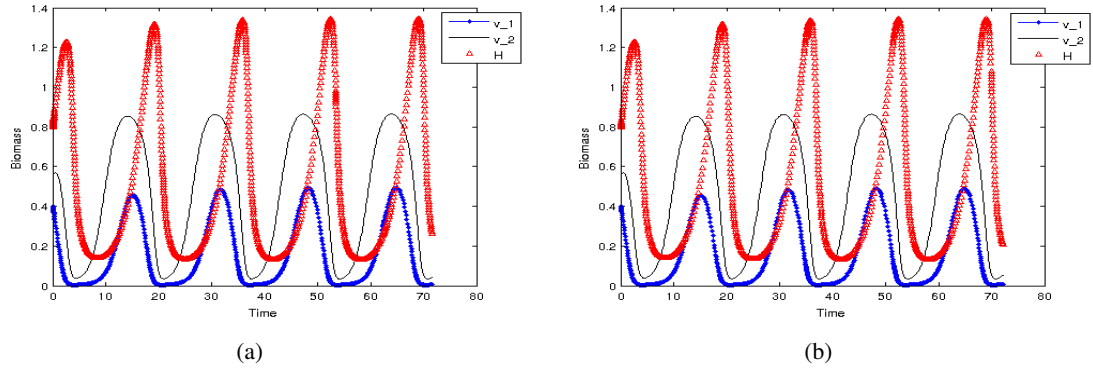


Figure 4.1: Simulations for the two-patch model (4.1) (the (a) figure), and the reduced model on the manifold \mathcal{M}_0 (4.10) (the (b) figure). The numerical solutions were obtained using MATLAB solver *ode15s*, where both solutions started from the same initial conditions. For the parameter values in Table 4.1, the patterns demonstrated in the Figures 4.1(a) and 4.1(b) show that both vegetation biomasses oscillate at same level. The herbivore biomasses on the two patches also show an oscillatory behavior. In Figure 4.1(a) we summed the herbivore biomass on the both patches. This Figure shows that the behavior of the dynamics for the two-patch model (4.1) for small $\varepsilon = 0.01$ is the same as the dynamics for the reduced model (4.10). The minimum values for v_1 and v_2 are 0.0039 and 0.0342 respectively, while their maximum values are 0.4918, 0.8644 and 1.3446 respectively. The initial points were $v_1 = 0.4$, $v_2 = 0.55$ and $H = 0.8$.

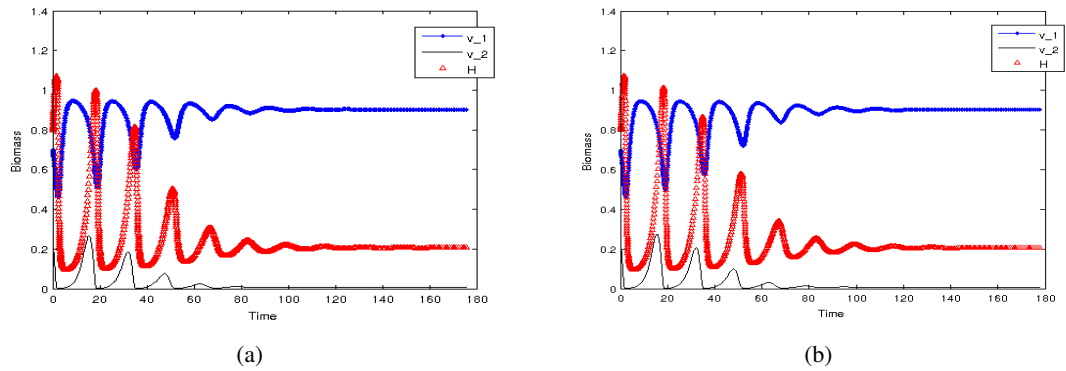


Figure 4.2: Numerical simulations for the two-patch model (4.1) (Figure 4.2(a)) and the reduced system (4.10) on the manifold \mathcal{M}_0 (Figure 4.2(b)). In these runs $\alpha_1 = 3.75$, $\alpha_2 = 2.5$, and the other parameters are shown in Table 4.1. The patterns show that the vegetation biomasses and herbivore biomasses oscillate and after short period of time they reach their stable equilibria. The initial points were $v_1 = 0.65$, $v_2 = 0.2$ and $H = 0.8$.

Parameter	Description	Value
η_1	$i_m K_1 / (r b_i)$	7.0
η_2	$i_m K_2 / (r b_i)$	5.25
ξ_1	$c i_m K_1 / (r b_g)$	2.625
ξ_2	$c i_m K_2 / (r b_g)$	1.9687
γ_1	K_1 / b_i	8.0
γ_2	K_2 / b_i	6.0
$\bar{\gamma}_1$	K_1 / b_g	4.0
$\bar{\gamma}_2$	K_2 / b_g	3.0
ρ_1	v_u / K_2	0.001
ρ_2	v_u / K_2	0.003
μ_1	$q m_p b_g / (r c i_m K_1)$	0.0027
μ_2	$q m_p b_g / (r c i_m K_2)$	0.0037
μ	$(m_p + q_s + q_0) / r$	0.1769
A_1	patch 1 area	50.0
A_2	patch 2 area	100.0
α_1	propensity of migrations	3.75
ζ_1	$A_1 K_1 / (A_2 K_2)$	3.0
ζ_2	$A_2 K_2 / (A_1 K_1)$	0.3333

Table 4.1: Parameters of the non-dimensionalized model (2.5). The second column gives the non-dimensionalized group of variables of the parameter in the first column. The third column gives the value used in this thesis. Note that these values are counted for all parameters except α_2 .

To study the long-term dynamics of the reduced two-patch model (4.10), we need to explore the stability of stationary solutions and the existence of periodic solutions. System (4.10) has the following equilibria

$$E_1 = (0, 0, 0) \quad (4.11a)$$

$$E_2 = (1, 1, 0) \quad (4.11b)$$

$$E_3 = (1, 0, 0) \quad (4.11c)$$

$$E_4 = (0, 1, 0) \quad (4.11d)$$

$$E_5 = (v_1^*, v_2^*, H^*), \quad (4.11e)$$

where (v_1^*, v_2^*, H^*) is associated with the positive nontrivial solutions to the following equations

$$v_1(1 - v_1) - \frac{\eta_1 \alpha_2 \xi_2 (v_1 - \rho_1)}{(1 + \beta_2 v_2)(1 + \gamma_1 (v_1 - \rho_1)) \left(\frac{\alpha_1}{1 + \beta_1 v_1} + \frac{\alpha_2 \xi_2}{1 + \beta_2 v_2} \right)} H = 0 \quad (4.12a)$$

$$v_2(1 - v_2) - \frac{\eta_2 \alpha_1 (v_2 - \rho_2)}{(1 + \beta_1 v_1)(1 + \gamma_2 (v_2 - \rho_2)) \left(\frac{\alpha_1}{1 + \beta_1 v_1} + \frac{\alpha_2 \xi_2}{1 + \beta_2 v_2} \right)} H = 0 \quad (4.12b)$$

$$\begin{aligned} & \frac{\xi_1 \xi_2 \alpha_2 (v_1 - \rho_1)}{(1 + \beta_2 v_2)(1 + \tilde{\gamma}_1 (v_1 - \rho_1)) \left(\frac{\alpha_1}{1 + \beta_1 v_1} + \frac{\alpha_2 \xi_2}{1 + \beta_2 v_2} \right)} + \frac{\xi_2 \alpha_1 (v_2 - \rho_2)}{(1 + \beta_1 v_1)(1 + \tilde{\gamma}_2 (v_2 - \rho_2)) \left(\frac{\alpha_1}{1 + \beta_1 v_1} + \frac{\alpha_2 \xi_2}{1 + \beta_2 v_2} \right)} \\ & - \frac{\mu_1 \alpha_2 \xi_2 (1 + \tilde{\gamma}_1 (v_1 - \rho_1))}{(1 + \beta_2 v_2)(v_1 - \rho_1) \left(\frac{\alpha_1}{1 + \beta_1 v_1} + \frac{\alpha_2 \xi_2}{1 + \beta_2 v_2} \right)} - \frac{\mu_2 \alpha_1 (1 + \tilde{\gamma}_2 (v_2 - \rho_2))}{(1 + \beta_1 v_1)(v_2 - \rho_2) \left(\frac{\alpha_1}{1 + \beta_1 v_1} + \frac{\alpha_2 \xi_2}{1 + \beta_2 v_2} \right)} - \mu = 0. \end{aligned} \quad (4.12c)$$

The equilibrium points E_1, E_2, E_3 and E_4 are all unstable equilibria (for more detail see Appendix A). System (4.12) is highly nonlinear (notice that $\tilde{\xi}_1, \tilde{\xi}_2, \tilde{\mu}_1$ and $\tilde{\mu}_2$ are functions of $v_1, v_2, \alpha_1, \alpha_2, \beta_1, \beta_2, A_1$ and A_2). It is not easy to get explicit expressions for the solutions v_1, v_2 and H from equations (4.12) as functions of at least one parameter. One can use graphics to illustrate the existence of positive solutions, such that $\rho_1 \leq v_1 \leq 1, \rho_2 \leq v_2 \leq 1$ and $H \geq 0$, for different parameter values.

Noticing that the third equation in (4.12) is only containing two variables namely v_1 and v_2 . One can eliminate H from the first two equations in (4.12), and hence obtain an equation containing only the variables v_1 and v_2 as follows

$$\frac{v_1(1 - v_1)(1 + \gamma_1(v_1 - \rho_1))}{\tilde{a}_1(v_1 - \rho_1)} - \frac{v_2(1 - v_2)(1 + \gamma_1(v_2 - \rho_2))}{\tilde{a}_2(v_2 - \rho_2)} = 0. \quad (4.13)$$

Now, from equation (4.13) and the third equation in (4.12), one can plot v_1 versus v_2 to determine the existence of fixed points. The points where the curves intersect each other represent the fixed points in v_1, v_2 plane, and by substituting these points back into the first (or the second) equation of system (4.12), we obtain the H values of the fixed points.

Using the parameter values showed in Table 4.1, and by choosing $\alpha_1 = 5.0$ and $\alpha_2 = 9.5$, we plotted equation (4.13) and the third equation in (4.12) using MATLAB, and we obtained the plot showed in Figure 4.3(a). The solid line represents equation (4.13), while the dashed line represents the third equation in (4.12). The two lines intersect at a single point with $v_1 = 0.46$, and $v_2 = 0.1388$, which represents the equilibrium of the two dimensional system. To obtain the third coordinate H for the equilibrium, we substituted the values of v_1 and v_2 back into the first equation in (4.12), and we obtained that $H = 1.4774$. The equilibrium point $(0.46, 0.1388, 1.4774)$ is a stable fixed point (see Appendix A).

To explore the effects of the migration properties α_1 and α_2 on the qualitative changes in the behavior of the equilibria (v_1^*, v_2^*, H^*) , we examined the equilibria for different values of α_1 and α_2 .

When the propensity to migrate from patch 1 is relatively high and the propensity of leaving the other patch is relatively small, for example $\alpha_1 = 15.0$ and $\alpha_2 = 3.5$ and using the other parameter values shown in Table 2.1, we again plotted v_1 versus v_2 and we obtained the graph showed in Figure 4.3(b). In this figure the two lines cross each other at $(0.966, 0.2544)$, and hence the corresponding value for the third coordinate H is 0.1846. The equilibrium point $(0.966, 0.2544, 0.1846)$ is unstable (see Appendix A for detailed calculations).

When both α_1 and α_2 are relatively small, for example for $\alpha_2 = 4.5$ and $\alpha_1 = 3.75$, Figure 4.4(a) shows that there exist two positive fixed points: at $(0.828, 0.1681, 0.8668)$, which is stable fixed point, and at $(0.989, 0.1539, 0.0653)$, which is an unstable fixed point (see Appendix A).

When $\alpha_1 = 3.75$ and $\alpha_2 = 10.5$, Figure 4.4(b) shows that the two curves intersect at two fixed points. The first fixed point $(0.414, 0.1452, 0.8764)$ is stable and the other fixed point $(0.989, 0.09146, 0.356)$ is unstable (for detailed calculations see Appendix A).

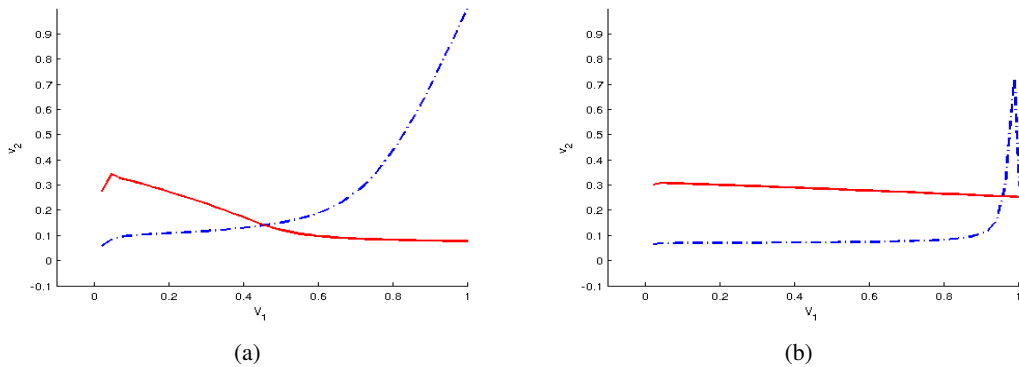


Figure 4.3: The nullclines of the reduced system (4.10) in v_1 and v_2 coordinates. In 4.3(a) $\alpha_1 = 5.0$ and $\alpha_2 = 9.5$. In 4.3(b) $\alpha_1 = 15.0$ and $\alpha_2 = 3.5$. The nullclines cross over at a single positive fixed points.

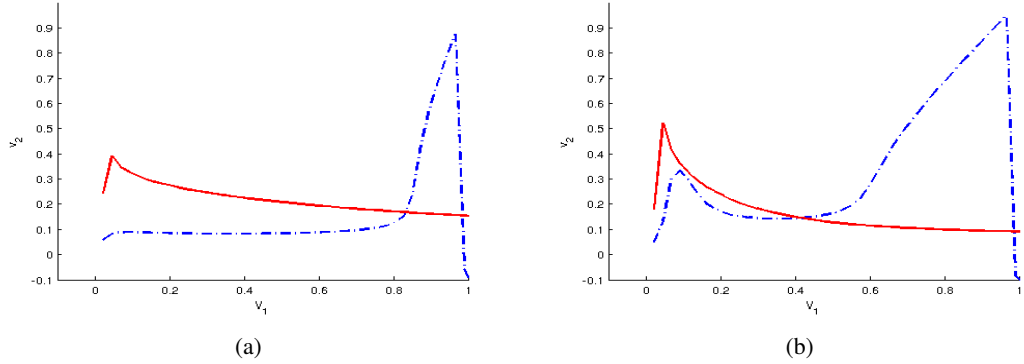


Figure 4.4: The nullclines for the system (4.10). The nullclines on the both figures intersect at two positive points. In 4.4(a) $\alpha_1 = 3.75$ and $\alpha_2 = 4.5$. In 4.4(b) $\alpha_1 = 3.75$ and $\alpha_2 = 10.5$.

α_1	α_2	The equilibrium	Eigenvalues	Stability type
		$E_1 = (0, 0, 0)$		unstable
		$E_2 = (1, 1, 0)$		unstable
		$E_3 = (1, 0, 0)$		unstable
		$E_4 = (0, 1, 0)$		unstable
5.0	9.5	(0.46, 0.1388, 1.4774)	$\lambda_1 = -0.2099 + 0.3282i$ $\lambda_2 = -0.2099 - 0.3282i$ $\lambda_3 = -1.669$	stable
15.0	3.5	(0.966, 0.2544, 0.1846)	$\lambda_1 = 0.2253 + 0.0976i$ $\lambda_2 = 0.2253 - 0.0976i$ $\lambda_3 = -0.9503$	unstable
4.5	3.75	(0.828, 0.1681, 0.8668)	$\lambda_1 = -0.2044 + 0.3236i$ $\lambda_2 = -0.2044 - 0.3236i$ $\lambda_3 = -0.7876$	stable
4.5	3.75	(0.989, 0.1539, 0.0653)	$\lambda_1 = 0.0696, \lambda_2 = 0.5821,$ $\lambda_3 = -0.9839$	unstable
3.75	10.5	(0.414, 0.1452, 0.8764)	$\lambda_1 = -0.0996 + 0.3696i$ $\lambda_2 = -0.0996 - 0.3696i$ $\lambda_3 = -0.4163$	stable
3.75	10.5	(0.989, 0.09146, 0.356)	$\lambda_1 = 0.0572 + 0.2986i$ $\lambda_2 = 0.0572 - 0.2986i$ $\lambda_3 = -1.0083$	unstable

Table 4.2: Table showing the equilibrium points for the reduced two-patch model (4.10) and their corresponding eigenvalues. These values were obtained numerically using the parameter values shown in Table 4.1, and the values for α_1 and α_2 correspond with their values in Figure 4.3 and 4.4. The calculations were carried out in Appendix A.

In Figure 4.4(b), the numerical explorations show that there may be another point where the lines can cross each other over the region for $v_2 < 0.1$ and $v_1 < 0.001$.

From the graphical illustrations (4.3) and (4.4), and from the stability analysis of the equilibria obtained from Figure 4.3 and (4.4) (see Appendix A for more detail), it appears that the number of fixed points and their stability change when the migration propensity parameters α_1 and α_2 are changed. This shows that the amount of animal migrations may stabilize or destabilize the two-patch system. So, it will be more convenient to examine the stability and the behavior of the system over the parameter space of migration propensities. In Section 4.3, we will study the existence of positive stationary solutions over the parameter space of α_2 , using the parameters continuation software AUTO (Doedel et al. [2007]).

4.2 The dynamics of the two-patch model for small $\varepsilon > 0$

For sufficiently small $\varepsilon \neq 0$, Theorem 3.3 assures that the manifold \mathcal{M}_0 persists as a perturbed manifold \mathcal{M}_ε , diffeomorphic and normally hyperbolically stable. It is easy to show that the manifold \mathcal{M}_0 is not a manifold to the flow of (4.1) with ε different from zero. Therefore,

$$\mathcal{M}_\varepsilon \neq \mathcal{M}_0.$$

Denote by \mathbb{R}_+^n the following

$$\mathbb{R}_+^n = \{x \in \mathbb{R}^n \mid x \geq 0\}.$$

Assume that \mathcal{P} has the following properties

- (I) \mathcal{P} is a C^r function, for $r < \infty$,
- (II) $\mathcal{P}(0) = 0$, and $D\mathcal{P}(0) = 0$.

If \mathcal{P} satisfies (I) and (II), then Theorem 3.4 tells us that the manifold \mathcal{M}_ε can be expressed as a graph of the function \mathcal{P} as follows

$$\mathcal{M}_\varepsilon = \{(v_1, v_2, h_1, H, \varepsilon) \in \mathbb{R}_+^5 \mid v_1 \geq 0, v_2 \geq 0, H > 0, h_1 = \mathcal{P}(v_1, v_2, H, \varepsilon)\}, \quad (4.14)$$

and (4.14) is locally invariant under (4.2).

Theorem 4 of Carr [1981] states that $\mathcal{P} = \mathcal{O}(\varepsilon)$ uniformly in other variables, so we can formally express \mathcal{P} as follows

$$h_1 = \mathcal{P} = \mathcal{H}^0 + \varepsilon \mathcal{H}^1(v_1, v_2, H) + \varepsilon^2 \mathcal{H}^2(v_1, v_2, H) + \dots \quad (4.15)$$

Inserting (4.15) into the third equation of (4.2) we get

$$\begin{aligned} \frac{dh_1}{d\tau} = \varepsilon (\mathcal{H}^0 + \varepsilon \mathcal{H}^1 + \dots) & \left[\frac{\xi_1(v_1 - \rho_1)}{1 + \bar{\gamma}_1(v_1 - \rho_1)} - \mu_1 \frac{1 + \bar{\gamma}_1(v_1 - \rho_1)}{v_1 - \rho_1} - \mu \right] \\ & + m_2 (H - \mathcal{H}^0 - \varepsilon \mathcal{H}^1 - \dots) - m_1 (\mathcal{H}^0 + \varepsilon \mathcal{H}^1 + \dots). \end{aligned}$$

\mathcal{P} is a C^r , hence we omit the terms $\mathcal{O}(\varepsilon^k)$ $k > 1$ and we obtain

$$\begin{aligned} \frac{dh_1}{d\tau} = \varepsilon (\mathcal{H}^0 + \varepsilon \mathcal{H}^1) & \left[\frac{\xi_1(v_1 - \rho_1)}{1 + \bar{\gamma}_1(v_1 - \rho_1)} - \mu_1 \frac{1 + \bar{\gamma}_1(v_1 - \rho_1)}{v_1 - \rho_1} - \mu \right] \\ & + m_2 (H - \mathcal{H}^0 - \varepsilon \mathcal{H}^1) - m_1 (\mathcal{H}^0 + \varepsilon \mathcal{H}^1). \end{aligned} \quad (4.16)$$

Differentiating (4.15) with respect to τ we obtain

$$\frac{dh_1}{d\tau} = \frac{\partial \mathcal{H}^0}{\partial \tau} + \varepsilon \frac{\partial \mathcal{H}^1}{\partial \tau}. \quad (4.17)$$

Since \mathcal{H}^0 is constant with respect to τ , we have $\frac{d\mathcal{H}^0}{d\tau} = 0$ and then (4.17) became as follows

$$\frac{dh_1}{d\tau} = \varepsilon \frac{\partial \mathcal{H}^1}{\partial \tau}. \quad (4.18)$$

From the Chain Rule we have from (4.18)

$$\frac{dh_1}{d\tau} = \varepsilon \left(\frac{\partial \mathcal{H}^1}{\partial v_1} \frac{dv_1}{d\tau} + \frac{\partial \mathcal{H}^1}{\partial v_2} \frac{dv_2}{d\tau} + \frac{\partial \mathcal{H}^1}{\partial H} \frac{dH}{d\tau} \right) = \mathcal{O}(\varepsilon^2). \quad (4.19)$$

That is because the changes $\frac{\partial \mathcal{H}^1}{\partial v_1}$, $\frac{\partial \mathcal{H}^1}{\partial v_2}$ and $\frac{\partial \mathcal{H}^1}{\partial H}$ are constant and, $\frac{dv_1}{d\tau}$, $\frac{dv_2}{d\tau}$ and $\frac{dH}{d\tau}$ are all of $\mathcal{O}(\varepsilon)$.

Comparing the both sides of (4.16) and (4.19) for the orders of ε , we obtain

$$\begin{aligned} \mathcal{O}(\varepsilon^0): \quad \mathcal{H}^0 &= \frac{m_2 H}{(m_1 + m_2)} \\ \mathcal{O}(\varepsilon): \quad \mathcal{H}^1 &= \frac{\mathcal{H}^0}{m_1 + m_2} \left[\frac{\xi_1(v_1 - \rho_1)}{1 + \bar{\gamma}_1(v_1 - \rho_1)} - \frac{\mu_1 (1 + \bar{\gamma}_1(v_1 - \rho_1))}{v_1 - \rho_1} - \mu \right], \end{aligned}$$

and hence we have

$$\begin{aligned} \mathcal{H}^\varepsilon(v_1, v_2, H) &= \mathcal{H}^0(v_1, v_2, H) + \varepsilon \mathcal{H}^1(v_1, v_2, H) + \mathcal{O}(\varepsilon^2) \\ &= \frac{m_2 H}{m_1 + m_2} \left(1 + \frac{\varepsilon}{m_1 + m_2} \left[\frac{\xi_1(v_1 - \rho_1)}{1 + \bar{\gamma}_1(v_1 - \rho_1)} - \frac{\mu_1 (1 + \bar{\gamma}_1(v_1 - \rho_1))}{v_1 - \rho_1} - \mu \right] \right) + \mathcal{O}(\varepsilon^2). \end{aligned}$$

Therefore, after determining the function \mathcal{H}^ε , and according to Theorem 3.4, the reduction of the

two-patch model (4.4) to the manifold \mathcal{M}_ε , for small $\varepsilon > 0$ is given by the following system

$$\begin{aligned} \frac{dv_1}{dt} &= v_1(1-v_1) - \frac{\eta_1(v_1-\rho_1)}{1+\gamma_1(v_1-\rho_1)} \Psi(v_1, v_2, \varepsilon) H \\ \frac{dv_2}{dt} &= v_2(1-v_2) - \frac{\eta_2(v_2-\rho_2)}{1+\gamma_2(v_2-\rho_2)} (1-\Psi(v_1, v_2, \varepsilon)) H \\ \frac{dH}{dt} &= \left[\frac{\xi_2(v_2-\rho_2)}{1+\bar{\gamma}_2(v_2-\rho_2)} - \frac{\mu_2(1+\bar{\gamma}_2(v_2-\rho_2))}{v_2-\rho_2} - \mu + \left\{ \frac{\xi_1(v_1-\rho_1)}{1+\bar{\gamma}_1(v_1-\rho_1)} \right. \right. \\ &\quad \left. \left. - \frac{\mu_1(1+\bar{\gamma}_1(v_1-\rho_1))}{v_1-\rho_1} - \frac{\xi_2(v_2-\rho_2)}{1+\bar{\gamma}_2(v_2-\rho_2)} + \frac{\mu_2(1+\bar{\gamma}_2(v_2-\rho_2))}{v_2-\rho_2} \right\} \Psi(v_1, v_2, \varepsilon) \right] H, \end{aligned} \quad (4.20)$$

where

$$\Psi(v_1, v_2, \varepsilon) = \frac{m_2}{m_1+m_2} \left(1 + \frac{\varepsilon}{m_1+m_2} \left[\frac{\xi_1(v_1-\rho_1)}{1+\bar{\gamma}_1(v_1-\rho_1)} - \frac{\mu_1(1+\bar{\gamma}_1(v_1-\rho_1))}{v_1-\rho_1} - \mu \right] \right).$$

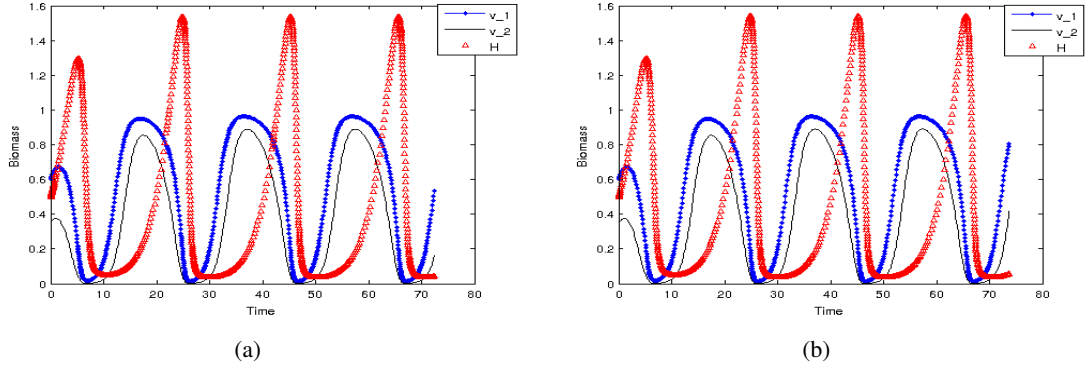


Figure 4.5: Numerical simulations shows the dynamics of the two-patch model (4.1) (Figure 4.5(a)) and the reduced system on the manifold \mathcal{M}_ε (4.20) (Figure 4.5(b)). In these figures, the patterns show that the vegetation biomasses on both patches oscillate. The total herbivore biomasses on the two patches also showed an oscillatory behavior. We used the parameter values showed in Table 4.1, with $A_1 = 50$, $A_2 = 100$, $\varepsilon = 0.01$ and $\alpha_2 = 1.50$. In the figures v_1 oscillates between 0.0143 and 0.9621, v_2 oscillates between 0.0025 and 0.8898, and H oscillates between 0.0358 and 1.5403. The initial points were $v_1 = 0.6$, $v_2 = 0.35$ and $H = 0.5$.

System (4.20) has the same equilibrium points E_1, E_2, E_3 and E_4 as system (4.10). The non-trivial equilibria (v_1^*, v_2^*, H^*) for system (4.20) are given by the positive solutions to the following

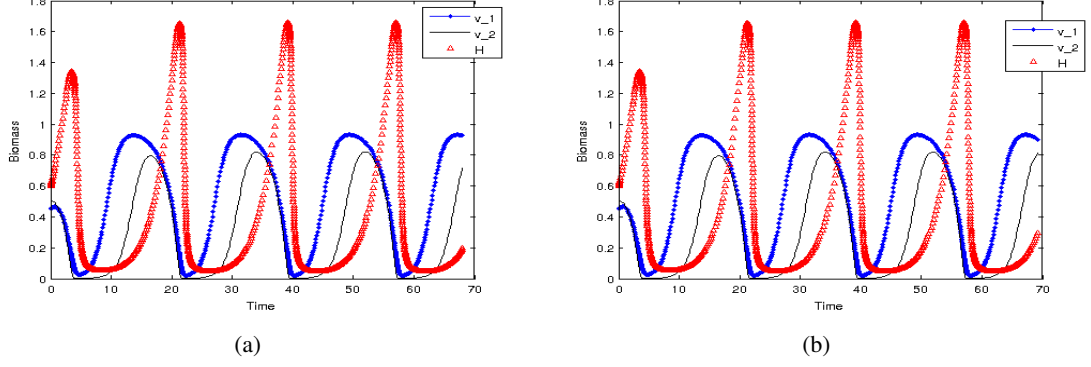


Figure 4.6: Simulations for the two-patch model (4.1) (Figure 4.6(a)), and the reduced system on the manifold \mathcal{M}_ε (4.20) (Figure 4.6(b)). In this figure we used the parameter values showed in Table 4.1 with $\varepsilon = 0.01$ and $\alpha_1 = \alpha_2 = 4$. The initial points were $v_1 = 0.45$, $v_2 = 0.5$ and $H = 0.6$.

system

$$\begin{aligned}
 v_1(1 - v_1) - \frac{\eta_1(v_1 - \rho_1)}{1 + \gamma_1(v_1 - \rho_1)} \Psi(v_1, v_2, \varepsilon) H &= 0 \\
 v_2(1 - v_2) - \frac{\eta_2(v_2 - \rho_2)}{1 + \gamma_1(v_2 - \rho_2)} (1 - \Psi(v_1, v_2, \varepsilon)) H &= 0 \\
 \frac{\xi_2(v_2 - \rho_2)}{1 + \tilde{\gamma}_2(v_2 - \rho_2)} - \frac{\mu_2(1 + \tilde{\gamma}_2(v_2 - \rho_2))}{v_2 - \rho_2} - \mu + \left[\frac{\xi_1(v_1 - \rho_1)}{1 + \tilde{\gamma}_1(v_1 - \rho_1)} \right. \\
 \left. - \frac{\xi_2(v_2 - \rho_2)}{1 + \tilde{\gamma}_2(v_2 - \rho_2)} - \frac{\mu_1(1 + \tilde{\gamma}_1(v_1 - \rho_1))}{v_1 - \rho_1} + \frac{\mu_2(1 + \tilde{\gamma}_2(v_2 - \rho_2))}{v_2 - \rho_2} \right] \Psi(v_1, v_2, \varepsilon) &= 0
 \end{aligned} \tag{4.21}$$

Again, system (4.21) is highly nonlinear, and the number of the parameters involved in the system is large, so it is difficult to obtain explicit expressions for $v_1(t)$, $v_2(t)$ and $H(t)$ using analytical methods. Numerical bifurcation analysis will be more convenient in this case, to examine the existence and the stability of positive equilibria, Hopf bifurcation, and the existence of periodic orbits, when the migration parameter α_2 takes different values.

In the following section, we will use the continuation software package AUTO-07p (Doedel et al. [2007]), to obtain bifurcation diagrams for the reduced two-patch systems (4.10) and (4.20), in which the migration propensity parameter α_2 is used as a bifurcation parameter. In all runs of the AUTO programs, we fixed all the parameters using the parameter values in Table 4.1, and α_2 varied between 0 and 15. This will allow us to study the behavior of the system over this period for the parameter α_2 , and in turn this will help to examine the effects of density dependent migrations on the stability of the system.

4.3 Numerical results for the reduced systems

Having a quick look back at the systems of equations (4.12) and (4.21), one can observe that the nonlinearity and the large number of parameters make it more difficult to obtain the nontrivial positive equilibria using analytical methods. Using direct calculations, we showed that the reduced systems (4.10) and (4.20) have the same trivial equilibrium points E_1, E_2, E_3 and E_4 . Stability analysis showed that these equilibrium points are unconditionally unstable (see Appendix A). For the nontrivial equilibria E_* , from the graphical illustrations and stability analysis (see Appendix A), we showed that the existence and the stability of E_* depends on the choice of the parameters α_1 and α_2 . In this section, we are interesting in examining the existence and the stability of the nontrivial positive stationary solutions for the reduced two-patch systems (4.10) and (4.20), over the parameter space of α_2 . To do that we varied the migration propensity parameter α_2 between 0 and 15 (for the parameter values in Table 4.1, and when $\alpha_1 = 3.75$ and $\alpha_2 > 15$, we found that the behavior of the system after this point remains the same as the behavior at $\alpha_2 = 15$) and we obtained bifurcation diagrams in one family of parameters.

The outputs that obtained from AUTO programs provided us with families of stationary solutions, Hopf bifurcations, and families of periodic orbits. At the end of the following section we presented some numerical simulations using MATLAB, to support our findings.

4.3.1 Bifurcations of the reduced systems

For the reduced two-patch system (4.10), if we started AUTO programs from any of the non coexistence fixed points E_1, E_2, E_3 or E_4 to compute families of stationary solutions, the program will not detect any other different fixed points rather than the starting point.

To examine the existence of the nontrivial equilibria $E_* = (v_1^*, v_2^*, h^*)$ we started AUTO from any arbitrary fixed point (v_1^*, v_2^*, h^*) , that is different from $E_i, i = 1, \dots, 4$. Since we are interested in obtaining the equilibria E_* for different values of α_2 , we first computed special cases of the equilibria, that is, when we chose $\alpha_2 = 0$ in (4.12). The system in this case has four equilibrium points (v_1^*, v_2^*, H^*) , namely $E_*^1 = (0, v_2^{1*}, h^{1*})$, $E_*^2 = (1, v_2^{1*}, h^{1*})$, $E_*^3 = (0, v_2^{2*}, h^{2*})$ and $E_*^4 =$

$(1, v_2^{2*}, h^{2*})$, where

$$v_2^{1*} = \frac{2\bar{\gamma}_2\mu_2 + \mu + \sqrt{(4\xi_2\mu_2 + \mu^2)}}{2(\xi_2 - \bar{\gamma}_2^2\mu_2 - \bar{\gamma}_2\mu)}$$

$$v_2^{2*} = \frac{2\bar{\gamma}_2\mu_2 + \mu - \sqrt{(4\xi_2\mu_2 + \mu^2)}}{2(\xi_2 - \bar{\gamma}_2^2\mu_2 - \bar{\gamma}_2\mu)}$$

$$h^{1*} = -\frac{(v_2^{1*} - 1)(1 + \gamma_2 v_2^{1*})}{\eta_2}$$

and

$$h^{2*} = -\frac{(v_2^{2*} - 1)(1 + \gamma_2 v_2^{2*})}{\eta_2}.$$

We started our AUTO programs from the equilibrium point E_*^4 using the parameter values given in Table 4.1. The resulting bifurcation diagrams are shown in Figure 4.8. These diagrams show the existence of stable and unstable fixed points, Hopf bifurcations (the figures on the left), and families of periodic orbits (the figures on the right). The dashed lines in these bifurcation diagrams indicate unstable fixed points or unstable periodic orbits, while the solid lines indicate stable fixed points or stable periodic orbits. In Table 4.3 we showed the bifurcation points along with their values and their labels.

4.3.1.1 The bifurcation diagrams for the reduced system of $\varepsilon = 0$

From the point $\alpha_2 = 0$, a branch of unstable fixed points continue until α_2 reaches "2" (see Table 4.3 for the corresponding α_2 value), where a supercritical Hopf bifurcation appears in the system that stabilizes the fixed points. A branch of unstable periodic orbits bifurcate from the Hopf point at "2". These unstable periodic orbits change their direction through the fold or a saddle node bifurcation point at "9". While α_2 decreases, the periodic orbits remain stable until they reach $\alpha_2 = 0$, where the dynamics beyond that value are not of our interest. The branch of fixed points at "2" remains stable until it reaches "3", when another Hopf bifurcation occurs in the system and the stability of the fixed points changes. Another unstable branch of periodic orbits bifurcates from the Hopf point at "3" and changes its direction and its stability at the fold point "14", and it continues until it reaches the end point at $\alpha_2 = 15$. At "3" the branch of unstable fixed points continues until it reaches the saddle node bifurcation at "4", where it changes its direction and remains unstable while α_2 decreases. The branch changes its direction again at the saddle node bifurcation at "5" and the fixed points remains unstable until a supercritical Hopf bifurcation point appears at "6", when the fixed points becomes stable and the branch continues until another Hopf bifurcation appears at "7", when the branch of fixed points becomes unstable. Branch of unstable periodic orbits bifurcates

4. NUMERICAL RESULTS

from the Hopf point at "6" and continues until it connects the other Hopf bifurcation at "7".

In the domain $2.419 < \alpha_2 < 3.0846$, the system exhibits only stable fixed points, and there is no other closed orbits in the phase space for α_2 being in this range and for the parameter values showed in Table 4.1. In this case, if the system started at any point near one of these stable equilibria then it would be attracted to one of these stable equilibria. In Figure 4.7 we showed an example for one of these cases when $\alpha_2 = 2.5$; another example showed in Figure 4.10, and the outputs aided this result.

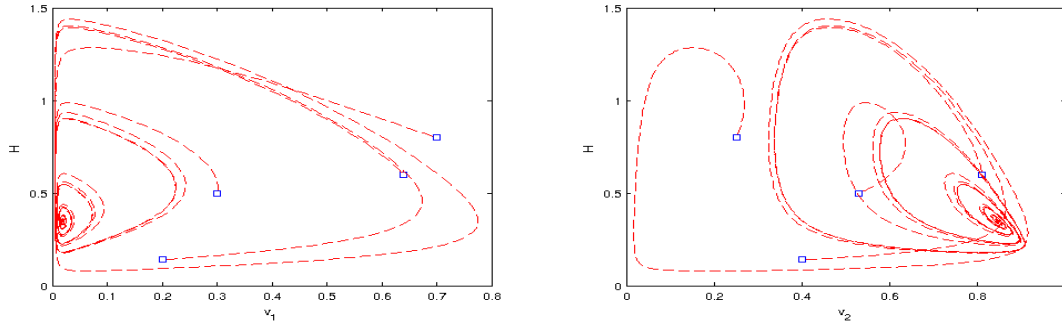


Figure 4.7: Phase plane for the reduced two-patch model (4.10) when $\alpha_2 = 2.5$. In this figure we started the solutions from four different points indicated by small squares, and it shows that all the solutions will tend to a single stable fixed point in the phase plane.

Label	Bifurcation type	α_2	v_1	v_2	H
1	End point	0.00000	1.00000	0.1583	0.3126
2	Hopf bifurcation	2.30029	0.816619	0.033031	0.43646
3	Hopf bifurcation	5.29291	0.430321	0.023233	0.60131
4	Fold point	5.5512	0.32589	0.033529	0.58688
5	Fold point	2.84308	0.019085	0.337149	0.55207
6	Hopf bifurcation	3.01878	0.01172	0.445478	0.55625
7	Hopf bifurcation	7.29233	0.01607	0.820912	0.37021
9	Fold point	2.419	0.88015	0.224266	0.9173
13	Fold point	3.0846	0.86659	0.45075	1.31405

Table 4.3: The bifurcation points and turning points from the bifurcation diagram 4.8, for the reduced two-patch model (4.10). In this table we labeled each point with the same label that appears on the bifurcation diagram 4.8.

4. NUMERICAL RESULTS

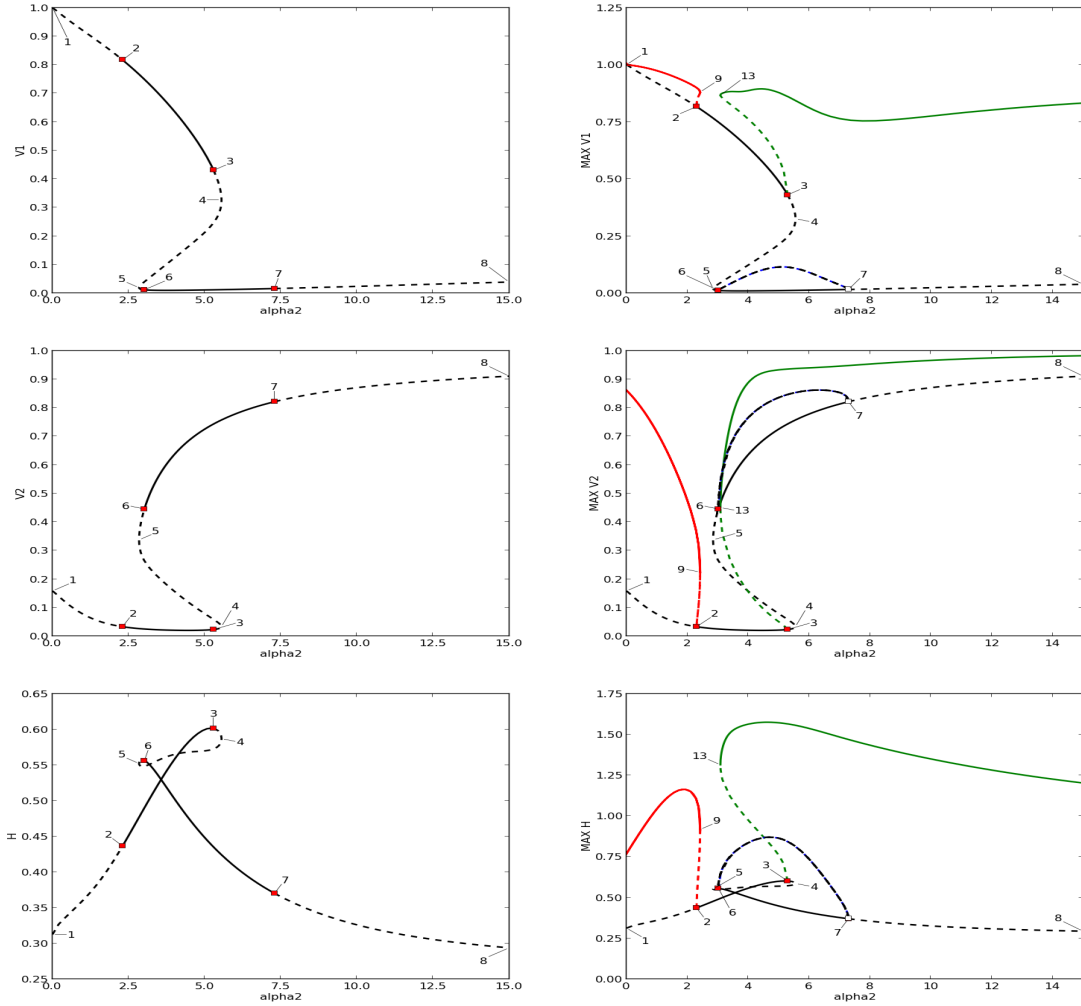


Figure 4.8: Bifurcation diagrams for the reduced two-patch model (4.10). It ranges over the parameter space of α_2 and plots the fixed points, fold points, Hopf bifurcation points, and periodic orbits of the system at these values. The figures on the left show only the fixed points, fold points, and Hopf bifurcation points (indicated by squares). The solid lines correspond to stable fixed points, and dashed lines indicate unstable fixed points. The figures on the right, show the periodic orbits that bifurcate from the Hopf points. The dashed lines in periodic orbits indicate unstable periodic solutions, while the solid lines indicate stable periodic orbits.

4. NUMERICAL RESULTS

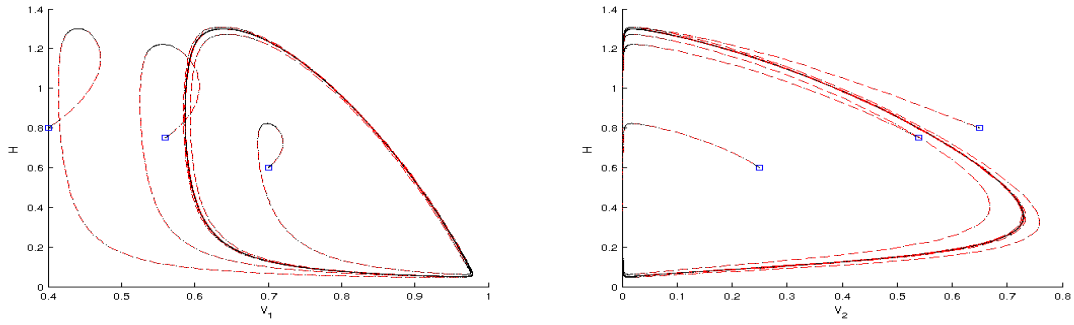


Figure 4.9: Simulation for the reduced two-patch model (4.10), for $\alpha_2 = 1.5$, showing a single stable limit cycle. The other parameters used are shown in Table 4.1. The initial points were indicated by small squares.

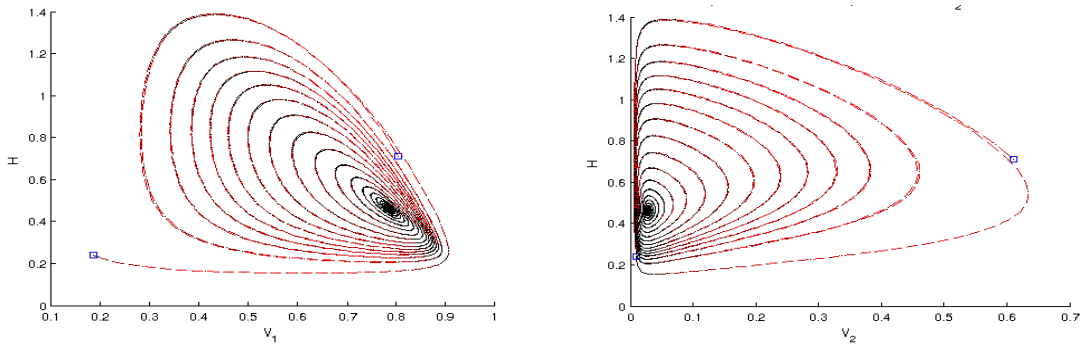


Figure 4.10: Simulation for the reduced two-patch model (4.10), for $\alpha_2 = 3$, and for the other parameters shown in Table 4.1. The output shows that a single stable fixed point appears in the system.

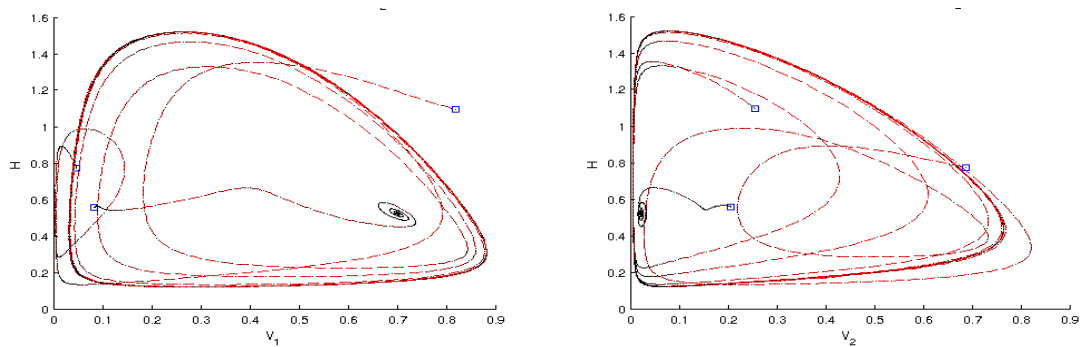


Figure 4.11: Phase plane corresponding to $\alpha_2 = 5.29636$ and the other parameters shown in Table 4.1. The outputs show that the solutions will either tend to a single stable fixed point, or a single stable limit cycle in the phase plane.

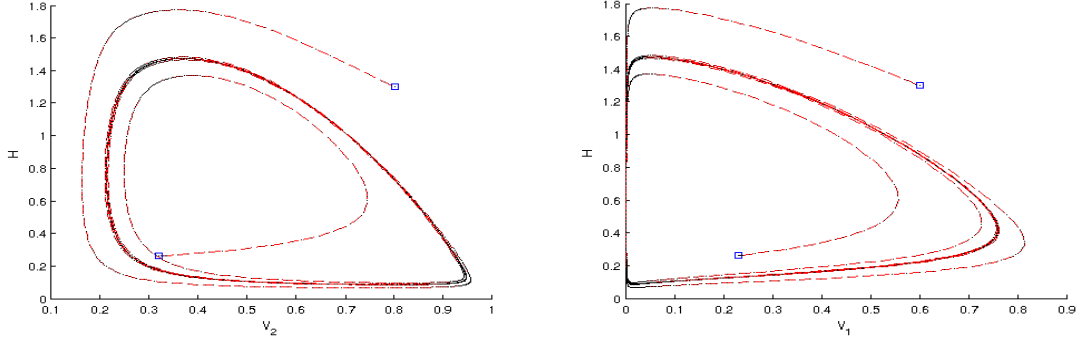


Figure 4.12: Phase plane corresponding to $\alpha_2 \geq 11$, and the other parameters shown in Table 4.1. The outputs show that all the solutions will be attracted to a single stable limit cycle in the phase plane. The behavior of the system after this point will remain the same.

4.3.1.2 The bifurcation diagrams for the reduced system when $\varepsilon > 0$

For the reduced system (4.20) for $\varepsilon > 0$, we started our AUTO programs from the equilibrium point $(1, v_2^*, h^*)$, where

$$v_2^* = 1/2 \frac{2\xi_2 \rho_2 - 2\mu_2 \bar{\gamma}_2^2 \rho_2 + 2\mu_2 \bar{\gamma}_2 + \mu - 2\mu \bar{\gamma}_2 \rho_2 - \sqrt{4\xi_2 \mu_2 + \mu^2}}{\xi_2 - \mu_2 \bar{\gamma}_2^2 - \bar{\gamma}_2 \mu}$$

and

$$h^* = \frac{v_2^* (1 - v_2^*) (1 + \gamma_2 (v_2^* - \rho_2))}{\eta_2 (v_2^* - \rho_2)},$$

using the parameter values in Table 4.1 and we obtained the bifurcation diagrams shown in Figure 4.13. We listed in Table 4.4 all the bifurcation points and the end points along with their labels, as they appear in the diagrams (4.13).

The diagrams (4.8) and (4.13) for the aggregated systems for $\mathcal{O}(\varepsilon^0)$ and for $\mathcal{O}(\varepsilon)$ respectively, have the same overall picture.

The region where the system exhibits only stable or (and) unstable fixed points for the bifurcation diagram 4.13 is $2.59073 < \alpha_2 < 3.30416$. For example, when $\alpha_2 = 2.98$, Figure 4.15 shows that all the solutions will be attracted to a single stable fixed point in the phase space.

Different numerical examples for different values of α_2 are shown in Figures 4.14, 4.16 and 4.17. In these figures the solutions were started from either unstable fixed point or unstable periodic orbit.

Label	Bifurcation type	α_2	v_1	v_2	H
1	End point	0.00000	1.00000	0.15837	0.31264
2	Hopf bifurcation	2.46356	0.81662	0.03303	0.43646
3	Hopf bifurcation	5.66983	0.43034	0.02323	0.60131
4	Fold point	5.94711	0.32583	0.33540	0.58687
5	Fold point	3.04869	0.01912	0.33691	0.55205
6	Hopf bifurcation	3.23726	0.01173	0.44520	0.55626
7	Hopf bifurcation	7.83216	0.01610	0.82120	0.36996
9	Fold point	2.59073	0.88015	0.22425	0.91731
13	Fold point	3.30416	0.86658	0.45074	1.31395

Table 4.4: The bifurcation points, turning points and their labels as they appear in the bifurcation diagram 4.13 for the reduce a two-patch model (4.20).

4. NUMERICAL RESULTS

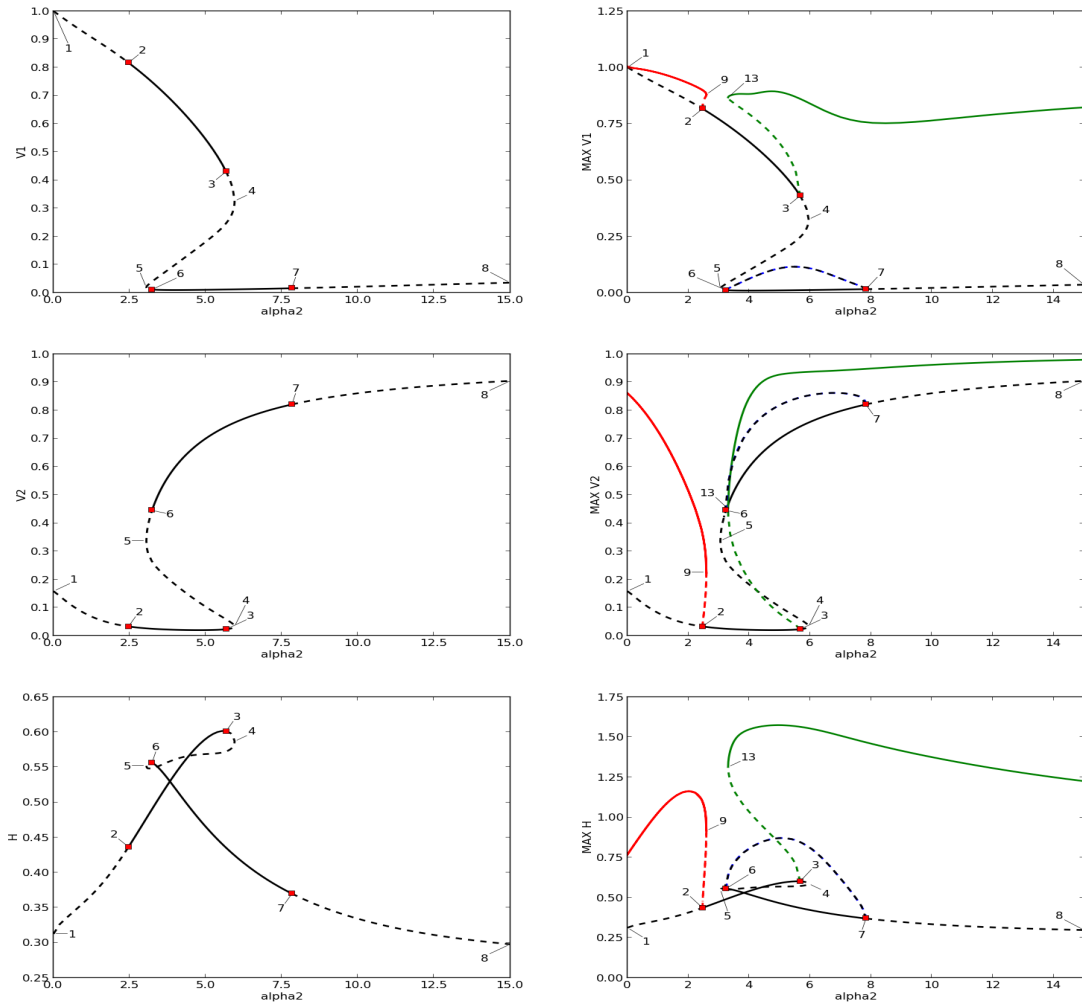


Figure 4.13: Bifurcation diagrams for the reduced two-patch model (4.20) for $\varepsilon = 0.001$. The figures on the left show the fixed points, fold points, and Hopf bifurcation points (four points indicated by small squares). In the figures to the left, the solid lines correspond to stable fixed points, and the dashed lines indicate unstable fixed points. The figures on the right show the families of periodic orbits that bifurcate from the Hopf points. The dashed lines in periodic orbits indicate instability, while the solid lines indicate stability.

4. NUMERICAL RESULTS

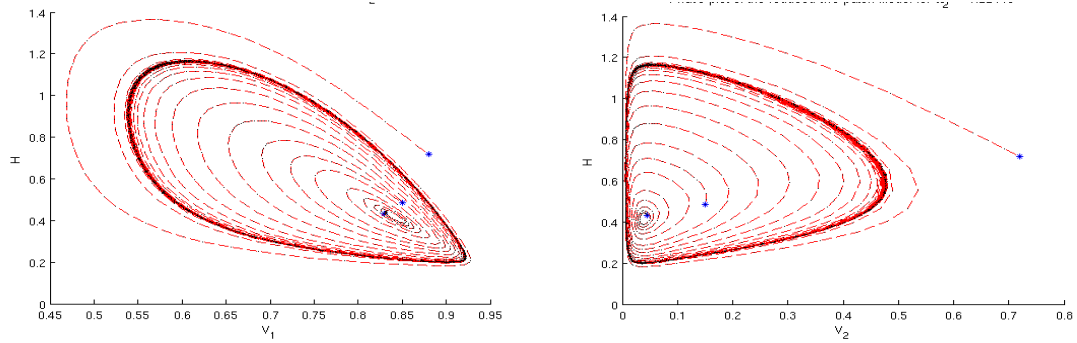


Figure 4.14: Simulation for the reduced system (4.20) for $\varepsilon = 0.001$, $\alpha_2 = 1.25$ and for the parameter values showed in Table 4.1. In this run, the solutions were started near the unstable fixed point and from two arbitrary points in the phase plane. The output shows that all the solutions will be attracted to a single stable limit cycle.

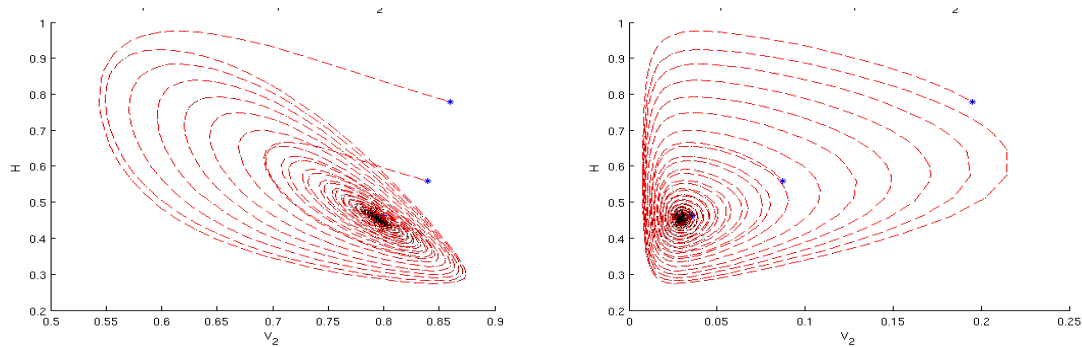


Figure 4.15: Simulations for the reduced system (4.20) for $\varepsilon = 0.001$, $\alpha_2 = 2.98$ and for the other parameter values shown in Table 4.1. The solutions were started near the unstable fixed point and two arbitrary points near the stable equilibrium. The output shows that a single stable fixed point attract all the solutions.

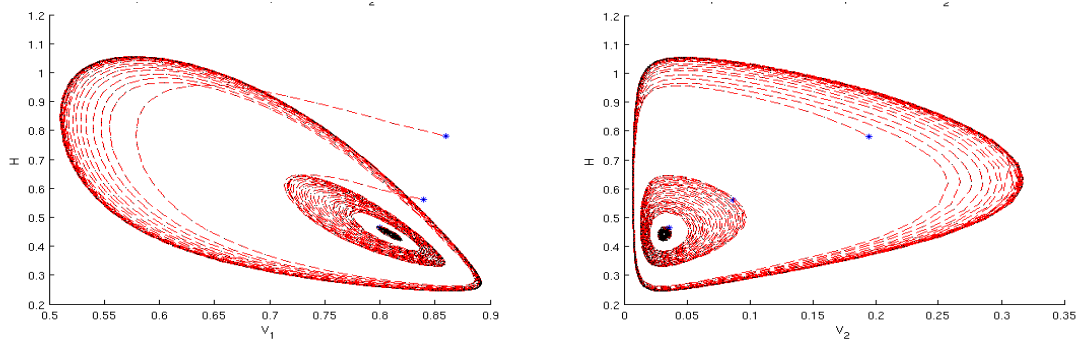


Figure 4.16: Simulation for the reduced system (4.20) for $\varepsilon = 0.001$, $\alpha_2 = 3.7$ and for the other parameter values shown in Table 4.1. The solutions were started near the two unstable fixed points and near the unstable periodic orbit. The output shows that one of the points will be attracted to stable fixed point, and the other points will be attracted to a single stable periodic orbit in the phase space.

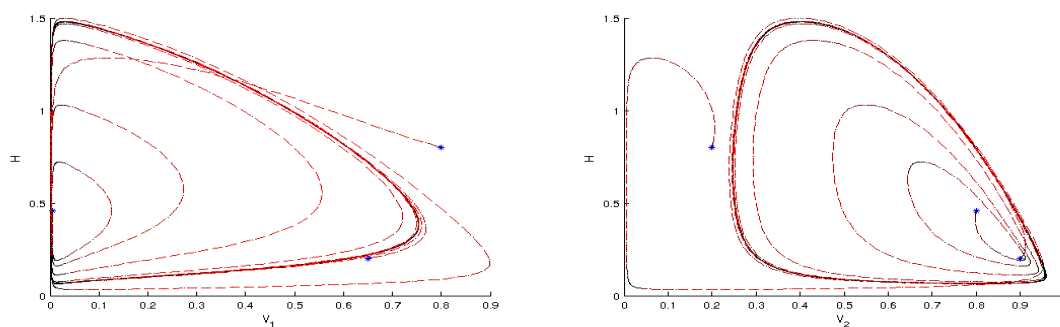


Figure 4.17: Simulation for the reduced system (4.20) for $\varepsilon > 0$ for $\varepsilon = 0.001$, $\alpha_2 = 7.3$ and for the other parameter values shown in Table 4.1. We started the solutions from three different arbitrary points. The outputs show that all the solutions would be attracted to the stable periodic orbit in the phase plane.

4. NUMERICAL RESULTS

The explorations of the dynamics of the reduced two-patch models (4.10) and (4.20) for more than one parameter, or for a parameter other than α_2 will not be considered in this thesis. As we stated before, the purpose of this chapter was to study the dynamics of the two-patch model (2.5) for different values of animal migrations, to see whether or not a density-dependent migrations can stabilize or destabilize multi-patch systems. We choose α_2 as bifurcation parameter to examine the dynamics of the reduced two-patch systems under different migration propensities. From the numerical simulations 4.9-4.17, we observed that the reduced systems provided different kinds of dynamics when the migration parameter α_2 varies. One can ask a question, will the reduced systems show structures different from what we had observed, when we choose a different set of parameters?

When the carrying capacity of patch 1 is larger than the carrying capacity of patch 2, and if the area of patch 1 is larger than patch 2 area, then in this case we expect that the animals will prefer to stay on patch 1, because the amount of the available food on this patch is much larger, and the large area will help animals to expand over this patch.

As an example, we choose the propensity α_2 of migration from patch 1 to patch 2 to be relatively small, and we varied α_2 between 0 and 40. In this run, we set $K_1 = 200$, $K_2 = 150$, $A_1 = 100$, $A_2 = 50$, $\alpha_1 = 4.5$, and the other parameters as given in Table 4.1. The resulting bifurcation diagram is shown in Figures 4.18. We observed that the whole bifurcation diagram is shifted to the right as compared to the bifurcation diagram 4.8. In these figures, when the migration propensity from patch 1 towards patch 2 is larger than or equal the migration propensity from patch 2 to patch 1 ($\alpha_2 \leq \alpha_1$), then the system in this case has an unstable fixed point and stable periodic orbits in the phase space with MAX_{v_1} is almost at the carrying capacity of v_1 , where on patch 2, MAX_{v_2} takes smaller values. In this case, as the animals leave patch 1 at higher migration rates and aggregate more on patch 2, the vegetation on patch 1 grows much faster and reaches its maximum carrying capacity. For larger values of α_2 we observed that the system has two sets of unstable periodic orbits and a unique stable cycle with large values of MAX_H . When α_2 passes the turning point at “4”, the system has a stable periodic orbit with relatively large MAX_H , and one of the unstable periodic orbits disappear from the system.

For a different set of parameters, for example $K_1 = 250$, $K_2 = 150$, $\alpha_1 = 4.5$, $\rho_1 = 0.002$, $\rho_2 = 0.001$, and the other parameters as in Table 4.1, the resulting bifurcation diagram is shown in Figure 4.19. In these diagrams the structure of the periodic orbits is different from what we had in 4.18, as the nature of the Hopf bifurcations at “2”, “3”, “6” and “7” in these figures has changed. A family of unstable periodic orbits connects the two Hopf bifurcations at “2” and “3”, and another family of unstable periodic orbits connects the other two Hopf bifurcations at “6” and “7”. The bifurcation

4. NUMERICAL BIFURCATION ANALYSIS

at “13” in the diagrams 4.18 has disappeared from the system. The diagrams in 4.19 show that the whole system has no closed stable orbits.

As a conclusion, the dynamics and the nature of the Hopf bifurcations for the reduced two-patch models (4.10) and (4.20) will change when we choose different set of parameters other than α_1 and α_2 .

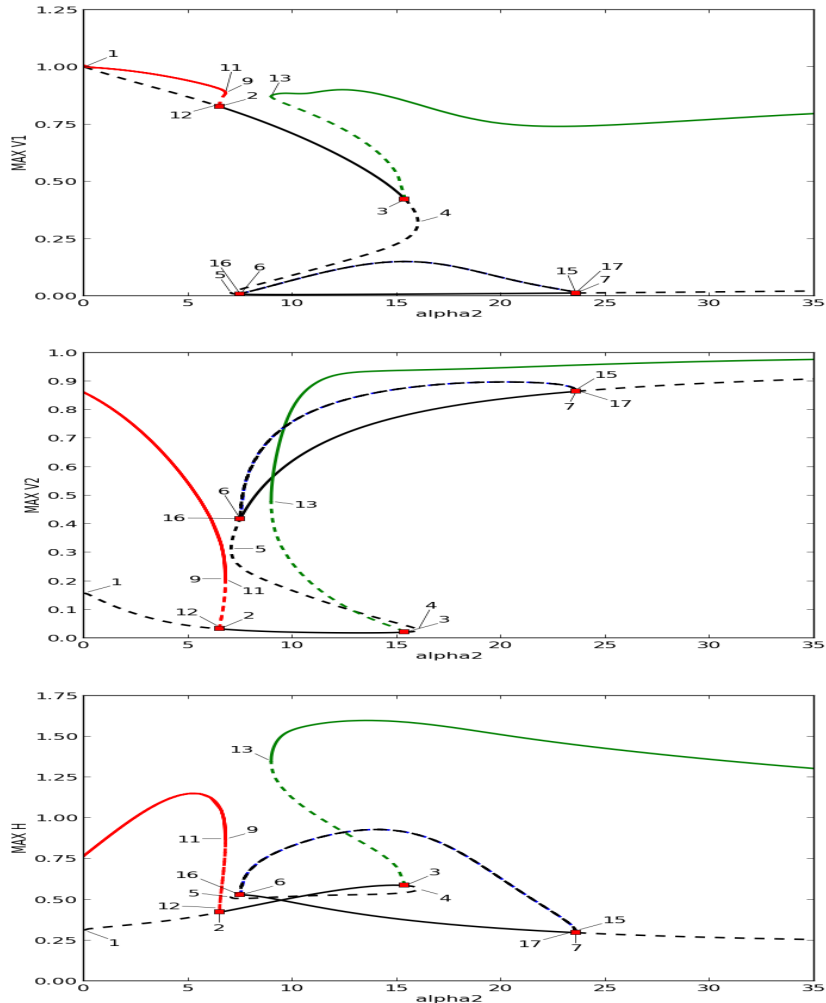


Figure 4.18: Bifurcation diagrams for the reduced two-patch model (4.10) when $K_1 = 200$, $K_2 = 150$, $\alpha_1 = 4.5$, and the other parameters shown in Table 4.1.

4.4 Conclusions

In this chapter, we provided analysis to the two-patch model (2.5), when only herbivores are allowed to migrate in both directions, and when the migrations occur faster in time. For simplicity and for the purpose of the mathematical analysis we used the total herbivore biomass H by summing the

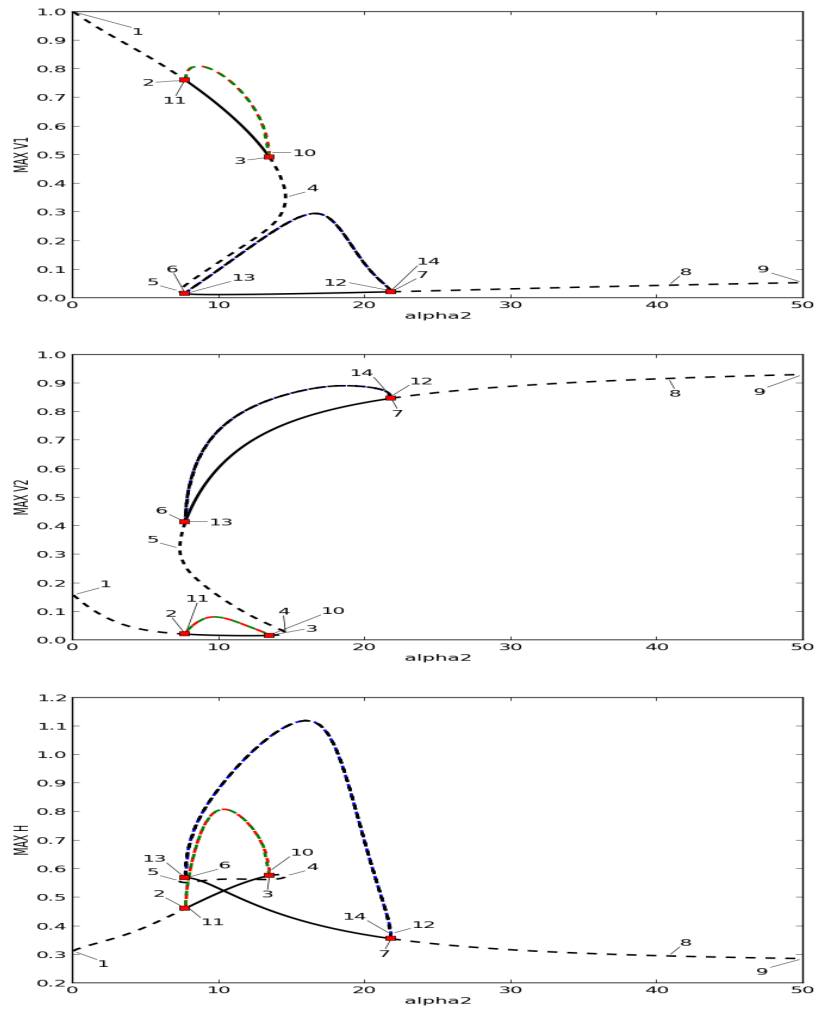


Figure 4.19: Bifurcation diagrams for the reduced two-patch model (4.10) when $K_1 = 250$, $K_2 = 150$, $\rho_1 = 0.002$, $\rho_2 = 0.001$, $\alpha_1 = 4.5$, and the other parameters shown in Table 4.1.

herbivore biomasses over the two patches. The model has two different time-scales, the fast and the slow time-scales. The existence of the two different time-scales in the model allowed us to use the geometric singular perturbation method to reduce the dimension of the two-patch model and obtain systems with fewer number of variables that govern the global dynamics, and hence are much easier to study their asymptotic behavior.

First, we proved that when $\varepsilon = 0$ in (2.5), then the fast system has a unique stable equilibrium, and the manifold of the fast equilibrium \mathcal{M}_0 is normally hyperbolically stable. The first reduced system results from the reduction of the dynamics to the manifold of the fast equilibrium \mathcal{M}_0 . Using the parameters values shown in Table 4.1, we provided some numerical results to show that the dynamics provided by the reduced system to the manifold \mathcal{M}_0 has the same features as the dynamics of the full system when ε is small (see Figures 4.1 and (4.2)).

When $\varepsilon \neq 0$ in (2.5), we proved that the manifold \mathcal{M}_0 is no longer a manifold of the equilibria for the system. Using results from Fenichel's Theorem 3.3, we proved the existence of a manifold \mathcal{M}_ε for the flow when ε is different from zero. We constructed an approximation to \mathcal{M}_ε and hence we used Fenichel's Theorem 3.4 to reduce the dimension of the two-patch model (2.5) to the manifold \mathcal{M}_ε . Using the parameter values shown in Table 4.1, we showed that the reduced system (4.20) on the manifold \mathcal{M}_ε has the same dynamics as the full system (2.5) (the results were shown in Figures 4.5 and 4.6). For the asymptotic behavior of the reduced systems (4.10) and (4.20), we proved that the both reduced systems have the same set of trivial equilibria.

To study the long-time behavior of the reduced systems, we explored the effects of animal migrations on the dynamics. The choice of α_2 to be the bifurcation parameter was because from the numerical simulations that we have obtained, we believe that animal propensity to migrate can affect the dynamics of the two-patch systems (4.10) and (4.20). Using the parameter values shown in Table 4.1, we provided some bifurcation diagrams, when α_2 is the only bifurcation parameter, and we obtained the diagrams 4.8 and 4.13. Each diagram has four Hopf bifurcations, so that families of periodic orbits are possible through these bifurcations. In these diagrams and for the set of the parameters in Table 4.1, we observed that the reduced two-patch systems (4.10) and (4.20) show different behavior when α_2 takes different values.

For example, in Figure 4.8, for $\alpha_2 \leq 2.30029$, the diagram shows that the system (4.10) has stable cycles with large values of v_1 . For $2.419 \leq \alpha_2 \leq 2.84308$ the diagram shows that the system has no closed orbits. When $3.0846 < \alpha_2 \leq 7.29233$, the diagram shows that the system has two sets of unstable cycles, and a unique stable limit cycle with large values of H . For $\alpha_2 > 7.29233$, the system has a unique stable cycle, with large H .

For the parameter values in Table 4.1, the bifurcation diagram 4.13 for the reduced two patch

4. CONCLUSIONS

model (4.10) has the same structure as the bifurcation diagram 4.8 for the reduced system (4.20). For a set of parameters different from the one listed in Table 4.1, we computed bifurcation diagrams for the reduced system (4.10), and the resulting figures showed a different structure of cycles.

For example, when $K_1 = 250$, $K_2 = 150$, $\rho_1 = 0.002$, $\rho_2 = 0.001$, and the other parameters in Table 4.1, we obtained the diagram 4.19. We observed that the whole system has no stable limit cycles. When $0 < \alpha_2 < 7.69928$ the system has no cycles of any type. When $7.31064 \leq \alpha_2 < 13.442$, the system has two unstable limit cycles, and when the migration propensity from patch 2 exceeds 20.1775, the cycles totally disappear from the system.

One can notice that most of the bifurcation diagrams and the simulation results that presented in this chapter were associated with large values of migration propensities. In our model, α_1 and α_2 are the propensity of migration parameters and their values do not give indications about the quality of vegetation on the local patches. On the other hand, the parameter β_i determine the palatability of the vegetation, and larger β_i indicates that the vegetation on patch i is more palatable. In our assumptions for the two-patch model we assumed that the migrations are proportional to migration propensities and reciprocal to the vegetation quality and the vegetation density on the patch. In our model the large values of α_i are more effective if β_i has smaller values. For example, if the quality of the vegetation on a patch is poor, and the propensity of leaving that patch is high, then the migration rate from that patch will be high, even if the vegetation density on the patch is high. In real systems such kind of migration behavior by animals can be seen, for example, as animals prefer to spend much time at the patches where the vegetation has a higher quality, and they leave the patch when the vegetation became less palatable, even if the biomass density of the vegetation is high.

As we pointed out previously in this section, the bifurcation diagrams for the reduced two-patch models (4.10) and (4.20), with the set of the parameters shown in Table 4.1, have intervals for the values of the parameter α_2 , where the system has no cycles. This result seems odd from the biological point of view. In the following sections we use the Morse decompositions and the Conley index theory to show that these diagrams are correct (from the mathematical point of view) and that AUTO has not failed to detect closed orbits for α_2 in that interval.

The work that we will be carrying out in Chapter 5 is purely mathematical and will not include any biological interpretations.

Chapter 5

Analyzing the bifurcation diagrams using Conley index and Morse decomposition theory

5.1 Introduction

Figure 5.1 below shows the bifurcation diagram for the reduced two-patch model (4.10) when $\varepsilon = 0$, $\alpha_1 = 4.5$ and the other parameters are shown in Table 4.1. In this diagram we observed that for $1.8116526400 < \alpha_2 < 3.8522743822$ there are no closed orbits in the system, and only stable fixed points or (and) unstable fixed points appear in the phase space. For $3.8522743822 \leq \alpha_2 < 4.7449008984$ families of unstable periodic orbits appear in the system. In Figures 5.3-5.6 we show some numerical simulations to describe the dynamics for some α_2 over this particular range of the parameter. One could ask, why the system for the parameter values in this range crashes to a single fixed point? Is there any possibility that the trajectories will tend to one of the limit cycles in the phase space? To get more explanations about the dynamics of the system showed in 5.1, we use Morse decomposition and the Conley index theorems.

In this chapter we use Morse decompositions and Conley index theorems to understand the global behavior of flows presented by the bifurcation diagrams for the reduced two-patch models (4.10) and (4.20). In the Morse decomposition theorem the qualitative behavior of the flow is determined by what is called Morse sets, Morse decompositions and the trajectories connecting these different sets (Mischaikow and Mrozek [2002]). Conley index theory (Conley [1978]; Mischaikow [1999]; Mischaikow and Mrozek [2002]) provides a set of tools for studying the dynamics of the general flow.

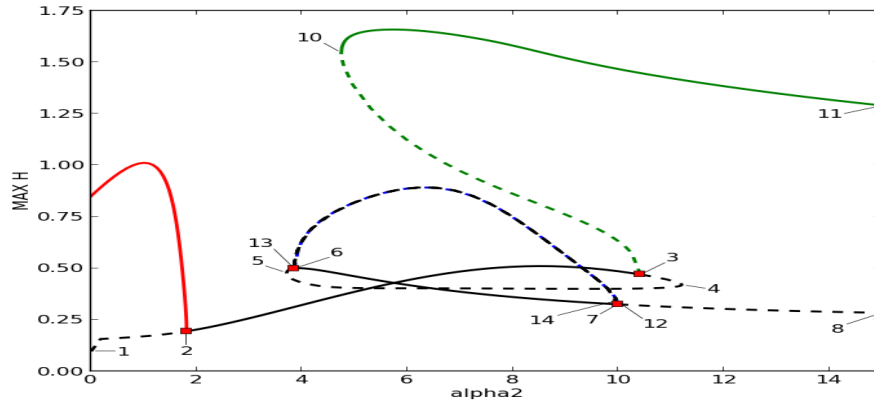


Figure 5.1: Bifurcation diagram illustrates the reduced two-patch model when $\varepsilon = 0$, where α_2 considered as a bifurcation parameter. In this figure $\alpha_1 = 4.5$ and the other parameter values are given in Table 4.1. Solid lines correspond to stable fixed points and stable periodic orbits, dashed lines correspond to unstable fixed points and unstable periodic orbits. Hopf bifurcations are indicated by squares. All bifurcations are labeled.

α_2	v_1	v_2	H	Unstable fixed point type	Name
1.5	0.939024	0.878049	0.294512	unstable fixed point	u_1
2.07143				no unstable fixed points in the system	u'_1
3.42				no unstable fixed points in the system	u'_2
3.73	0.0096	0.3354	0.4783	unstable fixed point	u_2
4.2251	0.0256098	0.187805	0.414024	unstable fixed point	u_3
	0.0256098	0.678049	0.717073	a point on unstable periodic orbit	R_1
5.75	0.0682927	0.119512	0.405488	unstable fixed point	u_4
	0.0981707	0.246341	0.8.79268	a point on unstable periodic orbit	R_2
	0.802439	0.836585	1.13963	a point on unstable periodic orbit	R_3
8.58714	0.0649752	0.0519802	0.398515	unstable fixed point	u_5
	0.134282	0.0519802	0.584777	a point on unstable periodic orbit	R_4
	0.615099	0.888614	0.766708	a point on unstable periodic orbit	R_5
10.2143	0.0170732	0.0365854	0.32439	unstable fixed point	u_6
	0.166463	0.853659	0.409756	unstable fixed point	u_7
	0.405488	0.0121951	0.571951	a point on unstable periodic orbit	R_6
10.8929	0.0213415	0.863415	0.32439	unstable fixed point	u_8
	0.183537	0.0243902	0.409756	unstable fixed point	u_9
	0.247561	0.0097561	0.439634	unstable fixed point	u_{10}
12	0.0170732	0.878049	0.294512	unstable fixed point	u_{11}

Table 5.1: Table shows the values of the unstable stationary solutions for certain values of α_2 , from the bifurcation diagram 5.1. In this table we labeled each unstable stationary solution with either u_i (for unstable fixed points) or R_i (for unstable cycles).

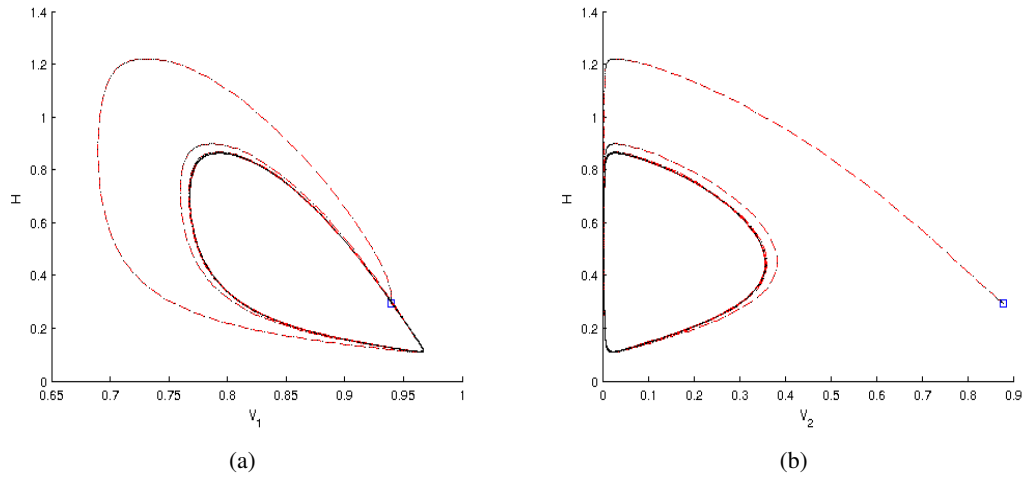


Figure 5.2: Phase plane corresponding to $\alpha_2 = 1.5$ in the bifurcation diagram 5.1. The solutions started near the unstable equilibrium point that is indicated by small square, and the long time dynamics show that the solution will be attracted to stable limit cycle in the phase plane.

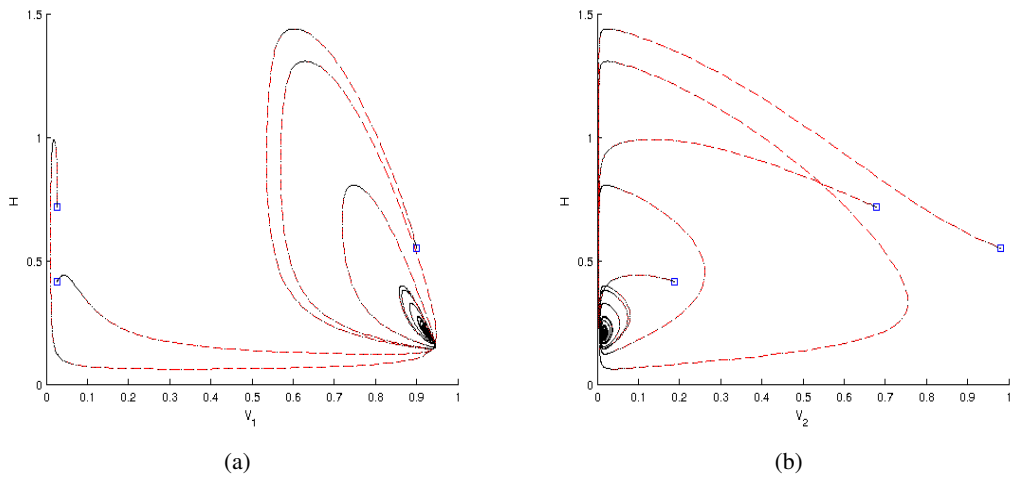


Figure 5.3: Phase plane corresponding to $\alpha_2 = 2.07143$ from the bifurcation diagram 5.1. In this case the system has only a single stable fixed point in the phase space. The solutions were started from three arbitrary initial points indicated by squares. A unique stable fixed point attract all the solutions.

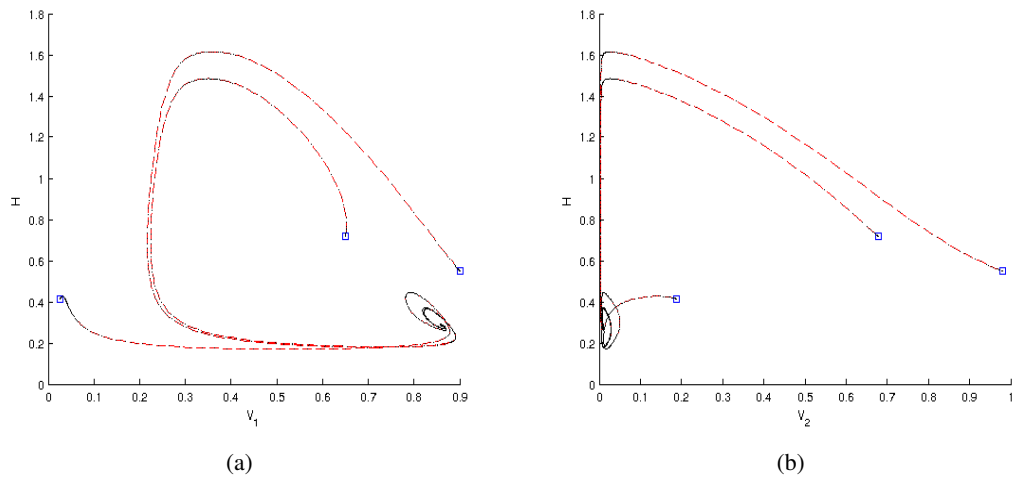


Figure 5.4: Phase plane corresponding to $\alpha_2 = 3.42$ from the bifurcation diagram 5.1. In this case only a single stable fixed point appear in the system. The solutions were started from three different initial points indicated by small squares. The figures show that all the solutions will be attracted to a single stable fixed point in the phase space.

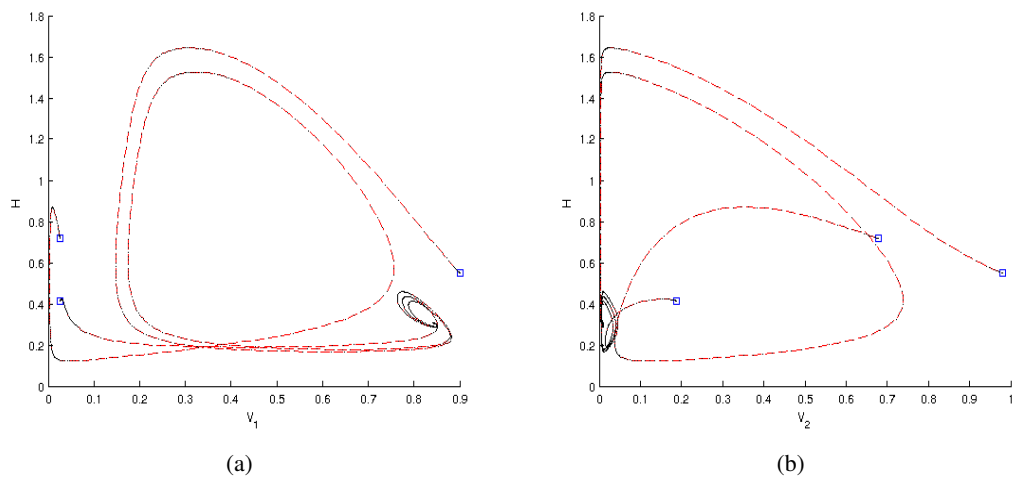


Figure 5.5: Phase plane corresponding to $\alpha_2 = 3.73$ from the bifurcation diagram 5.1. The system in this case has two fixed points, a stable fixed point and an unstable fixed point. In this run the solutions were started near the unstable fixed point and from two other arbitrary points indicated by squares. The unique stable fixed point attract all the solutions.

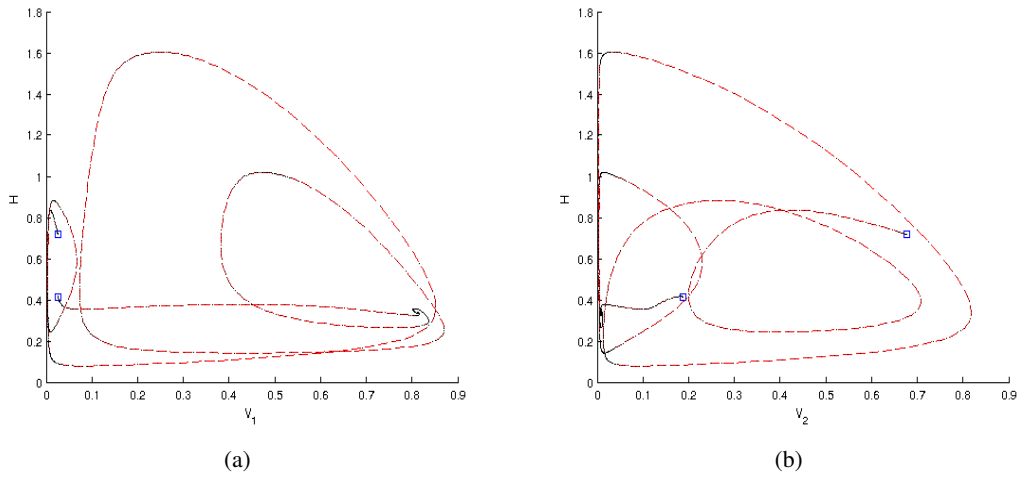


Figure 5.6: Phase plane corresponding to $\alpha_2 = 4.2251$. The system in this case has four stationary solutions, two stable fixed points, an unstable fixed point and an unstable periodic orbit. The initial solutions were indicated by small squares, where they started near the unstable fixed point and from a point on the unstable periodic orbit. Both solutions attracted to one of the stable fixed point in the phase space.

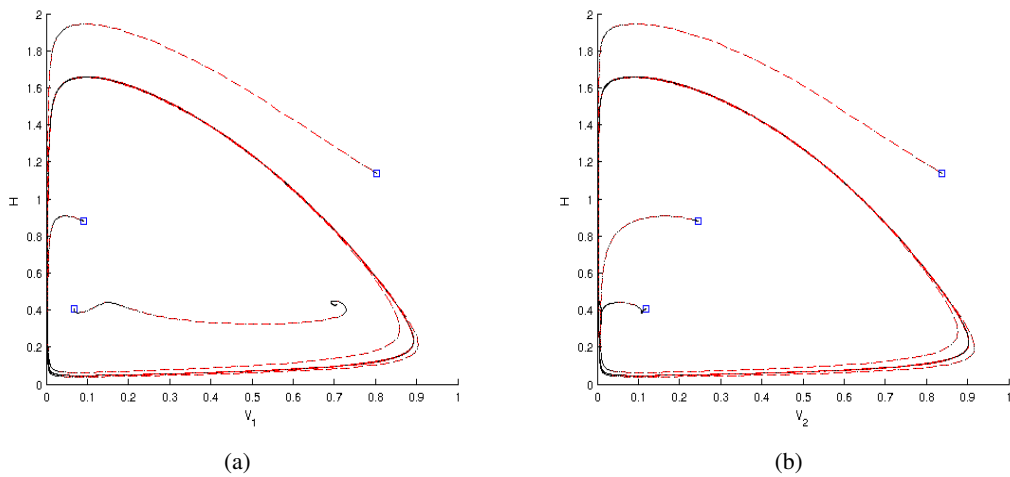


Figure 5.7: Phase plane corresponding to $\alpha_2 = 5.75$ from the bifurcation diagram 5.1. In this case the system has six stationary solutions, two stable fixed points, a stable periodic orbit, an unstable fixed point, and two unstable periodic orbits. The solutions were started near the unstable fixed point and from two other points near the unstable periodic orbits. The output shows that the point near the unstable fixed point will be attracted to one of the stable fixed points, while the points near the unstable periodic orbits will be attracted to the stable periodic orbit in the system.

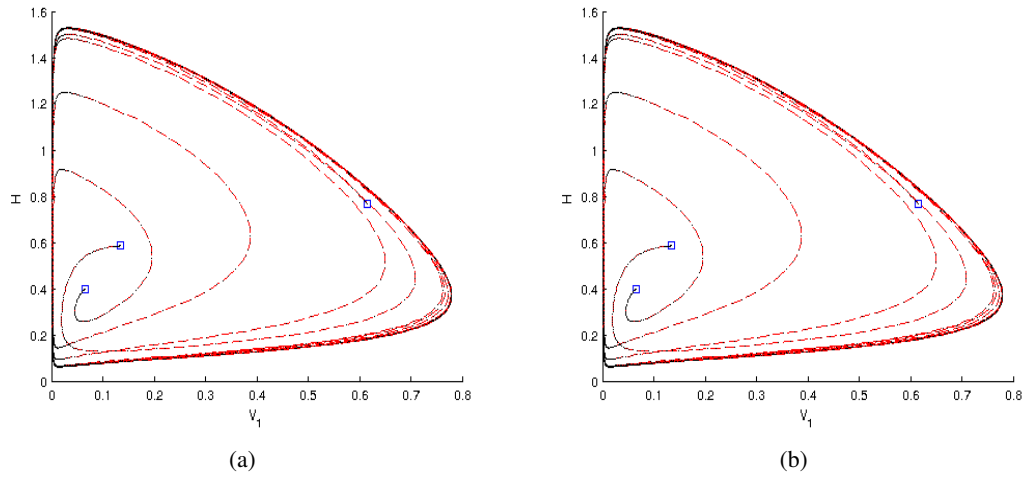


Figure 5.8: Phase plane corresponding to $\alpha_2 = 8.85714$ from the bifurcation diagram 5.1. The system in this case also contains six stationary solutions, two stable fixed points, a stable periodic orbit, an unstable fixed point, and two unstable periodic orbits. In these figures the initial solutions were started near the unstable stationary solutions and they are indicated by small squares. The output shows that all the solutions will be attracted to the stable periodic orbit.

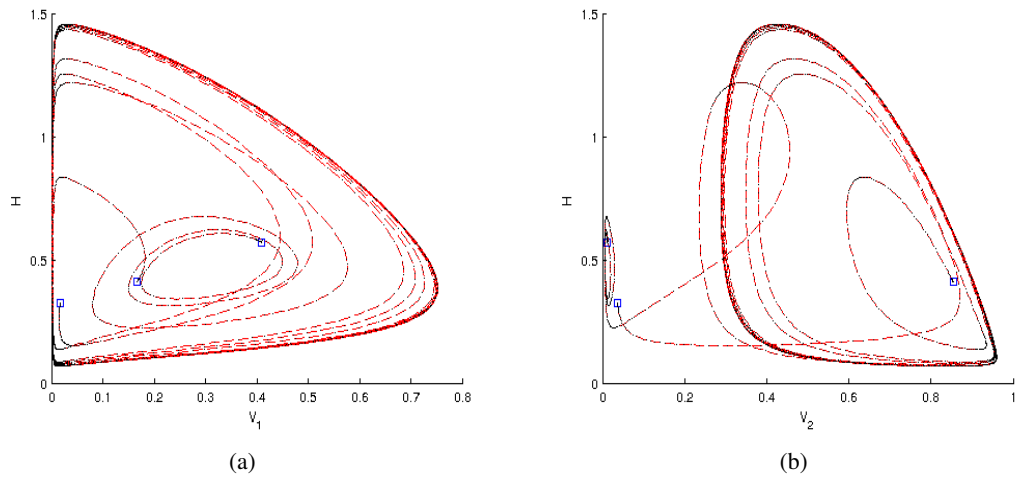


Figure 5.9: Phase plane corresponding to $\alpha_2 = 10.2143$ from the bifurcation diagram 5.1. In this case the system has five stationary solutions, a stable fixed point, two unstable fixed points, a stable periodic orbit, and an unstable periodic orbit. The solutions were started near the two unstable fixed points and from a point near the unstable periodic orbit. The output shows that all these solutions will be attracted to the single stable periodic orbit in the system.

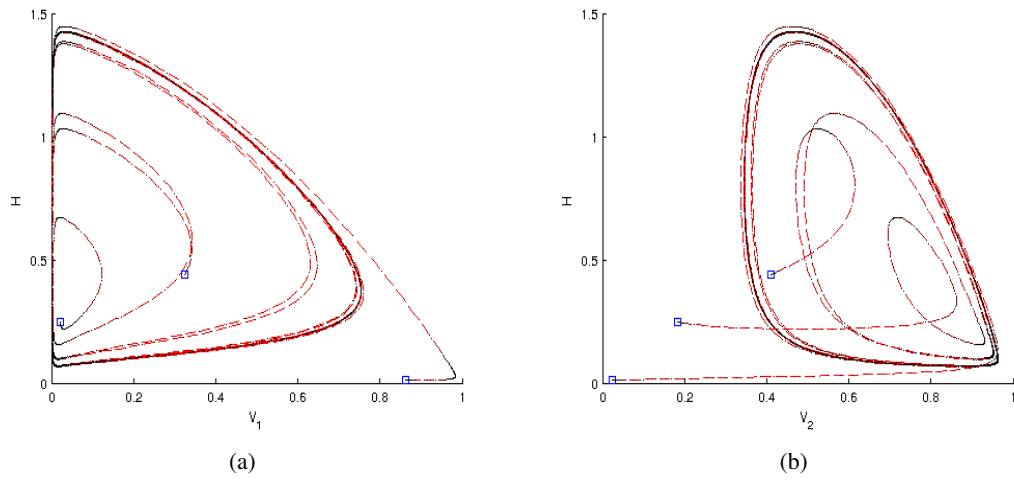


Figure 5.10: Phase plane corresponding to $\alpha_2 = 10.8929$ from the bifurcation diagram 5.1. The system in this case has four stationary solutions, three unstable fixed points, and a single stable periodic orbit. We started the solution from three points (indicated by small squares) near the unstable fixed points. The output shows that the solutions will be attracted to the single stable periodic orbit in the system.

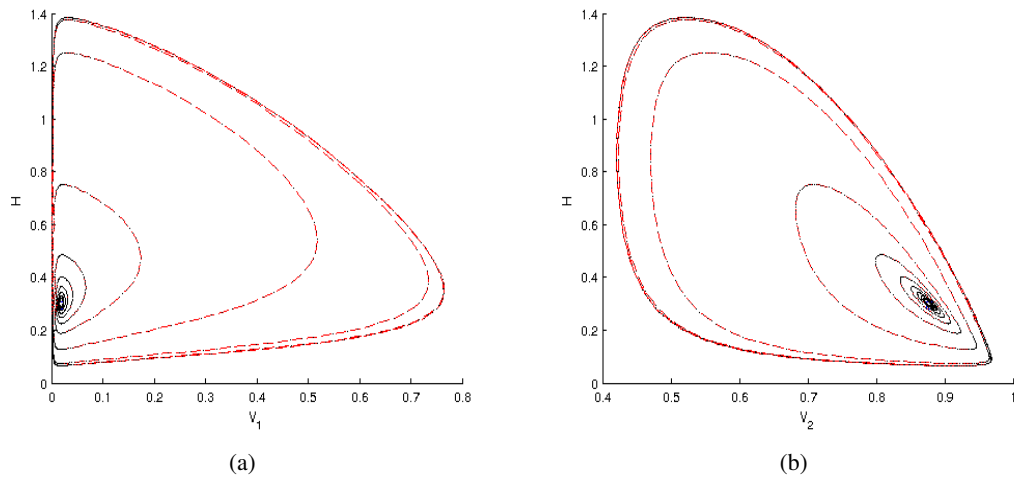


Figure 5.11: Phase plane corresponding to $\alpha_2 = 12$ from the bifurcation diagram 5.1. The system in this case contains two stationary solutions, an unstable fixed point and a stable periodic orbit. The solution were started from a point (indicated by small square) near the unstable fixed point. The stable periodic orbit attract the solution.

5.2 Methods

In the following sections we will use the Conley Index theory (Conley [1978]; Mischaikow [1999]; Mischaikow and Mrozek [2002]) and Morse Decomposition theorem to study the qualitative behavior of the reduced two-patch model shown in Figure 5.1. The work will be organized as follows. First we define an isolating invariant set S_μ , then decompose S_μ into smaller isolating invariant sets $\mathcal{M}(S_\mu)$. By assigning a partial order to each of the $\mathcal{M}(S_\mu)$, we obtain what is called the Morse decomposition. Conley index is a topological index that classifies the behavior of each of the Morse set by measuring how the trajectories leave and enter a small neighborhood of $\mathcal{M}(S_\mu)$. After determining the Conley indices, we compute what is called the homological Conley index for each Morse set. Then, we find the trajectories connecting Morse sets using what is called the ‘‘Connection Matrices’’ (Franzosa [1989]). Finally, we will find the connecting orbits between different Morse decompositions using the ‘‘transition matrices’’ (Franzosa and Mischaikow [1998]; McCord and Mischaikow [1992]).

We start briefly with theoretical background by reviewing some basic definitions from the dynamical systems, Morse decomposition theory and Conley index theory.

Let X be a compact metric space.

Definition 5.1 (Schneider and Barker [1973]).

The relation \sim is an equivalence relation if

- (i) *For all $x \in X$, $x \sim x$ (reflexivity).*
- (ii) *If $x \sim y$, then $y \sim x$ (symmetry).*
- (iii) *If $x \sim y$ and $y \sim z$, then $x \sim z$ (transitivity).*

The class of all elements equivalent to x is called the equivalence class of x .

Definition 5.2.

Let $\Lambda \subset \mathbb{R}^n$ be open. A map $\phi : \mathbb{R} \times X \times \Lambda \rightarrow X$ is said to be a Λ -parameterized flow if

- *ϕ is continuous.*
- *The restriction map $\phi_\mu : \mathbb{R} \times X \rightarrow X$ is a continuous flow for all $\mu \in \Lambda$.*

Definition 5.3.

The ω -limit set and the α -limit set of a subset $Y \subset X$ under a flow ϕ is defined as the following:

$$\omega(Y, \phi) := \bigcap_{t>0} cl(\phi([t, \infty), Y))$$

$$\alpha(Y, \phi) := \bigcap_{t>0} cl(\phi(-\infty, -t], Y).$$

5.2.1 Isolating invariant sets

The following definitions are important in the Morse decompositions and Conley index theorems.

Definition 5.4 (Mischaikow and Mrozek [2002]).

Let $N \subset \mathbb{R}^n$. Then $Inv(N, \phi) = \{x \in N | \phi(x, t) \in N; \forall t \in \mathbb{R}\}$ is referred to as the maximal invariant set in N .

Definition 5.5 (Isolating Neighborhood, Mischaikow and Mrozek [2002]).

A compact set $S \subset \mathbb{R}^n$ is an isolating neighborhood if $Inv(N, \phi) = S \subset Int(N)$, where $Int(N)$ denotes the interior of N .

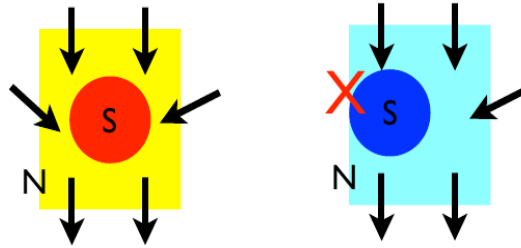


Figure 5.12: N : an isolating neighborhood of S

Next we define the neighborhood of an invariant set S that contains no other invariant sets. This is important because, to capture the flow near S , it is important to examine the flow in the small neighborhoods of S .

Definition 5.6 (Isolating Invariant Set, Mischaikow and Mrozek [2002]).

An isolating invariant set is a compact set S , for which there exists an isolating neighborhood N such that $S = Inv(N) \subset Int(N)$.

In other words, S is an isolating invariant set means that every trajectory that remains close to S belongs to S .

Hence isolating neighborhoods are robust with respect to perturbations, i.e. they persist or continue as the parameter changes, we need to formalize the notion of continuation.

Definition 5.7.

Let $N \subset X$ be compact, consider a parameterized flow $\phi : \mathbb{R} \times X \times \Lambda \rightarrow X$. Suppose $S_\mu = \text{Inv}(N, \phi_\mu)$. Then S_{μ_0} continues to S_{μ_1} if there exists a simply connected set $U \in \Lambda$ that contains μ_0 and μ_1 such that N is isolating for each $\mu \in U$.

In the following section, we introduce the Morse sets and Morse decompositions, then we define our Morse sets and Morse decompositions from the bifurcation diagram 5.1.

5.2.2 Morse decompositions

First we will give the definition of the partial order.

Definition 5.8 (Mischaikow and Mrozek [2002]).

A relation $>$ on a set P is called a partial order if it satisfies:

- (i) $p > p$ not true for any $p \in P$ (Strictness).
- (ii) $q > p$ and $r > q$ implies $r > p$ for all $p, q, r \in Q$ (Transitivity).

In addition, if $>$ satisfies

- (iii) for all $p, q \in P$, either $p > q$ or $q > p$

then the partial order called a total order.

Let $(P, >)$ denote the partially ordered set (or poset). The following is the definition of the Morse decompositions.

Definition 5.9 (Mischaikow and Mrozek [2002]).

Let S be an isolating invariant set. Let

$$\mathcal{M}(S) = \{M(p) \subset S \mid p \in P\}$$

be a collection of disjoint isolating invariant sets indexed by P . $\mathcal{M}(S)$ is a Morse decomposition of S if there exists a partial ordering $>$ on the indexing set P such that for all $x \in S \setminus \bigcup_{p \in P} M(p)$ there exist $p, q \in P$ such that $q > p$ and $\omega(x) \in M(q)$ and $\alpha(x) \in M(p)$.

Each $M(p)$ is referred to as a Morse set. Any partial ordering on P that satisfies the above condition is said to be an *admissible partial ordering*.

Let S_{μ_1} be an isolating invariant set for the flow ϕ_{μ_1} , $S_{\mu_1} = \text{Inv}(N, \mu_1)$, and let S_{μ_2} be an isolating invariant set for the flow ϕ_{μ_2} , $S_{\mu_2} = \text{Inv}(N, \mu_2)$. The following defines the continuation of Morse sets.

Definition 5.10 (Moeller [2005]).

Let $M(S_{\mu}) = \{M_{\mu}(p) | p \in P\}$ be a Morse decomposition for a parametrized flow ϕ_{μ} for each μ in the simply connected set $U \subset \Lambda$. A partial order “ $>$ ” on P is said to be continue over U if “ $>$ ” is admissible for each $\mu \in U$.

In other words, S_{μ_1} and S_{μ_2} are related by continuation. If $\mathcal{M}(S_{\mu_1}) = \{M_{\mu_1}(p) | p \in P\}$ and $M(S_{\mu_2}) = \{M_{\mu_2}(p) | p \in P\}$ are two Morse decompositions then M_{μ_1} continue to M_{μ_2} .

From the above definitions we note that Morse decomposition of a set S_{μ} is a collection of isolating invariant sets in S_{μ} , and each point in the set S_{μ} lies in a Morse set or on a trajectory connecting Morse sets.

Denote a stable fixed point by s , an unstable fixed point by u , an unstable periodic orbit by R and a stable periodic orbit by A .

From the bifurcation diagram 5.1 we have chosen ten values of the parameter α_2 , indicated by the vertical lines in Figure 5.13. For each α_2 , we labeled the sets of the stationary solutions and periodic orbits by M_{μ_i} , $i = 1, \dots, 10$, where each μ_i corresponds to a value of α_2 . Denote the set of equilibria corresponding to each μ_i by the following:

$$\begin{aligned} M_{\mu_1} &= \{u_1, A_1\}, M_{\mu_2} = \{s_1\}, M_{\mu_3} = \{s_2\}, M_{\mu_4} = \{u_2, s_3\}, \\ M_{\mu_5} &= \{u_3, R_1, s_4, s_5\}, M_{\mu_6} = \{u_4, R_2, R_3, s_6, s_7, A_2\}, \\ M_{\mu_7} &= \{u_5, R_4, R_5, s_8, s_9, A_3\}, M_{\mu_8} = \{u_6, u_7, R_6, s_{10}, A_4\}, \\ M_{\mu_9} &= \{u_8, u_9, u_{10}, A_5\}, \text{ and } M_{\mu_{10}} = \{u_{11}, A_6\}. \end{aligned} \tag{5.1}$$

In Figures 5.2-5.11, we used numerical simulations to show the long time dynamics by the system. In each of these figures, we started the simulations from points near the unstable stationary solutions (the unstable stationary solutions for each Morse set) that shown in Table 5.1, for each corresponding value of α_2 . From these simulation illustrations we are going to define the partial orders according to the flow direction. For example, if a trajectory starts at a point u and ends in a point s then we choose $u > s$.

In the following proposition we define partial orders for the sets $\mathcal{M}(S_{\mu_i}) = \{p | p \in P\}$.

Proposition 5.1.

The admissible partial orders $>_{\mu_i}$ for the sets $\mathcal{M}(S_{\mu_i}) = \{M_{\mu_i}(p) | p \in P\}$ are given by the following

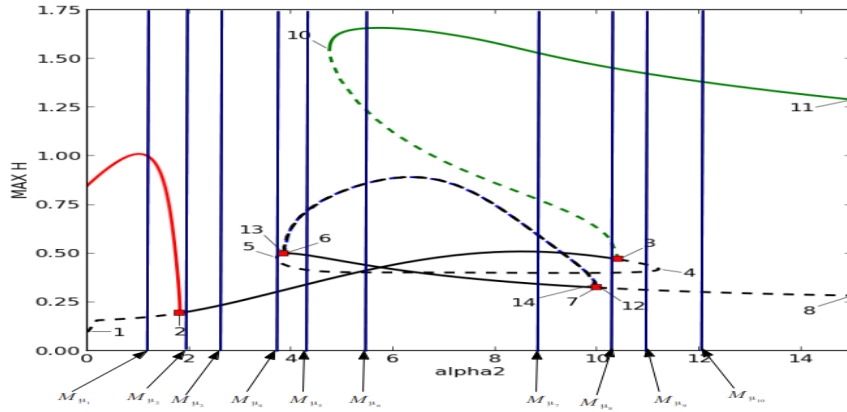


Figure 5.13: The Morse sets that obtained from the bifurcation diagram 5.1. Morse sets in this figure are labeled from M_{μ_1} to $M_{\mu_{10}}$ and each set consist of the stationary points that results from the intersection between the curves and the vertical lines.

(1) For $\alpha_2 = \mu_1$ we define $>_{\mu_1}$ by

$$u_1 >_{\mu_1} A_1.$$

(2) For $\alpha_2 = \mu_2$ and $\alpha_2 = \mu_3$ there are no partial orders to be defined,

(3) For $\alpha_2 = \mu_4$ we define $>_{\mu_4}$ by

$$u_2 >_{\mu_4} s_3.$$

(4) For $\alpha_2 = \mu_5$ we define $>_{\mu_5}$ by

$$u_3 >_{\mu_5} s_5, R_1 >_{\mu_5} s_5.$$

(5) For $\alpha_2 = \mu_6$ we define $>_{\mu_6}$ by

$$u_4 >_{\mu_6} s_6, R_2 >_{\mu_6} A_2, R_3 >_{\mu_6} A_2.$$

(6) For $\alpha_2 = \mu_7$ we define $>_{\mu_7}$ by

$$R_4 >_{\mu_7} A_3, R_5 >_{\mu_7} A_3, u_5 >_{\mu_7} A_3.$$

(7) For $\alpha_2 = \mu_8$ we define $>_{\mu_8}$ by

$$u_6 >_{\mu_8} A_4, u_7 >_{\mu_8} A_4, R_6 >_{\mu_8} A_4.$$

(8) For $\alpha_2 = \mu_9$ we define $>_{\mu_9}$ by

$$u_8 >_{\mu_9} A_5, u_9 >_{\mu_9} A_5, u_{10} >_{\mu_9} A_5.$$

(9) For $\alpha_2 = \mu_{10}$ we define $>_{\mu_{10}}$ by

$$u_{11} >_{\mu_{10}} A_6.$$

Proof:

From Definition (5.8) and from the numerical simulations 5.2-5.11 the proof is straight forward ■

As an obvious corollary, we have 10 Morse decompositions defined in the following proposition.

Proposition 5.2.

Consider the sets defined in (5.1) $\mathcal{M}(S_{\mu_i}) = \{M_{\mu_i}(p) \mid p \in P\}$, $i = 1, \dots, 10$ and consider the partial orders $>_{\mu_i}$, $i = 1, \dots, 10$ then, Morse decompositions are

$$\mathcal{M}(S_{\mu_i}) = \{M_{\mu_i}(p) \mid p \in (P_{\mu_i}, >_{\mu_i})\}, \quad i = 1, \dots, 10.$$

As we mentioned before, to understand the structure of the Morse decompositions we need to find the orbits connecting different Morse sets. The following is the definition of the connecting orbits between Morse sets.

Definition 5.11 (Moeller [2005]).

Given two Morse sets, $M_{\mu}(p)$ and $M_{\mu}(q)$, the set of connecting orbits between $M_{\mu}(p)$ and $M_{\mu}(q)$ in S_{μ} given by

$$C(M_{\mu}(q), M_{\mu}(p); S_{\mu}) := \{x \in S_{\mu} \mid \omega(x) \in M_{\mu}(p) \text{ and } \alpha(x) \in M_{\mu}(q)\}.$$

After establishing Morse decompositions from the bifurcation diagram 5.1, we need to look for the sets of connecting orbits between the different Morse sets. To do so, first for each element in the Morse sets $\{M_{\mu_i}(p) \mid p \in P\}$; $i = 1, \dots, 10$, we need to define a Conley index. Then, we need to find the possible connection matrices for the elements of each $\{M_{\mu_i}(p) \mid p \in P\}$.

5.2.3 Chain maps and graded modules braid

In this section we give some theoretical background about the chain maps and graded modules which are major principles in the Conley index theorem and the connection matrices.

Definition 5.12.

Let $n > 0$ be a natural number. The (geometric) n -simplex Δ^n is the space:

$$\Delta^n = \{((t_0, t_1, \dots, t_n) \in \mathbb{R}^{n+1} \mid t_i \geq 0, t_0 + t_1 + \dots + t_n = 1)\}$$

Definition 5.13.

Let X be a topological space.

- i) A singular n -simplex in X is a continuous map $\sigma : \Delta^n \rightarrow X$.
- ii) The singular n -chain group $C_n(X)$ is the free abelian group generated by the singular n -simplices in X . Its elements are called singular n -chains in X .

Definition 5.14 (Moeller [2005]).

Let $(P, >)$ be a poset. $I \subset P$ is said to be an interval if for r, p and q such that $p, q \in I$ and $r \in P$ with $q > r > p$ implies $r \in I$. Moreover, the set of intervals in P is denoted by $\mathcal{I}(P)$.

Definition 5.15 (Moeller [2005]).

Consider $I, J \in \mathcal{I}(P)$. I and J are said to be not comparable if for each $a \in I$ and $b \in J$ $a \not> b$ and $b \not> a$.

Denote the index filtration for the admissible ordering “ $>$ ” of M by \mathcal{N} , denote the set of all intervals in the partially ordered set of P by $\mathcal{I}(P, >)$,

Definition 5.16 (Moeller [2005]).

Let $I_i \in \mathcal{I}(P)$. The n -tuples of intervals in $(P, >)$ (denoted by $\mathcal{I}_n(P, >)$) is the ordered collection $(\mathcal{I}_2, \dots, \mathcal{I}_n)$ that satisfies

- (a) $\bigcup_{i=1}^n \mathcal{I}_i \in \mathcal{I}(P, >)$,
- (b) $p \in I_j, q \in I_k, j > k$ imply $p \not> q$.

If (IJ) is an adjacent pair (i.e., 2-tuple) intervals, then we set $IJ = I \cup J$. For more detail about index filtration see (Franzosa [1989]).

The boundary map (connection homomorphism) ∂_n defined by

$$\partial_n : C_n(M) \rightarrow C_{n-1}(M)$$

where $C_n(M)$ is an n -chain in M .

5. CHAIN MAPS AND GRADED MODULES BRAID

Definition 5.17.

Let C_n be an abelian group; then a simplicial chain complex is defined by the following:

$$\cdots \longrightarrow C_{n+1} \xrightarrow{\partial_{n+1}} C_n \xrightarrow{\partial_n} C_{n-1} \longrightarrow \cdots \longrightarrow C_1 \xrightarrow{\partial_1} C_0 \xrightarrow{\partial_0} 0.$$

Denote $C_n(J, G)$ by $C(J)$ for simpler notation.

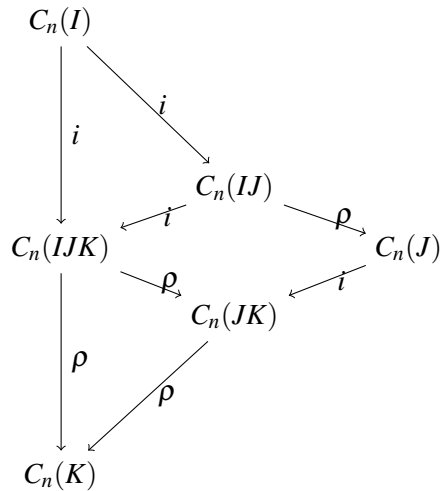
Definition 5.18 (Franzosa [1989]).

If $(I, J) \in \mathcal{S}_2(P, >)$, then the chain maps i, ρ are defined by

$$C(I) \xrightarrow{i(I,IJ)} C(IJ) \xrightarrow{\rho(IJ,J)} C(J)$$

with the following properties

- (i) $i(I, IJ)$ is injective and $\rho(IJ, J)i(I, IJ) = 0$,
- (ii) the chain map defined by $\rho(IJ, J), \rho : C(IJ)/\text{image}(i(I, IJ)) \rightarrow C(J)$ induces an isomorphism on homology,
- (iii) if I and J are noncomparable, then $\rho(IJ, J)i(I, IJ) = \text{id}|C(I)$,
- (iv) if $(I, J, K) \in \mathcal{S}_3(P, >)$, then braid diagram below, commutes.



The collection of the chain complex and chain maps is called the chain complex braid and denotes by $\mathcal{L}(\mathcal{N})$.

Definition 5.19.

5. CHAIN MAPS AND GRADED MODULES BRAID

A graded ring is a ring S together with a set of subgroups $S_d, i \geq 0$ such that

$$S = \bigoplus_{d \geq 0} S_d$$

is an abelian group, and $ab \in S_{i+j}$ for all $a \in S_i, b \in S_j$.

Definition 5.20.

If S is a graded ring, then a graded S -module (graded module) is an S -module M together with a set of subgroups $M_n, n \in \mathbb{Z}$ such that

$$M = \bigoplus_{n \in \mathbb{Z}} M_n$$

is an abelian group and $ab \in M_{i+j}$ for $a \in S_j, b \in M_i$.

The following is the definition of graded module braid.

Definition 5.21 (Franzosa [1988]).

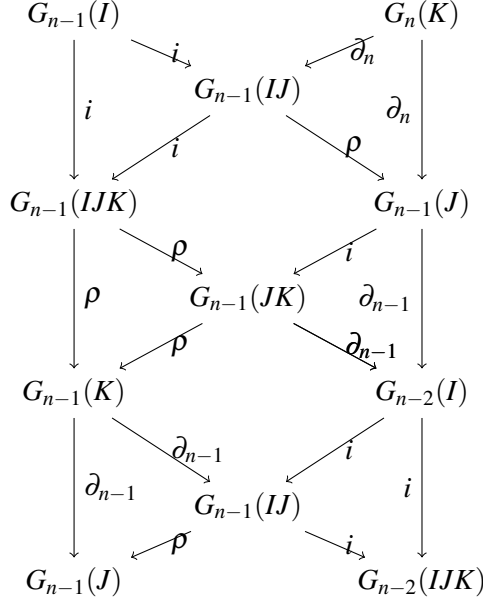
A graded module braid over $>$ is a collection of graded modules $\mathcal{G} = \mathcal{G}(>)$ and maps between the graded modules satisfying:

- 1- for each $\mathcal{I} \in \mathcal{I}(>, P)$ there is a graded module $G(I)$,
- 2- for each $(I, J) \in \mathcal{I}_2(P, >)$ there are maps

$$\begin{aligned} i(I, IJ) : G(I) &\longrightarrow G(IJ) \text{ of degree } 0, \\ \rho(IJ, I) : G(IJ) &\longrightarrow G(I) \text{ of degree } 0, \\ \partial(J, I) : G(J) &\longrightarrow G(I) \text{ of degree } -1 \end{aligned}$$

which satisfy

- (a) $\cdots \rightarrow G(I) \xrightarrow{i} G(IJ) \xrightarrow{\rho} G(I) \rightarrow \cdots$ is exact sequence,
- (b) if I and J are noncomparable, then $\rho(IJ, I)i(I, IJ) = \mathbf{id} \mid G(I)$,
- (c) if $(I, J, K) \in \mathcal{I}_3(P, >)$, then the following braid diagram commutes



In the following section we define the Conley index.

5.2.4 Conley index theory

The following definitions are necessary in defining the homology and Conley indices.

Definition 5.22 (Massey [1980]).

Let X be a topological space. Let $H_0(X), H_1(X), H_2(X), \dots$, be a sequence of abelian groups. For any continuous map $f : X \rightarrow Y$ define a sequence of homomorphisms f_* as follows

$$f_* : H_n(X) \rightarrow H_n(Y), \quad n = 0, 1, 2, \dots .$$

$H_n(X)$ is called the n -dimensional homology group of X , and f_* called the homomorphisms induced by f .

Let X be a topological space. Let

$$Z_n(X) = \text{Ker } \partial_n = \{u \in C_n(X) \mid \partial(u) = 0\} \quad (n > 0),$$

and

$$B_n(X) = \text{Image } \partial_{n+1} = \partial_{n+1}(C_{n+1}(X)) \quad (n \geq 0).$$

Then $H_n(X)$ can be defined by

$$H_n(X) = Z_n(X)/B_n(X), \quad \text{for } n > 0, \quad (5.2)$$

where Z_n/B_n is the quotient group defined by Z_n and B_n .

Definition 5.23 (Mischaikow and Mrozek [2002]).

A pointed space (Y, y_0) is a topological space Y with a distinguished point $y_0 \in Y$. Given a pair (N, L) of spaces with $L \subset N$,

$$N/L := (N/L \cup [L])$$

where $[L]$ denotes the equivalence class of points in L . N/L is usually use to denote the pointed space $(N/L, [L])$. The topology on $(N/L, [L])$ is defined as follows: a set $U \subset N \setminus L$ is open if U is open in N and $U \cap L = \emptyset$, or the set $(U \cap (N \setminus L)) \cup L$ is open in N . If $L = \emptyset$, then

$$(N/L, [L]) := (N \cup \{*\}, \{*\}),$$

where $\{*\}$ denotes the equivalence class consisting of the empty set.

The following is a definition of the index pair. This definition is important in defining homological Conley index.

Definition 5.24 (Mischaikow and Mrozek [2002]).

Let S be an isolating invariant set. A pair of compact sets (N, L) with $L \subset N$ is called an index pair for S if

- (1) $S = \text{Inv}(cl(N \setminus L))$ and $N \setminus L$ is an isolating neighborhood of S .
- (2) L is positively invariant in N , that is given $x \in L$ and $\phi([0, t], x) \subset N$, then $\phi([0, t], x) \subset L$.
- (3) L is an exit set for N , i.e. for a given $x \in N$ and $t_1 > 0$ such that $\phi(t_1, x) \in N$, then there exists $t_0 \in [0, t_1]$ for which $\phi([0, t_0], x) \subset N$ and $\phi(t_0, x) \in L$.

Theorem 3.5 in (Mischaikow [1989]) proves that if a set S is an isolating invariant set, then it has an index pair.

Now we are in a position to define the homological Conley index for an isolating invariant set.

Theorem 5.1 (Mischaikow and Mrozek [2002]).

Let (N, L) and (N', L') be index pairs for an isolating invariant set S . Then

$$(N/L, [L]) \sim (N'/L', [L']).$$

Definition 5.25 (Mischaikow and Mrozek [2002]).

Let S be an isolating invariant set with index pair (N, L) . The homological Conley index of S is defined by

$$CH_*(S) := H_*(N/L, [L]) \approx H_*(N, L). \quad (5.3)$$

Giving two sets related by continuation S_{μ_0} and S_{μ_1} , the following is the Conley continuation theorem.

Theorem 5.2 (Mischaikow and Mrozek [2002]).

Let S_{μ_0} and S_{μ_1} be isolating invariant sets related by continuation. Then

$$CH_*(S_{\mu_0}) \approx CH_*(S_{\mu_1}). \quad (5.4)$$

If x^* is a hyperbolic fixed point, the following theorem defines its homological Conley index.

Theorem 5.3 (Mischaikow and Mrozek [2002]).

Assume that x^* is a hyperbolic fixed point with an unstable manifold of dimension n . Then

$$CH_k(x^*) \approx \begin{cases} \mathbb{Z}_2 & \text{if } k = n \\ 0 & \text{otherwise.} \end{cases} \quad (5.5)$$

To find connection matrices for the Morse sets, we need to define what is called the attractor and the repeller sets and define their homological Conley indices.

Definition 5.26 (Moeller [2005]).

Given a compact invariant set, S , $\mathcal{A} \subset S$ is said to be an attractor if there is a neighborhood U of \mathcal{A} such that $\omega(U \cup S) = \mathcal{A}$. The dual repeller of \mathcal{A} in S is the compact set $\mathcal{R} = \{x \in S \mid \omega(x) \cap \mathcal{A} = \emptyset\}$. $(\mathcal{A}, \mathcal{R})$ refers to attractor-repeller pair for S .

The homological Conley index for a global attractor is defined in the following

Proposition 5.3 (Mischaikow and Mrozek [2002]).

If \mathcal{A} and \mathcal{R} are global attractor and repeller respectively for the dynamical system (X, ϕ) , then we

have

$$CH_k(\mathcal{A}) \approx \begin{cases} \mathbb{Z}_2 & \text{if } k = 1 \\ 0 & \text{if otherwise.} \end{cases} \quad (5.6)$$

$$CH_k(\mathcal{R}) \approx \begin{cases} \mathbb{Z}_2 & \text{if } k = 2 \\ 0 & \text{if otherwise.} \end{cases} \quad (5.7)$$

The following proposition defines the homological Conley index for each of our Morse sets using \mathbb{Z}_2 coefficients.

Proposition 5.4.

Given the Morse decomposition of Proposition 5.2, $\mathcal{M}(S_{\mu_i}) = \{M_{\mu_i}(p) \mid p \in (P_{\mu_i}, >_{\mu_i})\}$, $i = 1, \dots, 10$, then Conley index for each stable fixed point $s_i, i = 1, \dots, 10$, unstable fixed points $u_i, i = 1, \dots, 10$, stable periodic orbits $A_i, i = 1, \dots, 6$ and unstable periodic orbits $R_i, i = 1, \dots, 6$ as follows:

$$CH_k(s_i) = \begin{cases} \mathbb{Z}_2 & \text{if } k = 0 \\ 0 & \text{otherwise,} \end{cases}$$

$$CH_k(u_i) = \begin{cases} \mathbb{Z}_2 & \text{if } k = 1 \\ 0 & \text{otherwise,} \end{cases}$$

$$CH_k(A_i) = \begin{cases} \mathbb{Z}_2 & \text{if } k = 1 \\ 0 & \text{otherwise,} \end{cases}$$

and

$$CH_k(R_i) = \begin{cases} \mathbb{Z}_2 & \text{if } k = 2 \\ 0 & \text{otherwise.} \end{cases}$$

Proof:

The proof coming straight from the fact that stable hyperbolic fixed point s have zero dimensional unstable manifold, and the unstable hyperbolic fixed point u have one dimensional unstable manifold. Using the same arguments for the stable periodic orbit A and for the unstable periodic orbit R , we obtain the proof.

5.2.5 Connection matrices

The principle of connection matrices was first introduced by Conley in (Conley [1978]). These matrices give information about the existence of connecting orbits in a single flow (Morse decomposition).

First, we need to define what is called a long exact sequence of homological Conley indices for an index triple.

Definition 5.27 (Mischaikow and Mrozek [2002]).

Let M be an isolating invariant set and let $(\mathcal{A}, \mathcal{R})$ be an attractor repeller pair decomposition for M . An index triple for $(\mathcal{A}, \mathcal{R})$ is a collection of compact sets (N_2, N_1, N_0) where $N_0 \subset N_1 \subset N_2$ such that:

- (i) (N_2, N_0) is an index pair for M ,
- (ii) (N_2, N_1) is an index pair for \mathcal{R} ,
- (iii) (N_1, N_0) is an index pair for \mathcal{A} .

Let $C_n(N_i, N_j)$ denote the space of relative singular n -chains for (N_i, N_j) . Since $N_0 \subset N_1 \subset N_2$, we have the following short exact sequence

$$0 \rightarrow C_n(N_1, N_0) \rightarrow C_n(N_2, N_0) \rightarrow C_n(N_1, N_0) \rightarrow 0$$

and then its long exact sequence through homology is given by

$$\cdots \rightarrow H_n(N_1, N_0) \rightarrow H_n(N_2, N_0) \rightarrow H_n(N_1, N_0) \xrightarrow{\partial_n} H_{n-1}(N_2, N_1) \rightarrow \cdots$$

which is equivalent to

$$\cdots \rightarrow CH_n(\mathcal{A}) \rightarrow CH_n(M) \rightarrow CH_n(\mathcal{R}) \xrightarrow{\partial_n} CH_{n-1}(\mathcal{A}) \rightarrow \cdots$$

Let $C = \{C(p)\}_{p \in P}$ be a collection of graded modules. Mischaikow and Mrozek (Mischaikow and Mrozek [2002]) defined the following map Δ

$$\Delta : \bigoplus_{p \in P} CH_*(M(p)) \longrightarrow \bigoplus_{p \in P} CH_*(M(p)). \quad (5.8)$$

In matrix form, Δ can be written as the following

$$\Delta = [\Delta(p, q)]$$

where

$$\Delta(p, q) = CH_*(M(q)) \longrightarrow CH_*(M(p)).$$

The following is the definition of connection matrix.

Definition 5.28 (Connection Matrix, [Mischaikow \[1990\]](#)).

Δ is called connection matrix for the Morse set $\mathcal{M}(S)$ if the following properties satisfied

- (1) Δ is upper triangular.
- (2) $\Delta(p, q)(CH_k(M(p)) \subset CH_{k-1}(M(q)))$. (degree -1 map)
- (3) $\Delta^2 = 0$.
- (4) For every interval $I \in I(P, >)$

$$H_*\Delta(I) := \frac{Ker(\Delta(I))}{image(\Delta(I))} \approx CH_*(M(I))$$

. If $M(p)$ and $M(q)$ are a pair of Morse sets such that $(M(p), M(q)) \in \mathcal{I}_2(P, >)$, then

$$\Delta(pq) = \begin{bmatrix} 0 & \partial_*(M(p), M(q)) \\ 0 & 0 \end{bmatrix}.$$

The following theorem guarantees the existence of at least one connection matrix for a Morse decomposition.

Theorem 5.4 ([Franzosa \[1989\]](#)).

Given a Morse decomposition $\mathcal{M}(S)$ there exists at least one connection matrix.

Using the Morse decompositions defined in Proposition 5.2 and using the connection matrix Definition 5.28, we are able to compute connection matrices for each Morse set $M(S_{\mu_i})$.

Proposition 5.5.

There exist connection matrices for each of the Morse sets $\{M_{\mu_i}(p) | p \in P\}$.

Proof

For $\mathcal{M}(S_{\mu_1})$, the partial order is given by $u_1 >_{\mu_1} A_1$. Using the connection matrix defined in

5. CONNECTION MATRICES

Definition 5.28, we have

$$\Delta_{M_1} = \begin{matrix} & CH_0(A_1) & CH_1(u_1) \\ CH_0(A_1) & \begin{pmatrix} 0 & 1 \\ 0 & 0 \end{pmatrix} \\ CH_1(u_1) & \end{matrix} \quad (5.9)$$

For the Morse sets $\mathcal{M}(S_{\mu_2})$ and $M(S_{\mu_3})$, there are no partial orders defined for the flow in each set, so the only possible connection matrix is the zero matrix. For the Morse decompositions $\mathcal{M}(S_{\mu_4})$, from Proposition 5.1 we have the partial order $u_2 >_{\mu_4} s_3$, and hence a possible connection matrix is given by the following

$$\Delta_{M_4} = \begin{matrix} & CH_0(s_3) & CH_1(u_2) \\ CH_0(s_3) & \begin{pmatrix} 0 & 1 \\ 0 & 0 \end{pmatrix} \\ CH_1(u_2) & \end{matrix}. \quad (5.10)$$

For the Morse decomposition $\mathcal{M}(S_{\mu_5})$, the two possible partial orders that defined in Proposition 5.1 are $u_3 >_{\mu_5} s_5$ and $R_1 >_{\mu_5} s_5$. Using the definition of Δ in Definition 5.28 we have

$$\Delta_{M_5} = \begin{matrix} & CH_0(s_4) & CH_0(s_5) & CH_1(u_3) & CH_2(R_1) \\ CH_0(s_4) & \begin{pmatrix} 0 & 0 & 0 & 0 \\ 0 & 0 & 1 & 1 \\ 0 & 0 & 0 & 0 \\ 0 & 0 & 0 & 0 \end{pmatrix} \\ CH_0(s_5) & \\ CH_1(u_3) & \\ CH_2(R_1) & \end{matrix}. \quad (5.11)$$

For $\mathcal{M}(S_{\mu_6})$, the partial orders are defined by $u_4 >_{\mu_6} s_6$, $R_2 >_{\mu_6} A_2$ and $R_3 >_{\mu_6} A_2$. Then, from Proposition 5.1, we have

$$\Delta_{M_6} = \begin{matrix} & CH_0(s_6) & CH_0(s_7) & CH_0(A_2) & CH_1(u_4) & CH_2(R_2) & CH_2(R_3) \\ CH_0(s_6) & \begin{pmatrix} 0 & 0 & 0 & 1 & 0 & 0 \\ 0 & 0 & 0 & 0 & 0 & 0 \\ 0 & 0 & 0 & 0 & 1 & 1 \\ 0 & 0 & 0 & 0 & 0 & 0 \\ 0 & 0 & 0 & 0 & 0 & 0 \\ 0 & 0 & 0 & 0 & 0 & 0 \end{pmatrix} \\ CH_0(s_7) & \\ CH_0(A_2) & \\ CH_1(u_4) & \\ CH_2(R_2) & \\ CH_2(R_3) & \end{matrix}. \quad (5.12)$$

For the Morse set $\mathcal{M}(S_{\mu_7})$, we have the partial orders $R_4 >_{\mu_7} A_3$, $R_5 >_{\mu_7} A_3$ and $u_5 >_{\mu_7} A_3$. There-

5. CONNECTION MATRICES

fore, from the Proposition 5.28 we have

$$\Delta_{M_7} = \begin{array}{c} CH_0(s_8) \\ CH_0(s_9) \\ CH_0(A_3) \\ CH_1(u_5) \\ CH_2(R_4) \\ CH_2(R_5) \end{array} \begin{pmatrix} CH_0(s_8) & CH_0(s_9) & CH_0(A_3) & CH_1(u_5) & CH_2(R_4) & CH_2(R_5) \\ 0 & 0 & 0 & 0 & 0 & 0 \\ 0 & 0 & 0 & 0 & 0 & 0 \\ 0 & 0 & 0 & 1 & 1 & 1 \\ 0 & 0 & 0 & 0 & 0 & 0 \\ 0 & 0 & 0 & 0 & 0 & 0 \\ 0 & 0 & 0 & 0 & 0 & 0 \end{pmatrix}. \quad (5.13)$$

For the Morse decomposition $\mathcal{M}(S_{\mu_8})$, the orders defined in Proposition 5.1 are given by $u_6 >_{\mu_8} A_4$, $u_7 >_{\mu_8} A_4$ and $R_6 >_{\mu_8} A_4$. Using Definition 5.28, we have

$$\Delta_{M_8} = \begin{array}{c} CH_0(s_{10}) \\ CH_0(A_4) \\ CH_1(u_6) \\ CH_1(u_7) \\ CH_2(R_6) \end{array} \begin{pmatrix} CH_0(s_{10}) & CH_0(A_4) & CH_1(u_6) & CH_1(u_7) & CH_2(R_6) \\ 0 & 0 & 0 & 0 & 0 \\ 0 & 0 & 1 & 1 & 1 \\ 0 & 0 & 0 & 0 & 0 \\ 0 & 0 & 0 & 0 & 0 \\ 0 & 0 & 0 & 0 & 0 \end{pmatrix}. \quad (5.14)$$

For the Morse decomposition $\mathcal{M}(S_{\mu_8})$, Proposition 5.1 tells us that the partial orders are $u_8 >_{\mu_9} A_5$, $u_9 >_{\mu_9} A_5$ and $u_{10} >_{\mu_9} A_5$. From Proposition 5.28 we have $\Delta(A_5, u_8) = \partial(A_5, u_8) = 1$, $\Delta(A_5, u_9) = \partial(A_5, u_9) = 1$ and $\Delta(A_5, u_{10}) = \partial(A_5, u_{10}) = 1$. Therefore,

$$\Delta_{M_9} = \begin{array}{c} CH_0(A_5) \\ CH_1(u_8) \\ CH_1(u_9) \\ CH_1(u_{10}) \end{array} \begin{pmatrix} CH_0(A_5) & CH_1(u_8) & CH_1(u_9) & CH_1(u_{10}) \\ 0 & 1 & 1 & 1 \\ 0 & 0 & 0 & 0 \\ 0 & 0 & 0 & 0 \\ 0 & 0 & 0 & 0 \end{pmatrix}. \quad (5.15)$$

For the Morse decomposition $\mathcal{M}(S_{\mu_{10}})$, the only partial order is $u_{11} >_{\mu_{10}} A_6$. From Proposition 5.28 we have $\Delta(A_6, u_{11}) = \partial(A_6, u_{11}) = 1$. Hence, we have

$$\Delta_{M_{10}} = \begin{array}{c} CH_0(A_6) \\ CH_1(u_{11}) \end{array} \begin{pmatrix} CH_0(A_6) & CH_1(u_{11}) \\ 0 & 1 \\ 0 & 0 \end{pmatrix} \quad (5.16)$$

■

As we stated before, the connection matrix gives information about the existence of connecting orbits between the elements of a Morse set. To find connecting orbits between different Morse sets we need to define what is called "transition matrix". The following is a definition of the transition matrix between two different Morse sets.

Theorem 5.5 (Transition Matrix, [Mischaikow \[1989\]](#)).

Let $\mathcal{M}(S)$ and $\mathcal{M}(S')$ be isolating invariant sets related by continuation. If Δ_S and $\Delta_{S'}$ are connection matrices for Morse decompositions of $\mathcal{M}(S)$ and $\mathcal{M}(S')$ respectively, then there exists a matrix T consisting of degree-0 maps, such that $\Delta_S T + T \Delta_{S'} = 0$.

T is called the transition matrix (cf. [Conley \[1978\]](#); [Franzosa and Mischaikow \[1988, 1998\]](#); [Mischaikow \[1989\]](#)). This matrix gives information about the structure of orbits between different Morse sets.

Theorem 5.6 ([Mischaikow \[1990\]](#)).

Let the Morse set $\mathcal{M}(S_\mu)$ continue over an interval for the parameter μ as an attractor repeller, then $T(S_{\mu_1}, S_{\mu_0})$ is an isomorphism.

Let $\Delta^{1,0}$ denote the connection matrix for the Morse sets $\mathcal{M}(S_{\mu_0})$ and $\mathcal{M}(S_{\mu_1})$, then $\Delta^{1,0}$ with coefficients in \mathbb{Z}_2 is defined by the following

$$\Delta^{1,0} = \begin{bmatrix} \Delta_1 & T^{10} \\ 0 & \Delta_0 \end{bmatrix} \tag{5.17}$$

where Δ_0 and Δ_1 are the connection matrices for $\mathcal{M}(S_{\mu_0})$ and $\mathcal{M}(S_{\mu_1})$ respectively. T^{10} is the transition matrix that relate the Morse sets $\mathcal{M}(S_{\mu_0})$ and $\mathcal{M}(S_{\mu_1})$.

The transition matrix $T^{5,4}$ is given by the following

$$\Delta^{5,4} = \begin{matrix} & CH_0(s_4) & CH_0(s_5) & CH_1(u_3) & CH_2(R_1) & CH_2(s_3) & CH_2(u_2) \\ \begin{matrix} CH_0(s_4) \\ CH_0(s_5) \\ CH_1(u_3) \\ CH_2(R_1) \\ CH_2(s_3) \\ CH_2(u_2) \end{matrix} & \left(\begin{array}{cccccc} 0 & 0 & 0 & 0 & a & b \\ 0 & 0 & 1 & 1 & c & d \\ 0 & 0 & 0 & 0 & e & f \\ 0 & 0 & 0 & 0 & g & h \\ 0 & 0 & 0 & 0 & 0 & 1 \\ 0 & 0 & 0 & 0 & 0 & 0 \end{array} \right) \end{matrix}.$$

5. CONNECTION MATRICES

We only need to determine the values of a, b, c, d, e, f, g and h , which are the entries of the transition matrix $T^{5,4}$. Since $T^{5,4}$ is of degree -1 , we directly obtain that $b = 0, d = 0, e = 0$, and $g = 0$, and hence

$$T^{5,4} = \begin{pmatrix} a & 0 \\ c & 0 \\ 0 & f \\ 0 & h \end{pmatrix}.$$

From the definition of the connection matrix we have the property $\Delta^{5,4} \circ \Delta^{5,4} = 0$, and hence we have $a = 0$ and $f + h + c = 0$. Since the entries of the connection matrix are either 0 or 1, the only solution to the equation $f + h + c = 0$ is $f = h = c = 0$ and hence the matrix $\Delta^{5,4}$ becomes

$$\Delta^{5,4} = \begin{matrix} & CH_0(s_4) & CH_0(s_5) & CH_1(u_3) & CH_2(R_1) & CH_2(s_3) & CH_2(u_2) \\ \begin{matrix} CH_0(s_4) \\ CH_0(s_5) \\ CH_1(u_3) \\ CH_2(R_1) \\ CH_2(s_3) \\ CH_2(u_2) \end{matrix} & \begin{pmatrix} 0 & 0 & 0 & 0 & 0 & 0 \\ 0 & 0 & 1 & 1 & 0 & 0 \\ 0 & 0 & 0 & 0 & 0 & 0 \\ 0 & 0 & 0 & 0 & 0 & 0 \\ 0 & 0 & 0 & 0 & 0 & 1 \\ 0 & 0 & 0 & 0 & 0 & 0 \end{pmatrix} \end{matrix}.$$

This result shows that the Morse sets M_4 and M_5 , with the connection matrices defined by Δ_4 and Δ_5 , respectively, have no connection between them and the only possible transition matrix is the zero matrix.

Now, for the Morse sets M_5 and M_6 , we know that M_5 does not contain stable cycles, where M_6 has a unique stable limit cycle. We look for possible connections between the elements of M_5 and

M_6 . First we define the connection matrix $\Delta^{6,5}$ as the following

$$\Delta^{6,5} = \begin{pmatrix} 0 & 0 & 0 & 1 & 0 & 0 & a & b & c & d \\ 0 & 0 & 0 & 0 & 0 & 0 & a_1 & b_1 & c_1 & d_1 \\ 0 & 0 & 0 & 0 & 1 & 1 & a_2 & b_2 & c_2 & d_2 \\ 0 & 0 & 0 & 0 & 0 & 0 & a_3 & b_3 & c_3 & d_3 \\ 0 & 0 & 0 & 0 & 0 & 0 & a_4 & b_4 & c_4 & d_4 \\ 0 & 0 & 0 & 0 & 0 & 0 & a_5 & b_5 & c_5 & d_5 \\ 0 & 0 & 0 & 0 & 0 & 0 & 0 & 0 & 0 & 0 \\ 0 & 0 & 0 & 0 & 0 & 0 & 0 & 0 & 1 & 1 \\ 0 & 0 & 0 & 0 & 0 & 0 & 0 & 0 & 0 & 0 \\ 0 & 0 & 0 & 0 & 0 & 0 & 0 & 0 & 0 & 0 \end{pmatrix}$$

To find $\Delta^{6,5}$ we only need to determine the entries of the transition matrix T^{65} . Since T^{65} is of degree -1 , then

$$T^{65} = \begin{pmatrix} a & b & 0 & 0 \\ a_1 & b_1 & 0 & 0 \\ 0 & b_2 & 0 & 0 \\ a_3 & b_3 & c_3 & 0 \\ 0 & 0 & 0 & d_4 \\ 0 & 0 & 0 & d_5 \end{pmatrix}.$$

From the property that $(\Delta^{6,5})^2 = 0$, we obtain that $a_3 = 0$, $b_1 = 0$ and $b_3 = 0$ and the following equalities

$$\begin{aligned} c_3 + b &= 0, \\ c_3 + b_2 &= 0, \\ d_4 + d_5 + b_2 &= 0. \end{aligned}$$

Since the entries of $\Delta^{6,5}$ are either 0 and 1, we immediately obtain that $c_3 = b = b_2 = d_4 = d_5 = 0$.

Therefore,

$$T^{65} = \begin{pmatrix} a & 0 & 0 & 0 \\ a_1 & 0 & 0 & 0 \\ 0 & 0 & 0 & 0 \\ 0 & 0 & 0 & 0 \\ 0 & 0 & 0 & 0 \\ 0 & 0 & 0 & 0 \end{pmatrix}.$$

To determine the values of a and a_1 , we consider the properties of the flow over the interval $\mu_5 \leq \alpha_2 \leq \mu_6$. We argue that s_4 continues over this interval as an attractor, and hence we have $a = 1$. Using the same arguments, s_5 also continues as an attractor over the interval $\mu_5 \leq \alpha_2 \leq \mu_6$, and hence $a_1 = 1$.

This concludes that the transition matrix T^{65} for the Morse sets M_5 and M_6 is given by

$$T^{65} = \begin{pmatrix} 1 & 0 & 0 & 0 \\ 1 & 0 & 0 & 0 \\ 0 & 0 & 0 & 0 \\ 0 & 0 & 0 & 0 \\ 0 & 0 & 0 & 0 \\ 0 & 0 & 0 & 0 \end{pmatrix}.$$

5.3 Conclusions

In this chapter, we have proved that the bifurcation diagrams of Chapter 4 were correct, using the Morse decomposition and the Conley index theory. The connection matrices that we have obtained provided results aided the numerical simulations 5.2, 5.3, 5.4, 5.5, 5.6, 5.7, 5.8, 5.9, 5.10 and 5.11. The connection matrices that we have obtained provided results aided the numerical simulations. By providing the transition matrices $T^{4,5}$ and $T^{5,6}$ we proved that there are no connections between the Morse sets $\mathcal{M}(S_{\mu_4})$ and $\mathcal{M}(S_{\mu_5})$ and between $\mathcal{M}(S_{\mu_5})$ and $\mathcal{M}(S_{\mu_6})$. Note that, the set $\mathcal{M}(S_{\mu_4})$ corresponds to a value of α_2 where the system has no closed orbits and $\mathcal{M}(S_{\mu_5})$ correspond to an α_2 value when the system has fixed points and unstable closed orbits.

These results confirm that, given the connection matrices $\Delta_{M_4}, \Delta_{M_5}$ and Δ_{M_6} , the bifurcation diagram 5.1 for the reduced two-patch model (4.10) is the only possible diagram for the given set of parameters shown in Table 4.1. Therefore, for the values of α_2 where the system has no cycles, the results obtained in this chapter prove that the bifurcation diagrams of Chapter 4 are correct.

5. CONNECTION MATRICES

Note that the connection matrix for a given Morse set is not unique, unless the only possible matrix is the zero matrix. Here in this chapter, we only computed a single connection matrix for each of the Morse sets. One can compute other possible connection matrices and then explore the possibility of the existence of transition matrices different from what we have obtained. To do that is beyond the scope of this thesis.

Chapter 6

Two-patch model in a seasonal environment

6.1 Introduction

It has long been recognized that rainfall is an important factor that influences plant growth in savanna environments. The vegetation growth occurs when the soil is sufficiently moist from rainfall and stored moisture, and ceases when the soil becomes dry ([Owen-Smith \[2002a\]](#)). In most savanna systems, rainfall occurs seasonally and, as a consequence, the vegetation growth occurs seasonally in the places where the growth depends on the water from rainfall. Therefore, in the modelling of the vegetation growth, it is essential to include rainfall and soil moisture as factors that alter the vegetation growth.

The actual processes of the vegetation growth and the changes in the soil moisture depends on many factors, for examples such as atmospheric factors (temperature, humidity, sun light, etc.), soil profiles (slope, saturation, depth, etc.), and vegetation cover, etc. Hence, it is difficult to include all these factors and incorporate them in one model to study these processes. Making simplified assumptions will allow us to model vegetation growth as a function of soil moisture.

In this chapter we attempt to consider a seasonal two-patch model, where the vegetation growth depends on the daily rainfall using assumptions from Richardson and Hahn's model ([Richardson and Hahn \[2007\]](#)). The proposed model assumes that the water is only available to the vegetation roots in two soil layers. Moreover, the soil moisture in these two layers change through precipitation, evaporation, vegetation, and soil properties (loss by deep percolation and by surface drainage). The model will not address the feedback processes associated with soil moisture dynamics (the movement of water), and atmospheric factors such as temperature and humidity. By considering

the assumptions from the two-patch model (2.5) regarding the changes in animal densities on each patch due to growth, death and migrations, and using some simplified assumptions from (Richardson and Hahn [2007]), we construct a simple two-patch model describes the changes in the soil moisture in the two layers, and the corresponding changes in the vegetation growth, herbivore utilization and senescence.

The proposed seasonal model for the changes in vegetation biomasses on each patch consist of two sub-models, the first sub-model describes the changes in the soil moisture (rainfall, run-off, infiltration, drainage, evaporation and transpiration), while the second sub-model consider the changes in the vegetation biomass (live vegetation and dead vegetation) and the changes in the herbivore biomass.

6.2 Soil moisture model background

Dye (Dye [1984]) presented a model for the vegetation growth as a function of rainfall and soil moisture. Later, Richardson and Hahn reformulated his model using differential equations to model soil moisture, grass growth, and animal intake (Richardson and Hahn [2007]). In this model, a daily rainfall is an input, furthermore, the daily rainfall was partitioned into run-off and infiltration. Richardson and Hahn (Richardson and Hahn [2007]), assumed that the growth of the vegetation components is affected by soil moisture, where soil moisture is partitioned into three horizons A , B , C , and evaporation and transpiration remove water from different horizons.

In the following sections, we describe two sub models, based on some modified assumptions from Richardson and Hahn's model (Richardson and Hahn [2007]), to model a seasonal vegetation growth in a two patches environment. The first sub-model is concerned with the changes in the soil moisture in two horizontal layers and the second sub-model associated with the changes in vegetation biomasses (green vegetation and dry vegetation).

6.3 Model formulations

Assume that there are two discrete patches of vegetation, inhabited by a single herbivore species. After rainfall, we assume that the water is either run-off (by surface drainage) or infiltrate to the soil and stored in two horizontal layers A and B , that are accessible to the vegetation roots. The layers A and B have maximum capacities w_{amax} and w_{bmax} , respectively. When the amount of water in the first layer A reaches its maximum capacity w_{amax} , then the water drains to the second layer B . After the second layer reaches its maximum capacity w_{bmax} , then water infiltrate deeper into the soil to

areas where it can not be reached by the vegetation roots. In order to examine spatial heterogeneity and its impact on the model species, we consider a difference in land structure between the two patches. We distinguish between the two patches by assuming that one patch is a run-on patch. In this case all water from the rainfall infiltrates into the soil and the run-off amount is zero. We further assume that the vegetation biomass is partitioned to live vegetation and dead vegetation. The growth of the live vegetation depends on the soil moisture, while the increment in the dead vegetation biomass results from the senescence of the green vegetation. The general structure of the model in a single patch is showed in Figure 6.1.

6.3.1 Soil moisture

In this section we describe the changes in the soil moisture as a function of rainfall, infiltration, deep drainage, evaporation and transpiration. Firstly, we assume that the water loss from the top layer is due to evaporation, drainage and transpiration, while the lost in the water in the layer B is due to transpiration and deep drainage. Rainfall, infiltration and runoff are assumed to be instantaneous events as these events are rapid compared to evaporation and transpiration.

The general feature of the model that describing the changes in the soil moisture is given by the following

$$\text{The soil moisture in } a = \text{Infiltration} - \text{Evaporation} - \text{Transpiration} - \text{Drainage}_a$$

$$\text{The soil moisture in } b = \text{Drainage}_a - \text{Transpiration} - \text{Drainage}_b.$$

6.3.1.1 Rainfall

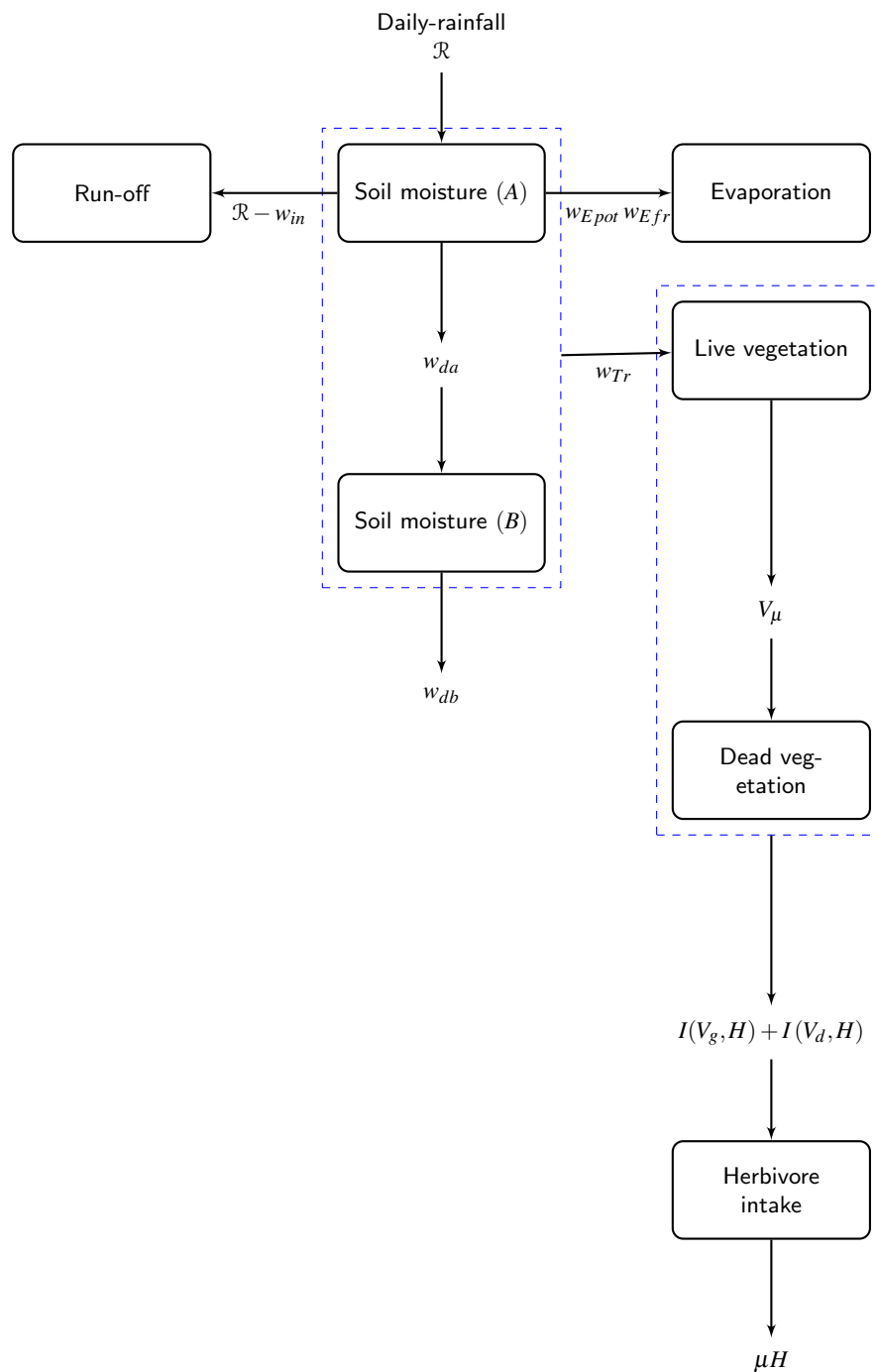
In our model we consider the occurrence of a daily rainfall during the wet season. To obtain a daily rainfall we will generate random daily rainfall \mathcal{R} , using some MATLAB built in functions.

6.3.1.2 Infiltration

In the run-on patch we assume that the amount of the surface drainage is zero, hence the water infiltration w_{in} is equal to the amount of water from the rainfall \mathcal{R} . For the run-off patch, Richardson and Hahn (Richardson and Hahn [2007]) assumed that, when the rainfall is less than 12mm , then the amount of water that infiltrates into the soil is equal to the amount of rainfall, otherwise they used a quadratic equation to describe the infiltration. The instantaneous change in water infiltration

6. SOIL MOISTURE

Figure 6.1: Schematic outline the seasonal model. The soil layers partitioned into two layers and the deep drainage. The water from rainfall infiltrate to the first layer, where the run-off and evaporate only remove water from this layer. Transpiration remove water from both layers. The vegetation roots reach the two top layers A and B . Vegetation biomass partitioned to green vegetation and dry vegetation. Herbivores consume from both types.



is given by the following

$$w_{in} = \begin{cases} \mathcal{R}, & \mathcal{R} < 12 \\ 1.05\mathcal{R} - 0.0054\mathcal{R}^2 - 0.4, & \mathcal{R} \geq 12. \end{cases} \quad (6.1)$$

We assume that the run-off amount is equal to the difference between the rainfall and the water infiltration, hence

$$\text{Run-off} = \mathcal{R} - w_{in}.$$

The values of water stores in each layer is calculated each day following a rainfall event as follows: The instantaneous change in the layer *A* due to infiltration and drainage is described by

$$w_a = w_{in} - w_{da}, \quad (6.2)$$

where w_{da} is the amount of water drained from the layer *A*.

For the layer *B* we have

$$w_b = w_{da} - w_{db}, \quad (6.3)$$

So, the amount of water on each layer at the beginning of each day is equals to the instantaneous amount plus the water from the previous day.

6.3.1.3 Evaporation

As we assumed before the evaporation will only remove water from the upper layer *A*. We further assume that the evaporation is affected by two main factors, the above ground vegetation cover and the water availability in the top soil layer.

The actual water evaporation is estimated as a function of the potential evaporation rate and the amount of water in the layer *A* as follows ([Richardson and Hahn \[2007\]](#))

$$w_E = w_{Efr} \times w_{Epot}, \quad (6.4)$$

where w_{Efr} is the fraction of the potential evaporation which is related to the amount of water stored in the surface layer w_a (see Appendix A for more detail), and w_{Epot} is the potential evaporation.

6.3.1.4 Transpiration

The rate of transpiration by the vegetation roots is a function of water availability in the layers that accessible to vegetation roots, and the green vegetation biomass (Dye [1984]). The rate of transpiration w_{Tr} can be estimated as the following

$$w_{Tr} = w_m \times w_{pTr} \times V_g \times w_{aEmax}$$

where w_m is the soil moisture index, V_g is the live vegetation biomass, w_{pTr} is the potential transpiration rate (see Appendix A for more detail), and w_{aEmax} is the maximum rate of evaporation.

The amount of water that is removed from each layer depends on the transpiration quantities, soil depth of each layer and the proportion of the accessible water in the horizons (Richardson and Hahn [2007]). Thus

$$w_{Tri} = w_{fi} \times w_{Tr}, \quad i = a, b, \quad (6.5)$$

where w_{fi} is the water available for the vegetation as a fraction of total storage.

The changes in the soil moisture in each horizon, due to evaporation and transpiration is described by the following differential equations

$$\begin{aligned} \frac{dw_a}{dt} &= w_a - w_{Tra} - w_E \\ \frac{dw_b}{dt} &= w_b - w_{Trb} \end{aligned} \quad (6.6)$$

In the following section we present a model that describes the changes in the vegetation biomass due to growth, senescence and grazing.

6.3.2 Vegetation growth

In the model, the vegetation biomass is partitioned into live (green) vegetation biomass and the dead (dry) vegetation biomass, where herbivore consumes from both vegetation types. The model describes the growth, utilization, senescence and decay in each category.

6.3.2.1 Green vegetation biomass

The changes in the green (live) vegetation biomass due to growth, senescence and grazing is described by the following differential equation

$$\frac{dV_g}{dt} = r_g V_g \left(1 - \frac{V_g}{K} \right) - \mu_g V_g - i_g \frac{(V_g - v_u)}{b_i + V_g - v_u} H, \quad (6.7)$$

6. SEASONAL TWO-PATCH MODEL

where K is the maximum live vegetation biomass, v_u is the ungrazable amount, i_g is the herbivore intake rate, b_i is the half saturation rate, μ_g is the death rate of green vegetation, and r_g is the growth rate of live vegetation and according to (Richardson and Hahn [2007]) it can be estimated as follows

$$r_g = k_s \times \delta w_{Tr} \times w_{Tr} \times r, \quad (6.8)$$

where r is the fractional growth rate, δw_{Tr} is the transpiration coefficient, k_s is the efficiency of synthesis of forage.

6.3.2.2 The changes in dry vegetation biomass

The increases in the dry vegetation biomass result from the green vegetation senescence, while it is decrease result from the removal through grazing and decay. Thus, the changes in the dead vegetation biomass is described by the following differential equation

$$\frac{dV_d}{dt} = \mu_g V_g - \mu_d V_d - I(V_d, H), \quad (6.9)$$

where μ_d is the decay rate in the dead vegetation biomass and $I(\mu_d, H)$ is the herbivore intake, in which

$$I(V_d, H) = i_d \frac{V_d H}{b_i + V_d}, \quad (6.10)$$

i_d is the herbivore intake rate from dry vegetation and b_i is the half saturation rate for eating.

6.4 The seasonal two-patch model

Now, we are in position to formulate a two-patch model in a seasonal environment, where the soil moisture is affected by a daily rainfall, evaporation, drainage and transpiration. The vegetation growth in turn depends on the soil moisture availability, and the changes in herbivore densities is according to the two-patch model (2.5).

Using the above assumptions, and considering the equations (6.6), (6.7), and (6.9), the two-patch

6. SEASONAL TWO-PATCH MODEL

herbivore/vegetation model in a seasonal patchy environment is given by the following system

$$\frac{dw_{a_i}}{dt} = w_{a_i} - w_{tra_i} - w_E \quad (6.11a)$$

$$\frac{dw_{b_i}}{dt} = w_{b_i} - w_{trb_i} \quad (6.11b)$$

$$\frac{dV_{g_i}}{dt} = r_{g_i} V_{g_i} \left(1 - \frac{V_{g_i}}{K}\right) - \mu_g V_{g_i} - i_g \frac{(V_{g_i} - v_u) H_i}{b_i + V_{g_i} - v_u} \quad (6.11c)$$

$$\frac{dV_{d_i}}{dt} = \mu_g V_{g_i} - \mu_d V_{d_i} - i_d \frac{V_{d_i} H_i}{b_i + V_{d_i}} \quad (6.11d)$$

$$\begin{aligned} \frac{dH_i}{dt} = & \left[c \left(i_g \frac{V_{g_i} - v_u}{b_g + V_{g_i} - v_u} + i_d \frac{V_{d_i}}{b_g + V_{d_i}} \right) - \bar{\mu} \right] H_i \\ & + \mathcal{L} \left[\frac{\alpha_j A_j H_j}{(1 + \bar{\beta}_j (V_{g_j} + V_{d_j})) A_i} - \frac{\alpha_i H_i}{1 + \bar{\beta}_i (V_{g_i} + V_{d_i})} \right]; i, j = 1, 2, \end{aligned} \quad (6.11e)$$

where c is the conversion rate from the consumed biomass into herbivore biomass, $\bar{\mu}$ is the herbivore death rate and \mathcal{L} is a constant to distinguish between the migration time scale and other demographic changes. The other parameters are as stated in Tables 2.1 and 4.1.

Consider the following change of variables

$$\tau = \frac{\varepsilon t}{r_g}, v_i = \frac{V_{g_i}}{K_i}, v_{d_i} = \frac{V_{d_i}}{K_i}, h_i = \frac{H_i}{K_i} \quad (6.12)$$

System (6.11) with the new variables (6.12) can be transform to the following system

$$\frac{d\bar{w}_{a_i}}{d\tau} = \varepsilon (\bar{w}_{a_i} - \bar{w}_{tra_i} - \bar{w}_E), \quad (6.13a)$$

$$\frac{d\bar{w}_{b_i}}{d\tau} = \varepsilon (\bar{w}_{b_i} - \bar{w}_{trb_i}), \quad (6.13b)$$

$$\frac{dv_i}{d\tau} = \varepsilon \left(v_i(1 - v_i) - \mu_{v_i} v_i - \eta_i \frac{(v_i - \rho_i) h_i}{1 + \gamma_i (v_i - \rho_i)} \right), \quad (6.13c)$$

$$\frac{dv_{d_i}}{d\tau} = \varepsilon \left(\mu_{v_i} v_i - \mu_{v_{d_i}} v_{d_i} - \bar{\eta} \frac{v_{d_i} h_i}{\gamma_i^{-1} + v_{d_i}} \right), \quad (6.13d)$$

$$\begin{aligned} \frac{dh_i}{d\tau} = & \varepsilon \left[\frac{\xi_i (v_i - \rho_i)}{1 + \bar{\gamma}_i (v_i - \rho_i)} + \frac{\bar{\xi}_i v_{d_i}}{\bar{\gamma}_i^{-1} + v_{d_i}} - \bar{\mu} \right] h_i \\ & + \left[\frac{\alpha_j \zeta_j h_j}{1 + \beta_j (v_j + v_{d_j})} - \frac{\alpha_i h_i}{1 + \beta_i (v_i + v_{d_i})} \right], \quad i, j = 1, 2 \end{aligned} \quad (6.13e)$$

where $\bar{w}_{a_i} = \frac{w_{a_i}}{r_g}$, $\bar{w}_{b_i} = \frac{w_{b_i}}{r_g}$, $\bar{w}_{tra_i} = \frac{w_{tra_i}}{r_g}$, $\bar{w}_E = \frac{w_E}{r_g}$, $\bar{w}_{trb_i} = \frac{w_{trb_i}}{r_g}$, $\eta_i = \frac{i_m K_i}{r_g b_i}$, $\bar{\eta} = \frac{i_d}{r_g}$, $\rho_i = \frac{v_u}{K_i}$, $\gamma_i = \frac{K_i}{b_i}$, $\mu_{v_i} = \frac{\mu_g}{r_g}$, $\xi_i = \frac{c i_g K_i v_{g_i}}{r_g b_g}$, $\bar{\xi}_i = \frac{c i_d}{r_g}$, $\beta_i = \bar{\beta}_i K_i$, and $\zeta_i = \frac{A_i K_i}{A_j K_{g_j}}$. For the description of the parameters see Tables 6.1, 6.2, and 6.3.

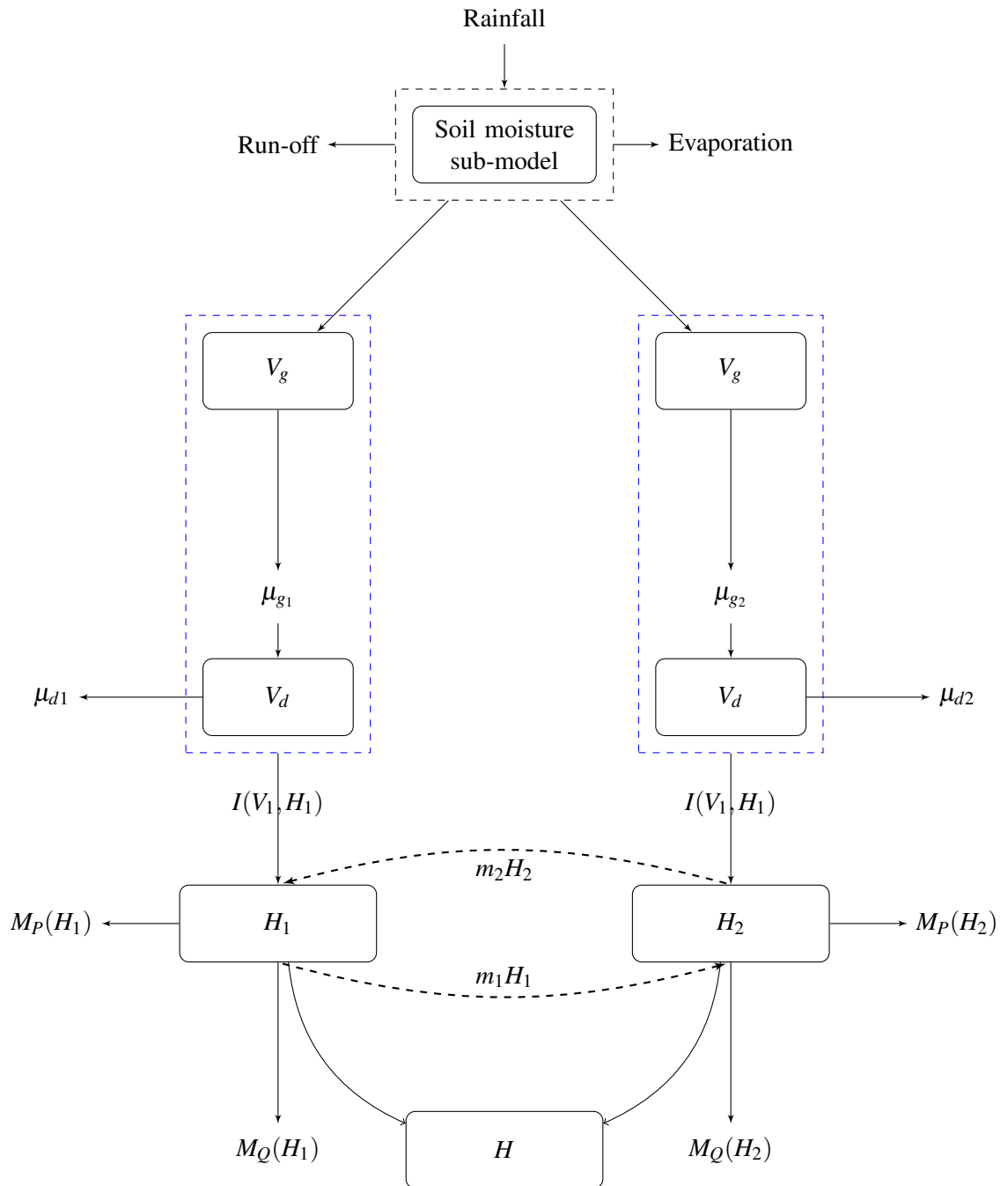


Figure 6.2: Diagram outline the two-patch model in a seasonal environment. The soil moisture sub model described with more detail in (6.1).

6. SEASONAL TWO-PATCH MODEL

Variable	Description	Unit
\mathcal{R}	Daily rainfall	mm
V_g	Live vegetation biomass (green)	kg/ha
V_d	Dead vegetation biomass (dry)	kg/ha
H	Herbivore biomass	kg/ha
w_{in}	Water infiltrating soil	mm/day
w_a	Water stored in layer a	mm
w_b	Water stored in layer b	mm
w_{da}	Water drained from the layer a	mm/day
w_{db}	Water drained from the layer b	mm/day
w_{tot}	The total amount of water stored in all horizons	mm/day
w_{Epot}	Potential water loss from soil by evaporation	mm/day
w_m	Soil moisture index for vegetation	–
w_{Efr}	Fraction of potential evaporation	–
w_E	Water lost from soil by evaporation	mm/day
$Days_{gra}$	Days since onset of growing season	kg /ha
k_s	Efficiency of synthesis of forage, guild	–
w_{Tr}	Transpiration coefficient for vegetation	–
wf_i	The water available for the vegetation as a fraction of total storage	–
w_{pTr}	Transpiration coefficient for guild	–
wfs_i	Water store i as % of effective depth of horizon	mm/day
w_{Tri}	Water transpired from layer $i = a, b$	mm/day
fr_v	Fraction of new growth of vegetation green	–
Fr_{dry}	The proportion of new growth of green vegetation	–
r_v	The fraction of the new growth of green vegetation	–
fr_v	The adjusted fraction allocated the green vegetation	–
Shoots	The above ground vegetation biomass	kg/ha

Table 6.1: Description of the variables in the seasonal two-patch model. The parameters are taken from (Richardson and Hahn [2007]).

Parameter	Description	Unit	Value
w_{amax}	Maximum water capacity of layer a	mm	10
w_{bmax}	Maximum water capacity of layer b	mm	15
w_{aEmax}	Maximum water capacity of layer b	mm	10
Sd_a	Soil depth of layer a	mm	35.2
Sd_b	Soil depth of layer b	mm	98.4
δw_{Tr}	Transpiration coefficient	–	1.8
μ_g	The death rate of live vegetation	day ⁻¹	0.001
μ_d	The death rate of dry vegetation	day ⁻¹	0.001

Table 6.2: Parameters value (Richardson and Hahn [2007])

6. SEASONAL TWO-PATCH MODEL

Parameter	Description	Value
K_{g_1} (vegetation carrying capacity of patch 1)		200
K_{g_2} (vegetation carrying capacity of patch 2)		150
η_1	$i_m K_{g_1} / (r_g b_i)$	18.1818
η_2	$i_m K_{g_2} / (r_g b_i)$	24.2424
ρ_1	v_u / K_{g_1}	0.001
ρ_2	v_u / K_{g_2}	0.003
γ_1	K_{g_1} / b_i	6
γ_2	K_{g_2} / b_i	8
μ_v	μ_g / r_g	—
μ_{v_d}	μ_d / r_g	—
ξ_1	$c_i K_{g_1} / r_g b_g$	5.1515
ξ_2	$c_i K_{g_2} / r_g b_g$	6.8687
ξ_i	$c_i d / r_g$	2.5758
β_1	$\beta_1 K_{g_1}$	40
β_2	$\beta_2 K_{g_2}$	20
ζ_1	$A_1 K_{g_1} / A_2 K_{g_2}$	1.5
ζ_2	$A_2 K_{g_2} / A_1 K_{g_1}$	0.6667
μ	$(m_p + q_s + q_0) / r_g$	0.3680
A_1 (patch 1 area)		100
A_2 (patch 2 area)		200

Table 6.3: Table represents the parameters value and the description of the non-dimensionlized seasonal two-patch model (6.13).

Looking at the two-patch model in a constant environment (2.5), and the two-patch model in a seasonal environment (6.13), one can see that the main difference between the two model is that the vegetation growth rate r in (2.5) is assumed to be constant, while in (6.13) the growth rate of the green vegetation r_g is assumed to be a time dependent and it depends on the seasonal rainfall and the soil moisture. From the mathematical point of view, the system of equations (2.5) is an autonomous system of perturbed differential equations, while system (6.13) is a nonautonomous system of perturbed differential equations, in the content of the time dependency of the rainfall. The mathematical analysis that were provided in Chapter 4 and Chapter 5, can not be applied directly to system (6.13) to study the dynamical behavior of the nonperturbed systems, and hence the suitable way for us to deal with (6.13) is to use numerical simulations.

6.5 Numerical simulations

The main objective of this section is to present some numerical illustrations to describe the dynamics of the seasonal two-patch model (6.13) for different values of the animal migration propensities.

As we stated in our assumptions for the seasonal two-patch model (6.13), the vegetation will only grow if there is enough amount of soil moisture that enabling the growth. We started the simulations at the middle of the growing season, assuming that the amount of the soil moisture is sufficient, and the above ground vegetation biomass is suitable to sustain animals growth.

To obtain a daily rainfall, first we partitioned the whole season into two equal intervals, six months as the raining season and the other six months as the dry season. We assume that the rainfall events only occur during the wet season, and each day of the wet season has the same probability that the rainfall can occur on that day. We used MATLAB to generate uniformly random numbers between 0 and the maximum anticipated precipitation (mm/day) during the wet season days, and we set the probability of raining to be zero during the dry season days.

The assumptions of the seasonal two-patch model stated that the change in the soil moisture due to the rainfall is an instantaneous event. We assume that patch 2 is the run-off patch and that is mean a portion of water from the rainfall will run off the patch, while in patch 1 we assume that there is no run off amount. Therefore, at the beginning of each day following a rainfall during the wet season, for patch 1 we directly added the water from the rainfall to the amount of the soil moisture on the patch, and for patch 2 we used the second equation in (6.1) to calculate the infiltration amount. The changes in the soil moisture due to evaporation and transpiration are described by the set of differential equations (6.13a) and (6.13b), and the detailed equations in Appendix B.

The parameter values for the numerical simulations of the seasonal two-patch model (6.13)

6. NUMERICAL SIMULATIONS

(except for the rainfall \mathcal{R}) are shown in Tables 6.2 and 6.3 and they were taken from (Richardson and Hahn [2007]) and (Owen-Smith [2004]). For the daily rainfall \mathcal{R} , we used the same generated data in all of our simulations (because here we are not interested in examining the effects of different rainfall patterns on the dynamics of the system).

We run the numerical simulations for two different values of ε , $\varepsilon = 0.01$ and 0.1 . This will allow us to examine the effects of the rapid migrations on the dynamics of the system. For each value of ε we obtained solutions for different values of migration propensity parameters α_1 and α_2 .

Firstly, in the case of the absence of migrations i.e. when $\alpha_1 = \alpha_2 = 0$, we started the solutions using the parameter values shown in Tables 6.2 and 6.3, and the output is shown in Figure 6.5. In these figures, the initial vegetation and the total herbivore biomasses were relatively low, and the output shows that the vegetation biomass density on patch 1 will increase faster than the vegetation biomass on patch 2. After a short period of time the vegetation biomass density reaches a high biomass and oscillate, and during this time the herbivore biomass increases and then stabilized at a high biomass. Note that the patch densities differ slightly. This result shows that the system has a global attractive cycle when there are no migrations.

Secondly, to examine the effects of different migration propensities on the dynamics of the two-patch model (6.13), we introduced different migration propensities to the system, and we obtained the Figures 6.6-6.9, using the same initial solutions, and using the parameter values shown in Tables 6.2 and 6.3. In each one of these outputs we used two different values for ε . For $\varepsilon = 0.01$ we obtained the figures that shown on the left columns, and in the figures in the right columns we set $\varepsilon = 0.1$.

For small migration propensities from patch 1 to patch 2, we obtained the outputs that are shown in Figures 6.6 and 6.7. Each row in these figures correspond to different values of α_1 and α_2 . In these cases, comparing the outputs to the case when there were no migrations (Figure 6.5), we observed that when the migrations are slow i.e. $\varepsilon = 0.1$ (the figures in the right column in Figures 6.6 and 6.7) the vegetation dynamics show a slightly difference, and the dynamics is almost the same as the dynamics in the case of no migrations (Figure 6.5). The total herbivore biomasses in these cases is higher than in the case when there were no migrations between the two-patches.

When the migrations are rapid, in our case when $\varepsilon = 0.01$, and when the migration propensities to leave patch 1 are small, we obtained the figures in the left columns and that are shown in Figures 6.6 and 6.7. In these figures, the dynamics is different from the dynamics that was produced in the two previous cases and that is when there were no migrations, and when the migrations were slow. The outputs show that for a short period of time the vegetation biomass on patch 1 increases and then decreases and, as the herbivore biomass decreases, the vegetation biomass start to increase again

6. NUMERICAL SIMULATIONS

until it reaches a high level and then decreases again. After a long period of time (approximately 15 years) the vegetation biomass show stable periodic behavior with relatively high vegetation biomass. Note that the area of patch 1 is smaller than patch 2 area, $A_1 < A_2$, but patch 1 has larger carrying capacity than patch 2, $K_1 > K_2$. Also the soil moisture on patch 1 is also larger than the soil moisture on patch 2. For patch 2, the vegetation biomass increases and after a shorter period of time the biomass stabilizes periodically (see the graph on the left column in Figure 6.7). The total herbivore biomass shows different behavior when the migrations are rapid. In these cases, in a short period of time, the herbivore biomass increases and, as the vegetation biomass decreases, the herbivore biomass also decreases. When the vegetation biomass starts to increase, the herbivore biomass increases and after a period of time (approximately 15 years) the biomass stabilizes at a high level.

When we assumed that the animals have large propensities to leave patch 1, the outputs are shown in Figures 6.8 and 6.9. When $\varepsilon = 0.1$, the output is represented by the graphs on the right columns, and they show that the dynamics is similar to the dynamics of the case when there were no migrations. When $\varepsilon = 0.01$, the outputs are represented by the left columns in Figures 6.8 and 6.9. Comparing with the case of no migrations, the results show that when $\alpha_1 \geq \alpha_2$, the total herbivore biomass grows to higher densities. When $\alpha_1 = 0.8$ and $\alpha_2 = 0.5$ (Figure (a) in 6.8 and 6.9), and when $\alpha_1 = \alpha_2 = 0.7$ (Figure (c) in 6.8 and 6.9), the results show the vegetation dynamics on patch 1 have similar behavior, where as the vegetation biomass on patch 2 when $\alpha_1 = 0.8$ and $\alpha_2 = 0.5$ oscillates at a lower values than in the case when $\alpha_1 = \alpha_2 = 0.7$. When $\alpha_1 = 0.8, \alpha_2 = 0.5$ and when $\alpha_1 = 0.6$ and $\alpha_2 = 0.4$, the total herbivore biomass in these cases will grow faster than when $\alpha_1 = \alpha_2 = 0.7$ and in the three cases the total herbivore biomasses will stabilize at high values.

From the above results one can see that the dynamics of the seasonal two-patch model (6.13), with the set of the parameter values that are shown in Tables 6.2 and 6.3, is sensitive to rapid migrations and to the migration propensities α_1 and α_2 , and the later result is similar to what we had obtained from the analysis of the reduced two patch models (4.10) and (4.20) in Chapter 4.

We started the solutions from different initial conditions, with different sets of migration propensities, and when we set $\beta_1 = \beta_2 = 10$, and $\varepsilon = 0.01$, where the other parameter values are shown in Tables 6.2 and 6.3, we obtained the outputs that shown in Figures 6.10 and 6.11. In these cases the system shows different kind of behavior in the long time dynamics.

In Figure 6.10, we assumed that the propensity of leaving patch 1 is small, moreover we set $\alpha_1 \leq \alpha_2$. In figures (a) and (b), we started the simulations from a relatively low biomass density of vegetation on both patches with a high total animal biomass, and we assumed that there are no

6. NUMERICAL SIMULATIONS

migrations between the patches (i.e. $\alpha_1 = \alpha_2 = 0$). The output shows that the herbivore biomass will stabilize at a high biomass density in comparison to the vegetation biomass, and the vegetation biomass shows a stable oscillatory behavior (see the figures in the first row). This result is consistent with the long time behavior that is shown in Figure 6.6, in which the system has a global attractive cycle when there is no migrations between the patches.

When we choose $\alpha_1 = 0.4$, and $\alpha_2 = 0.4$, the outputs are shown in Figure (6.10) (c) and (d). In this case, the system has global stable cycle, with high animal biomass density.

In Figure 6.10 (e) and (f), we used $\alpha_1 = 0.4$ and $\alpha_2 = 0.7$, the system also has a global attractive cycle with high biomass density of vegetation and total herbivore biomass.

These results conclude that when the migration propensity of leaving patch 1 is small and $\alpha_1 \leq \alpha_2$, then the system has a stable limit cycle. Notice that $K_1 > K_2$ and $A_1 < A_2$.

For large α_1 and $\alpha_1 \geq \alpha_2$, the outputs are shown in Figure 6.11.

When $\alpha_1 = 0.8$ and $\alpha_2 = 0.5$, the outputs are shown in Figure 6.11 (a) and (b). The result shows that the system in this case has a stable limit cycle with 5 different frequencies, each of 2 years length, with a high total herbivore biomass and with a relatively high vegetation biomass.

When $\alpha_1 = \alpha_2 = 0.7$, in the along term the output shows that there is a stable limit cycle in the system (see Figure 6.11 (c) and (d)).

In Figure 6.11 (e) and (f), we used $\alpha_1 = 0.6$ and $\alpha_2 = 0.4$. The result shows that the system has a global attractive limit cycle with 5 different frequencies of 2 years length.

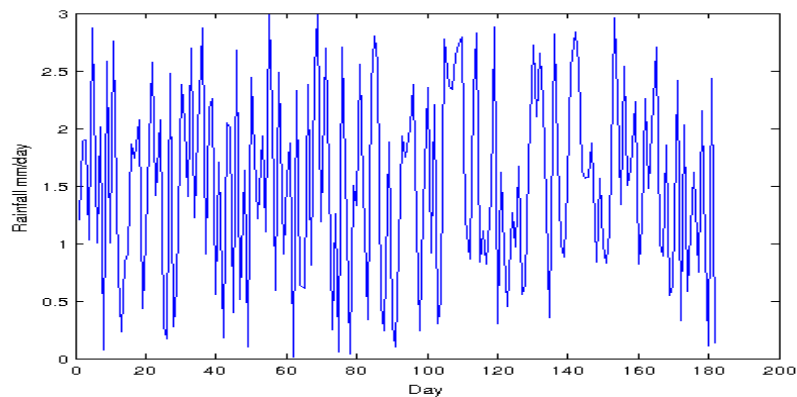
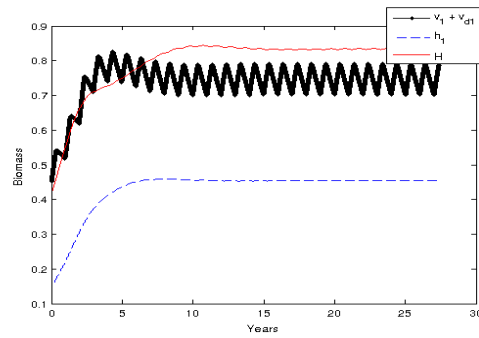
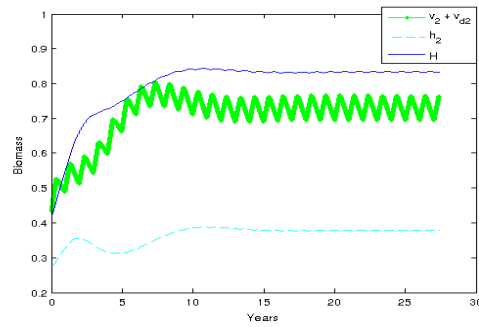


Figure 6.3: A sample of random daily rainfall showing the rainfall amount during the days of the raining season.

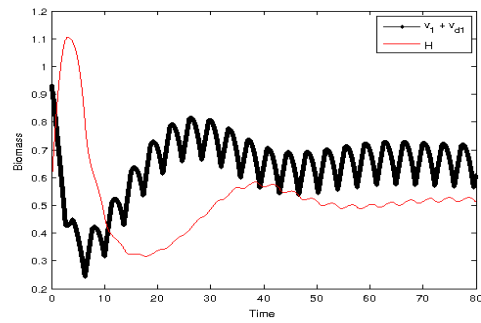


(a)

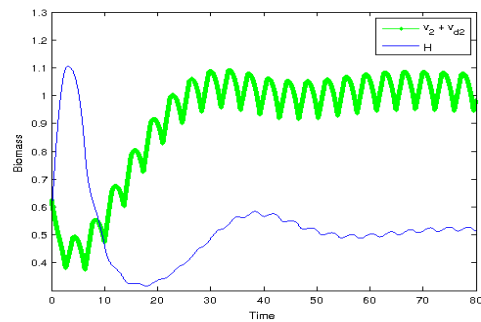


(b)

Figure 6.4: Numerical simulations for the seasonal two-patch model (6.13) when there are no migrations between the patches $\alpha_1 = \alpha_2 = 0$. The parameter values used are shown in Table 6.2 and Table 6.3. (a) patch 1 (b) patch 2. The initial points were $v_{g_1} + v_{d_1} = 0.46$, $v_{g_2} + v_{d_2} = 0.43$, $h_1 = 0.175$, $h_2 = 0.2667$ and $H = 0.42$.



(a)



(b)

Figure 6.5: Numerical simulation for the seasonal model (6.13) when we used a constant daily rainfall (the mean value of the generated data in Figure 6.3. The parameter values used are shown in Table 6.2 and Table 6.3. The initial values were $v_{g1} = 0.6$, $v_{g2} = 0.4$, $v_{d1} = 0.333$, $v_{d2} = 0.225$, $h_1 = 0.2667$, $h_2 = 0.0.3$ and $H = 0.42$.

6. NUMERICAL SIMULATIONS

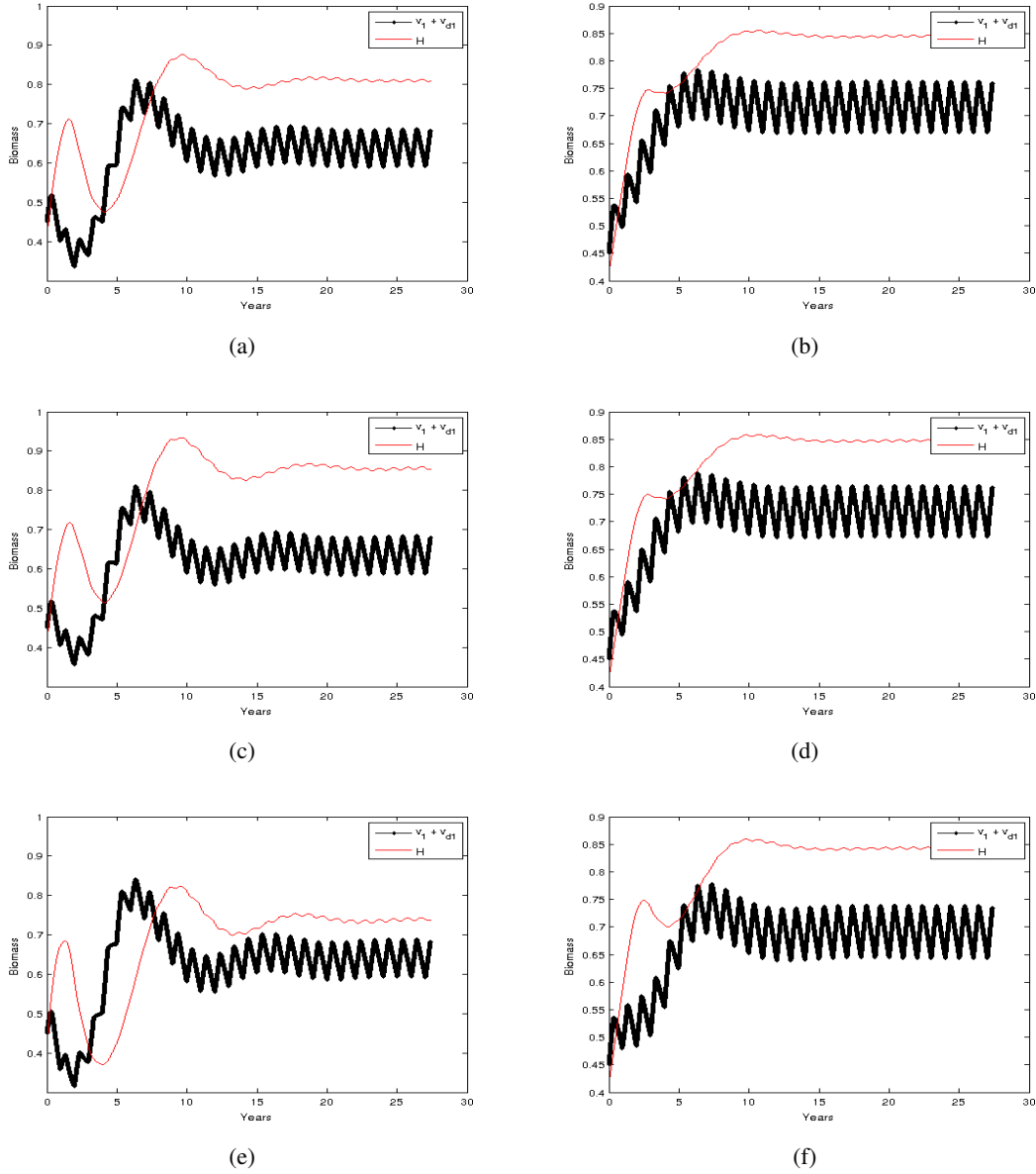


Figure 6.6: Numerical simulations for the seasonal two-patch model (6.13), showing the dynamics on patch 1. The parameter values used are shown in Table 6.2 and Table 6.3. In these simulations, the figures in the left column correspond to the solutions when $\varepsilon = 0.01$, where the figures in the right column correspond to $\varepsilon = 0.1$. In all these figures we used $\alpha_1 \leq \alpha_2$. The figures in each row associated with different values of α_1 and α_2 . Figures (a) and (b) correspond to $\alpha_1 = 0.3$ and $\alpha_2 = 0.4$. Figures (c) and (d) correspond to $\alpha_1 = \alpha_2 = 0.5$, while the figures (e) and (f) correspond to $\alpha_1 = 0.4$ and $\alpha_2 = 0.7$. The initial values were $v_{g_1} + v_{d_1} = 0.45$ and $H = 0.42$.

6. NUMERICAL SIMULATIONS

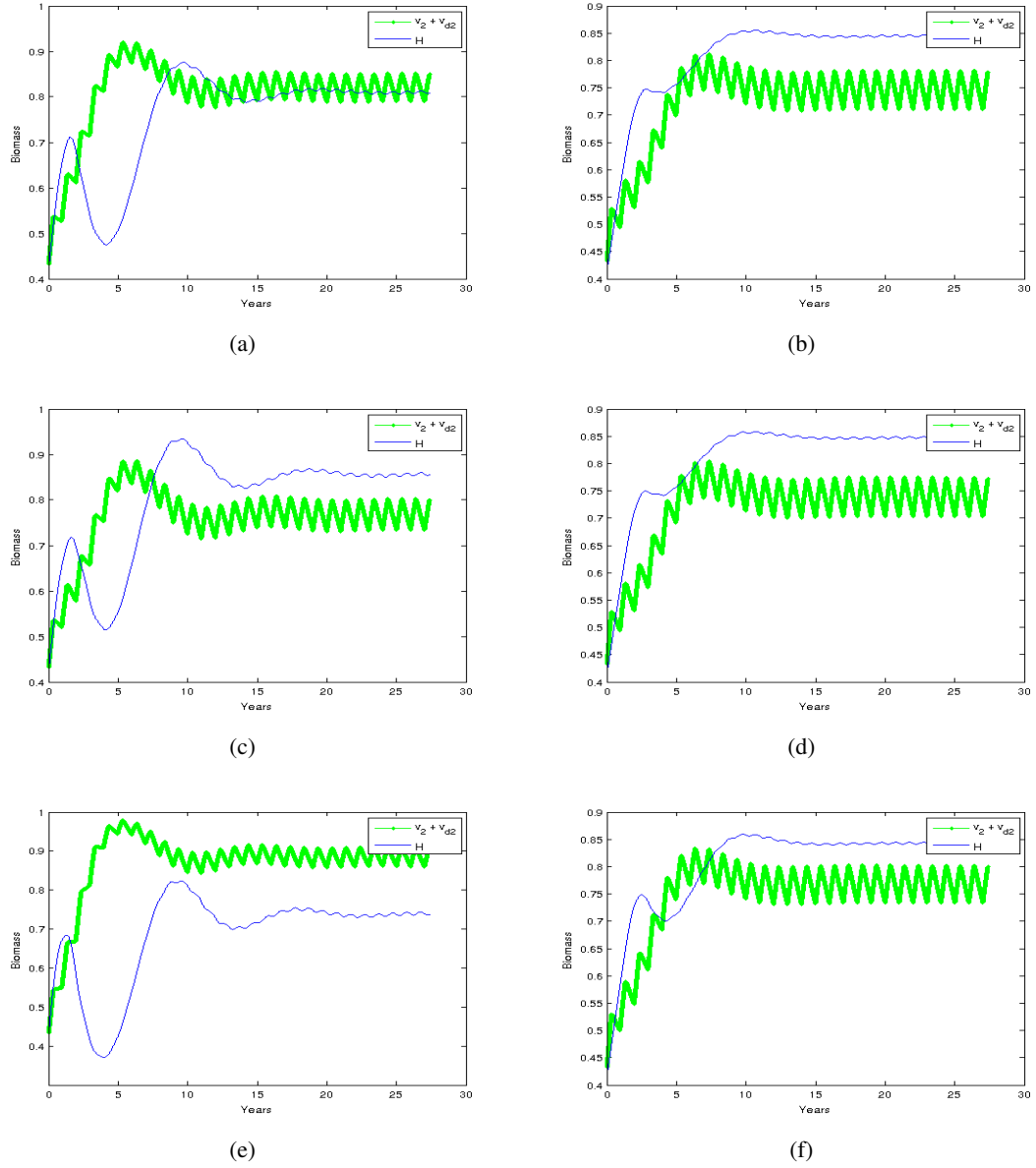


Figure 6.7: The dynamics on patch 2 for the seasonal two-patch model (6.13) when $\varepsilon = 0.01$ (the figures in the left column), and when $\varepsilon = 0.1$ (the figures in the right column). Figures (a) and (b) correspond to $\alpha_1 = 0.3$ and $\alpha_2 = 0.4$, while figures (c) and (d) correspond to $\alpha_1 = \alpha_2 = 0.5$, and figures (e) and (f) correspond to $\alpha_1 = 0.4$ and $\alpha_2 = 0.7$. The initial values were $v_{g_2} + v_{d_2} = 0.45$ and $H = 0.42$.

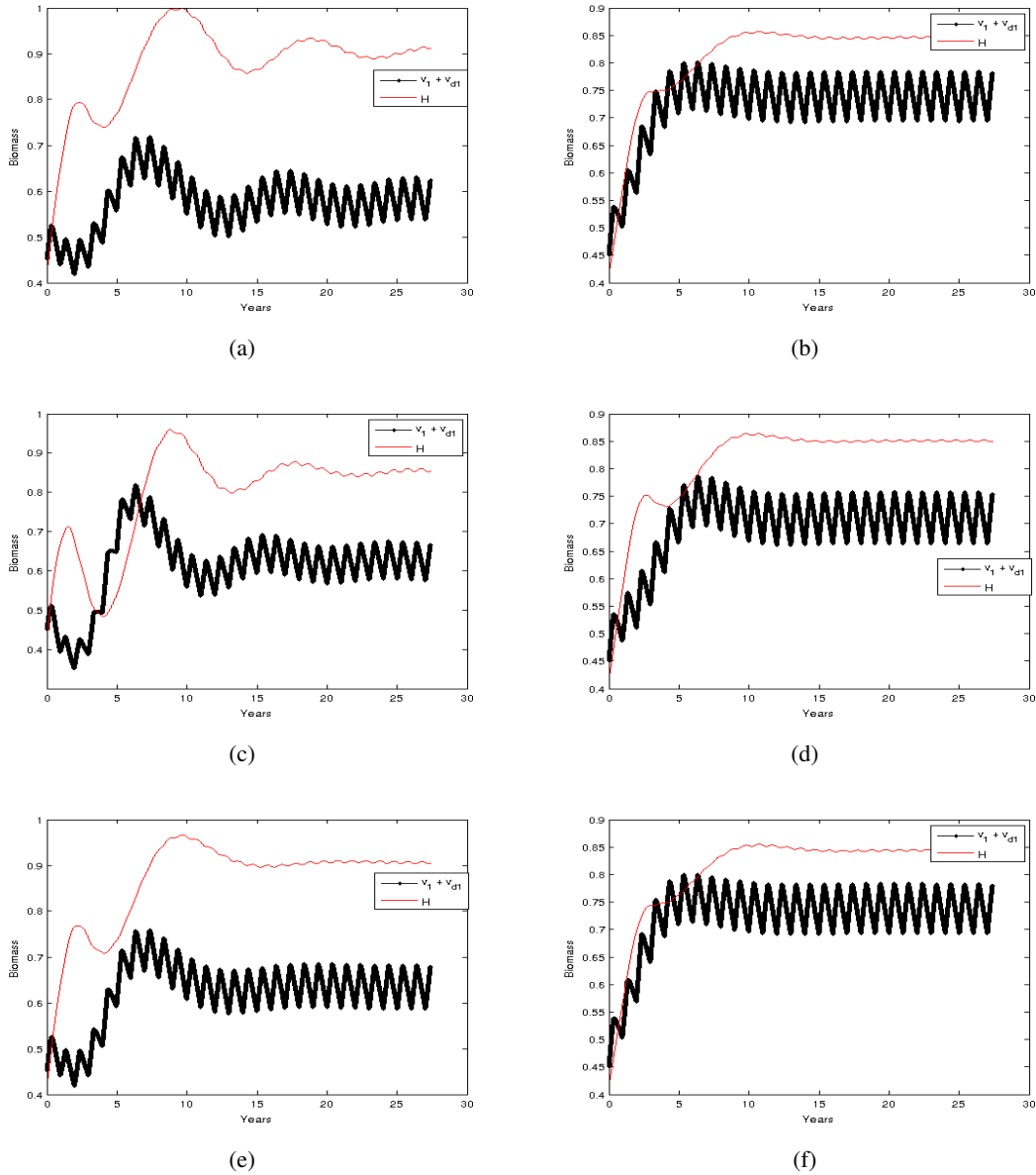


Figure 6.8: Numerical simulations for the seasonal two-patch model (6.13) show the dynamics on patch 1. The parameter values used are shown in Table 6.2 and Table 6.3. The figures in the left column correspond to $\varepsilon = 0.01$, and the figures in the right column correspond to $\varepsilon = 0.1$. In all figures we set $\alpha_1 \geq \alpha_2$. Figures (a) and (b) correspond to $\alpha_1 = 0.8, \alpha_2 = 0.5$. In (c) and (d), $\alpha_1 = \alpha_2 = 0.7$, and in figures (e) and (f) $\alpha_1 = 0.6$ and $\alpha_2 = 0.4$. The initial values were $v_{g1} + v_{d1} = 0.45$ and $H = 0.42$.

6. NUMERICAL SIMULATIONS

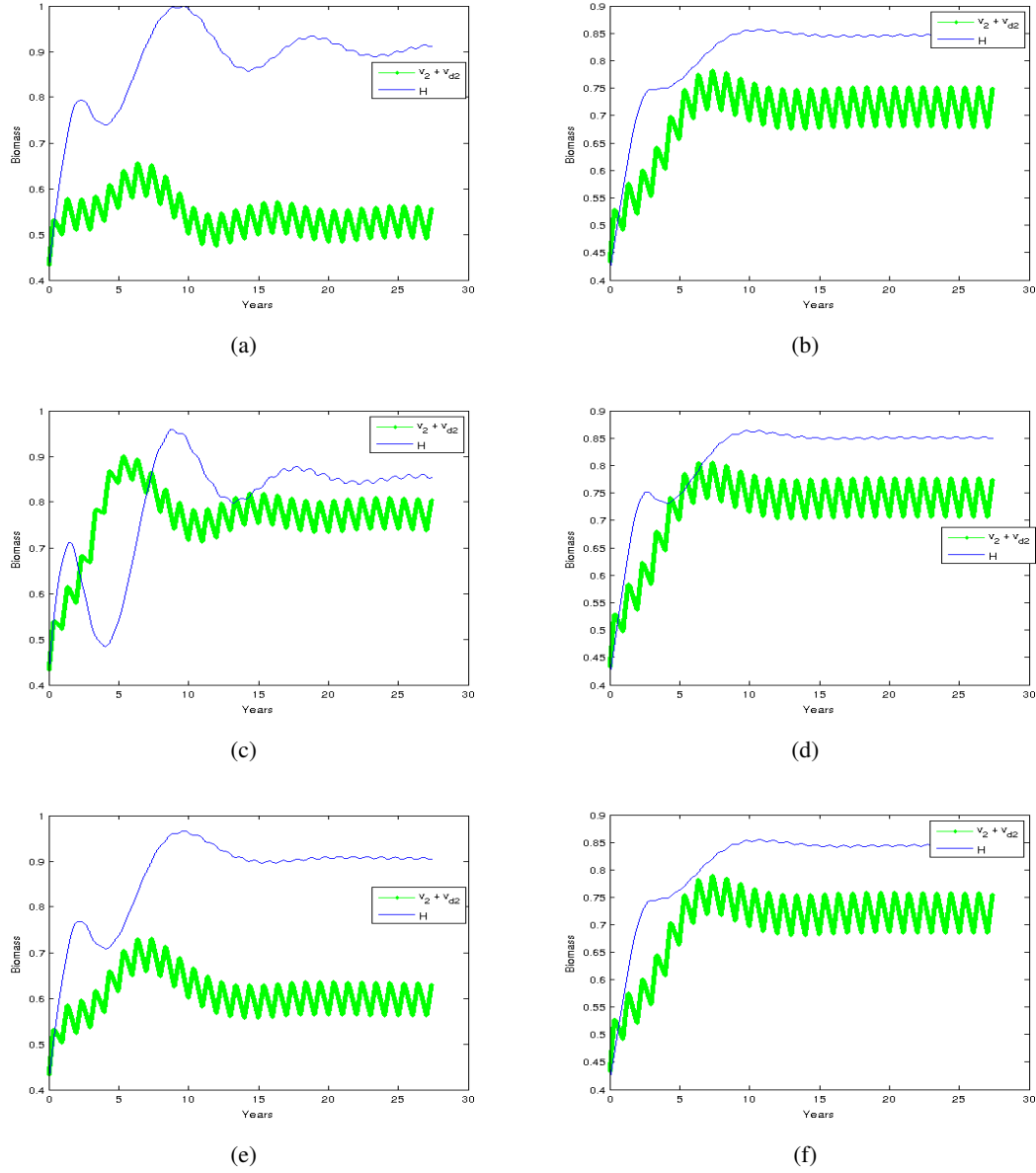


Figure 6.9: The dynamics on patch 2 for the seasonal two-patch model (6.13) when $\alpha_1 = 0.8$ and $\alpha_2 = 0.5$ (the figures in the first row), $\alpha_1 = \alpha_2 = 0.7$ (the figures in the second row) and when $\alpha_1 = 0.6$ and $\alpha_2 = 0.4$ (the figures in the third row). The figures in the left column correspond to $\varepsilon = 0.01$, where the figure on the right column correspond to $\varepsilon = 0.1$. The initial values were $v_{g_2} + v_{d_2} = 0.45$ and $H = 0.42$.

6. NUMERICAL SIMULATIONS

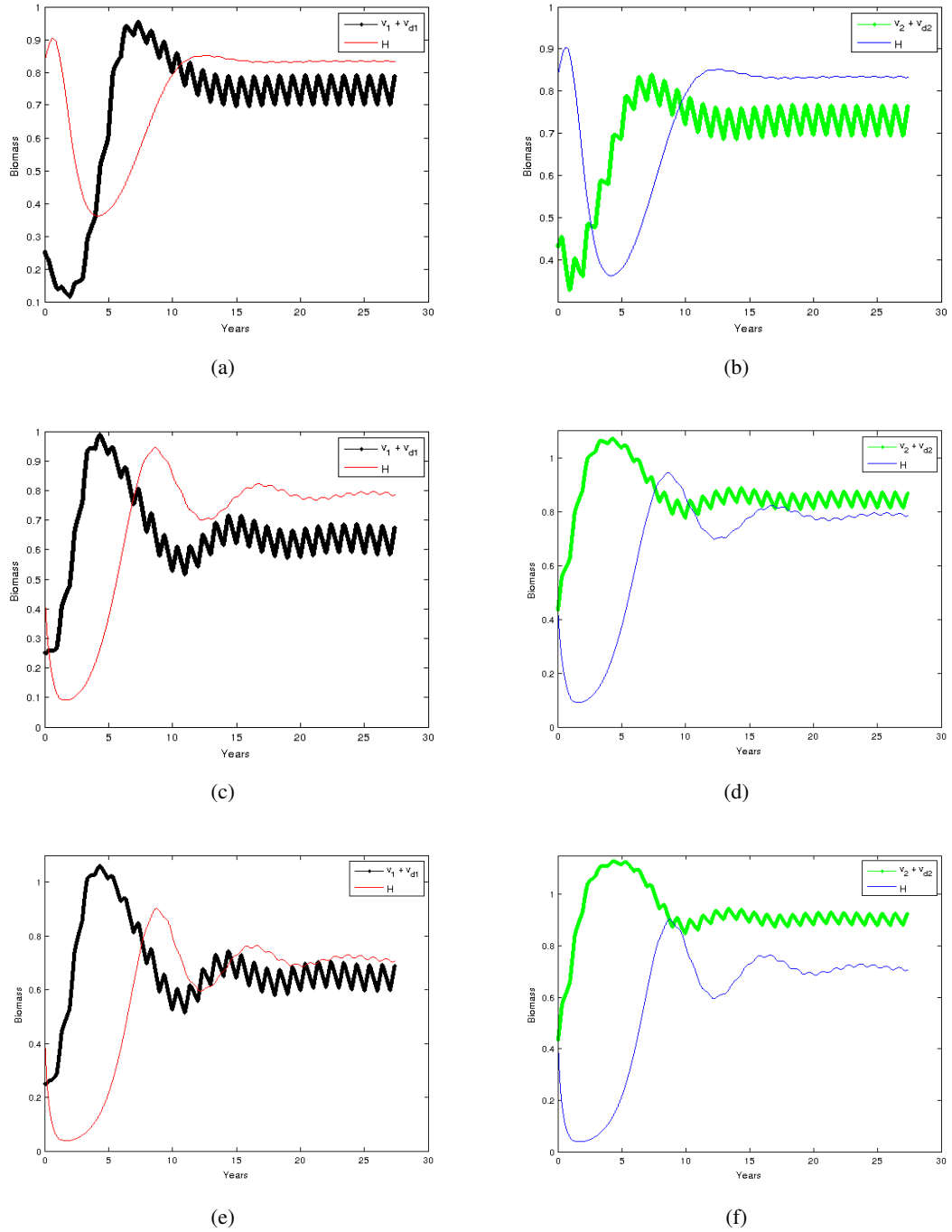


Figure 6.10: Numerical simulations show different behavior by the seasonal two-patch model (6.13), when we used $\beta_1 = \beta_2 = 10$, and the other parameters are shown in Tables 6.2 and 6.3. The dynamics on patch 1 is shown by the figures in the left column, and the figures in the right column show the dynamics on patch 2. We started the solutions from different initial points, and we set $\alpha_1 \leq \alpha_2$ in all these figures. When $\alpha_1 = \alpha_2 = 0.0$, the output is shown in the figures (a) and (b). In (c) and (d) we used $\alpha_1 = 0.3$ and $\alpha_2 = 0.4$ and in (e) and (f) $\alpha_1 = 0.4$ and $\alpha_2 = 0.7$. From top to bottom, the initial values were $(v_{g_1} + v_{d_1} = 0.25, v_{g_2} + v_{d_2} = 0.43, H = 0.85)$, $(v_{g_1} + v_{d_1} = 0.25, v_{g_2} + v_{d_2} = 0.43, H = 0.41)$ and $(v_{g_1} + v_{d_1} = 0.25, v_{g_2} + v_{d_2} = 0.43, H = 0.18)$, respectively.

6. NUMERICAL SIMULATIONS

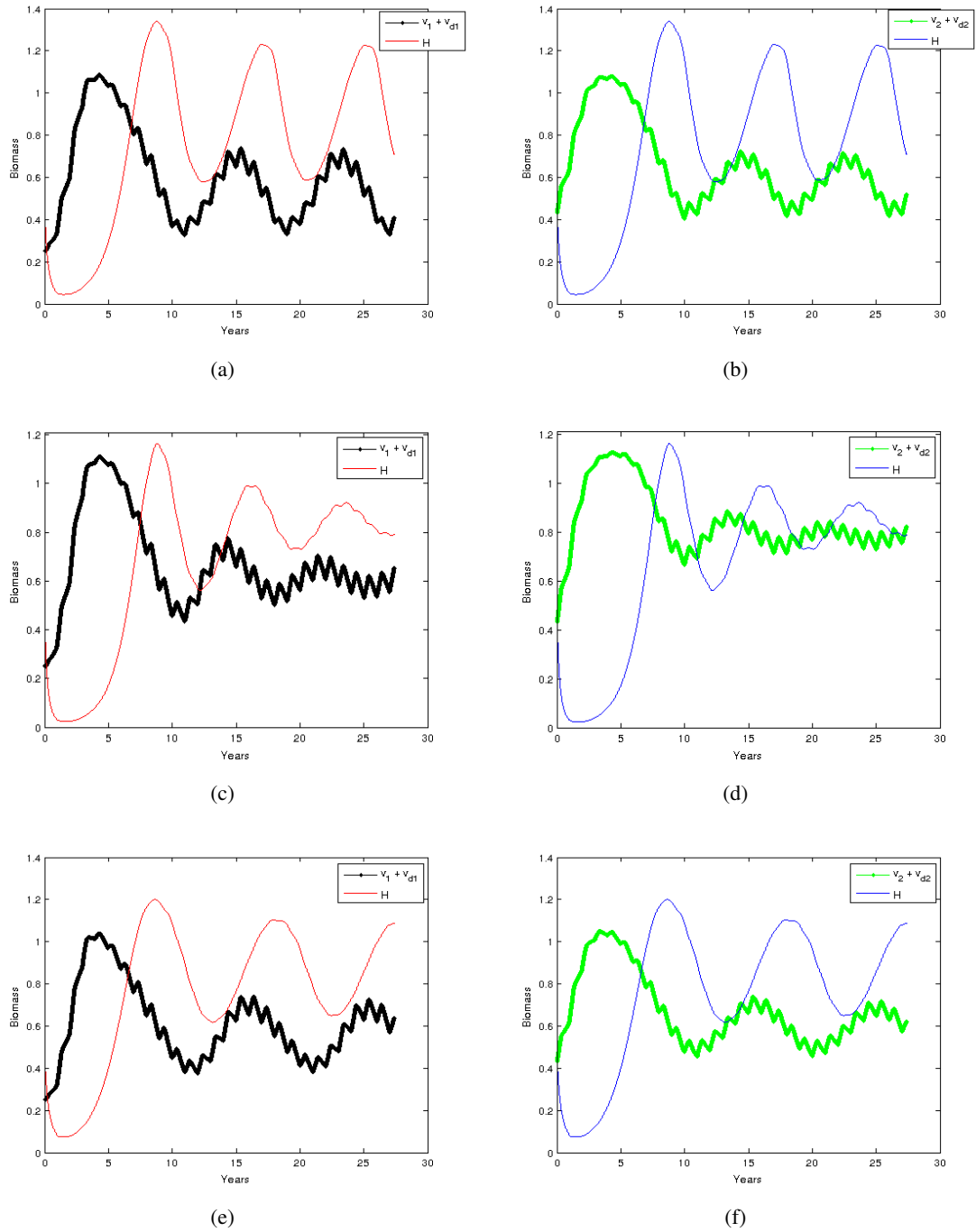


Figure 6.11: In these simulations we set $\alpha_1 \geq \alpha_2$. The dynamics on patch 1 is shown in the figures in the left column, where the figures in the right column show the dynamics on patch 2. In these figures we used $\beta_1 = \beta_2 = 10$, and the other parameters are given in Tables 6.2 and 6.3. In (a) and (b) $\alpha_1 = 0.8$ and $\alpha_2 = 0.5$, in (c) and (d) $\alpha_1 = \alpha_2 = 0.7$ and in (e) and (f) we used $\alpha_1 = 0.6$ and $\alpha_2 = 0.4$. The initial values used in the plots in this figure were the same, $(v_{g_1} + v_{d_1} = 0.25, v_{g_2} + v_{d_2} = 0.43, H = 0.38)$, $(v_{g_1} + v_{d_1} = 0.25, v_{g_2} + v_{d_2} = 0.43, H = 0.38)$.

6.6 Conclusions

In this chapter we extended the idea of the two-patch model that was introduced in Chapter 2 to include the effects of seasonal environment on the dynamics, by assuming that the vegetation growth depends on seasonal rainfall and on the soil moisture, using a simplified assumptions from (Richardson and Hahn [2007]). We assumed that in each patch the water from the rainfall will be stored in two horizontal soil layers which the vegetation roots can access and a portion of water from the rainfall will run off patch 2 (the run-off patch). The basic assumption of the seasonal model is that the vegetation will only grow when the amount of the soil moisture is sufficient.

We used numerical simulations to study the long time behavior of the model when the migration propensity parameters α_1 and α_2 vary. In these simulations we considered different factors that may change the behavior of the system along with the migration propensities, and that are the migration speed (the choice of ε), the initial conditions, and the quality of vegetation parameters β_1 and β_2 .

In the case when there were no migrations between the patches, the model is described by the local dynamics on each isolated patch, due to the changes to the soil moisture and the corresponding herbivore/vegetation interactions. When we used the parameter values shown in Tables 6.2 and 6.3, we observed that the long time behavior of the system for different initial conditions is the same and the system in these cases has global attractive cycles, with high biomass densities for both herbivore and vegetation (see Figure 6.5 and Figure 6.10 (a) and (b)). Comparing the vegetation densities on both patches, we observed that on patch 1 the biomass density is relatively high if compared with the vegetation on patch 2. Notice that we used $K_1 > K_2$ and the soil moisture of patch 1 is larger than that of patch 2.

When $\varepsilon = 0.1$, the migration is slow and the change in the local biomasses in each patch due to the migrations will be small. We used the parameter values shown in Tables 6.2 and 6.3 and, by using different values for the migration propensities α_1 and α_2 , we observed that the migrations have no big impact on the dynamics of the system. Moreover, we found that the model has the same long time behavior of the model when there were no migrations between the patches. The system in these cases has global attractive cycles, with high total herbivore and vegetation biomass densities (see the graphs in the right columns of Figures 6.6, 6.7, 6.8, and 6.9).

To model rapid migrations we set $\varepsilon = 0.01$. In this case the animals travel more frequently between the patches when the local vegetation density becomes smaller. When we used the parameter values in Tables 6.2 and 6.3, we observed that the behavior of the system in the short time dynamics is different, depending on the amount of the migration propensities, but the system has the same long time behavior (see the graphs in the left columns in Figures 6.6-6.9).

6. CONCLUSIONS

When animals have small propensity to leave patch 1 and $\alpha_1 \leq \alpha_2$, for the short time dynamics the vegetation on patch 2 will grow to higher densities and, as the animals aggregate more in patch 1, the vegetation in this patch will decrease. In the long term we see that the system has a stable cycle (see the graphs in the left columns in Figures 6.6 and 6.7).

When α_1 is large and $\alpha_1 > \alpha_2$, for the set of the parameter values in Tables 6.2 and 6.3, the long time behavior of the system is described by global attractive cycle, with smaller vegetation density on patch 2, relatively large vegetation density on patch 1 and high total herbivore density. Notice that the carrying capacity of patch 1 is larger than the carrying capacity of patch 2, $K_1 > K_2$ and patch 1 has a higher soil moisture amount (see the graphs in the left columns in Figures 6.8 and 6.9).

When we considered a lower quality of vegetation on both patches i.e, β_1 and β_2 have smaller value (in our case $\beta_1 = \beta_2 = 10$), and when the migration is fast $\varepsilon = 0.01$, we noticed that the dynamics of the system is different when the migration propensity parameters α_1 and α_2 take different values.

When $\alpha_1 \leq \alpha_2$, and for the other parameters that shown in Tables 6.2 and 6.3, the results show that the system have stable cycles (see Figure 6.10).

When animals have a large propensities to leave patch 1 ($\alpha_1 > \alpha_2$), the results show that the long time behavior of the system depends on the choice of α_1 and α_2 . For example, in the cases when $\alpha_1 = 0.8$, $\alpha_2 = 0.5$, and $\alpha_1 = 0.6$, $\alpha_2 = 0.4$, the results show that the system in these cases has a stable limit cycle with 5 different frequencies, each of 2 years length.

In our model, we assumed that the animal has no prior knowledge on how is palatable the vegetation on the other patch, or whether the other patch has a higher vegetation density biomass. When the local patch provide a lower quality of vegetation, then migration rates from this patch will be high.

Chapter 7

Concluding remarks

Number of mathematical models have been developed to study interacted species living in patchy environments (for instance see [Bernstein et al. \[1999\]](#); [Feng et al. \[2011\]](#); [Giulia et al. \[2012\]](#); [Neubert et al. \[2002\]](#); [Poggiale \[1998\]](#)). In this thesis, we have developed two mathematical models for herbivore and vegetation interactions, in constant and seasonal two-patch environments, where animals can migrate between the patches. The purpose of providing these models was to study the effects of herbivore migrations on the long time dynamics of the two-patch systems. In the following we give a brief summary to the work that has been done in this thesis.

We formulated a two-patch model for herbivore/vegetation interactions in a constant two-patch environment, by extending the metaphysiological model that proposed by Owen-Smith ([Owen-Smith \[2004\]](#)). In our model we considered the case when only animals are allowed to migrate between the two patches searching for food, where the animal leaves a patch when the local vegetation density becomes low, or when the vegetation quality is poor. Incorporating the propensity of migrations, the vegetation quality and the patch area in the density-depend migration has not well studied in the literature and by making these assumptions we have made significant contribution to improve existing models.

Furthermore, we have assumed that the process in the model have two different time scales, slow time-scale for the demographics changes and fast time-scale for the migration process. The resulting two-patch model consisted of a system of four perturbed ordinary differential equations.

Then, we applied the geometric singular perturbation theory to obtain unperturbed systems. Recently this theory has been applied in mathematical biology (see for instance [Auger et al. \[2012\]](#); [Hek \[2010\]](#); [Marva et al. \[2012\]](#); [Poggiale et al. \[2009\]](#)) and by using this theory here in this thesis we provided another example for application. The theory allowed us also to obtain two reduced systems of unperturbed ordinary differential equations, with fewer variables governing the global

dynamics, for different orders of ε (for $\mathcal{O}(\varepsilon^0)$ and $\mathcal{O}(\varepsilon^k)$, $k > 0$). First, we proved that the manifold of the fast equilibrium \mathcal{M}_0 (when $\varepsilon = 0$) is normally hyperbolically stable. This allowed us to use the results from Fenichel's first theorem to reduce the dynamics of the system to this manifold.

Second, we obtained a manifold \mathcal{M}_ε for $\varepsilon > 0$ and, by using the results from Fenichel's theorems we produced another reduced systems for $\mathcal{O}(\varepsilon)$. We provided numerical simulations to illustrate that the dynamics of reduced systems were the same as the dynamics of the full model for small $\varepsilon > 0$. The results obtained at this point were consistent with the results from the literature.

To have a close look at the effects of the density-dependent migrations on the dynamics of the reduced systems, we provided bifurcation diagrams using the parameter values presented in (Owen-Smith [2004]) and using different migration parameters. We used the propensity of migration parameter α_2 as the bifurcation parameter.

The resulting bifurcation diagrams have shown that for some values of α_2 the system has a unique stable cycle, whereas for some other values the system has three cycles, two unstable cycles and one stable cycle, with high values of total herbivore density biomass. This suggested that the propensity of migration has large impact on the global dynamics of the reduced two-patch systems. When we have made the carrying capacities K_1 and K_2 , $K_1 < K_2$, the ungrazable vegetation amounts ρ_1 and ρ_2 varied, we have obtained different bifurcation diagrams in which the behavior of the system is topologically different from what we had obtained before the diagrams showed that the whole system has no stable cycles. These results were consistent with the results from previous studies (Auger and de la Parra [2000]; Auger and Poggiale [1996]; Auger et al. [2000a]; Bernstein et al. [1999]; El Abdllaoui et al. [2007]; Mchich et al. [2007]).

Also the results showed that for certain choice of parameters, the system has no closed orbits and only fixed points appeared in the phase space for some values of α_2 , while for the other values of α_2 there were periodic orbits. This result have no biological explanations. To make sure that the resulting diagrams of the reduced two-patch models were correct (from the mathematical point of view), we used the Morse decomposition and the Conley index theorems. The Morse decomposition theorem allowed us to study the qualitative behavior of the flow using what is called Morse sets, Morse decompositions and the trajectories connecting these different sets. We considered one of the bifurcation diagrams and we decomposed it to ten sets that contained stationary solutions and periodic orbits for each corresponding value of α_2 . We constructed isolated invariant sets and, by assigning Conley index for each element of these sets, we obtained Morse decompositions. Then, we computed the homological Conley index for each element and then, we obtained connection matrices between the elements of each individual Morse set. Notice that the connection matrices are not unique. To see the possibility for the existence of connecting orbits between neighboring

Morse sets, we computed transition matrices.

We considered two cases. First, we calculated a transition matrix for one of the Morse sets M_{μ_4} that contained only fixed points and its neighboring Morse set M_{μ_5} that contained unstable closed orbit. The resulting transition matrix was the zero matrix. This suggested that there were no connections between the Morse sets M_{μ_4} and M_{μ_5} . Second, we considered the Morse set M_{μ_5} and the neighboring Morse set M_{μ_6} that contained a stable limit cycle. The results showed the existence of connecting orbits between the two Morse sets M_{μ_5} and M_{μ_6} , where two stable fixed points on M_{μ_5} continue over the interval of α_2 to two stable fixed points on M_{μ_6} . This result showed that the fixed points were not continue over α_2 to limit cycles.

The results concluded that, using the connection matrices (5.9)-(5.16), the bifurcation diagrams that we obtained using the parameters defined in Table 4.1 are correct.

The study of patch models in seasonal environments has not been well introduced in the literature. To examine the effects of seasonal environments on the dynamics of two-patch system, we extended the two-patch model (2.5) of Chapter 2, by assuming that the vegetation growth depends on the soil moisture and rainfall. We have used assumptions from the model by Richardson and Hahn (Richardson and Hahn [2007]), to model the changes in the soil moisture and the vegetation growth. We have used the same rules for the migrations as in the constant environment model (2.5) and we have constructed a system of perturbed ordinary differential equations describing the dynamics.

We have assumed that the change in the soil moisture due to the rainfall is an instantaneous event. In this case the model is described by a time dependent system of perturbed differential equations and we were not able to apply the results from Fenichel theorems or the results from Chapter 4.

We have presented some numerical results by considering two cases for the migration speed parameter ε and we have used different values for the migration propensities α_1 and α_2 and the vegetation quality parameters β_1 and β_2 . The results suggested that slow migrations have small impact on the dynamics of the system and, the long time dynamics have the same features as in the systems of isolated patches with no migrations. In the case of fast migrations, the dynamics of the system depended on the choice of the migration propensity parameters and, on the vegetation quality parameters. When the vegetation was palatable, the long time behavior of the system showed that the existence of a stable cycle with large total herbivore density.

When the vegetation quality was poor and the migration propensities were high, the results showed that system has stable limit cycles containing several frequencies.

The bifurcation diagrams that we have presented in this thesis were based on the migration

7. Concluding remarks

propensities α_1 and α_2 and the exploration of the dynamics when the vegetation quality changed have been done briefly in this thesis. It is clear that migrations, vegetation quality, patch size and the Holling-type functional response result in a system with potentially complicated behavior, with a large variety of dynamics governed by bifurcation parameters. Future work is needed to elucidate this.

Also, the analysis presented in Chapter 5 was based on certain connection matrices, for the future work we suggest that, one can use a general formula for all the possible connection matrices for each Morse set and then compute transition matrices based on that.

Bibliography

- Peter Abrams, Ross Cressman, and Vlastimil Křivan. The Role of Behavioral Dynamics in Determining the Patch Distributions of Interacting Species. *The American Naturalist*, 169(4): 505–518, 2007.
- Linda Allen. Persistence, Extinction, and Critical Patch Number for Island Populations. *Journal of Mathematical Biology*, 24:617–625, 1987.
- José Luis González Andújar and Joe N. Perry. Chaos, Metapopulations and Dispersal. *Ecological Modelling*, 65(3-4):255 – 263, 1993.
- Pierre Auger and Rafael Bravo de la Parra. Methods of Aggregation of Variables in Population Dynamics. *Life Sciences*, 323:665–674, 2000.
- Pierre Auger and Jean-Christophe Poggiale. Emergence of Population Growth Models: Fast Migration and Slow Growth. *Theoretical Biology*, 182:99–108, 1996.
- Pierre Auger, Sandrine Charles, Muriel Viala, and Jean-Christophe Poggiale. Aggregation and Emergence in Ecological Modelling: Integration of Ecological Levels. *Ecological Modelling*, 127:11–20, 2000a.
- Pierre Auger, Jean-Christophe Poggiale, and Sandrine Charles. Emergence of Individual Behaviour at The Population Level. Effects of Density-Dependent Migration on Population Dynamics. *Comptes Rendus de l'Académie des Sciences - Series {III} - Sciences de la Vie*, 323(1):119 – 127, 2000b.
- Pierre Auger, Rafael Bravo de la Parra, Jean-Christopher. Poggiale, Eva. Sánchez, and Thai Huu Nguyen. *Structured Population Models in Biology and Epidemiology*, chapter 5, pages 209–263. Springer-Verlag, Berlin Heidelberg, 2008a.
- Pierre Auger, Rafael Bravo de la Parra, Jean-Christophe Poggiale, Eva Sánchez, and Luis Sanz.

BIBLIOGRAPHY

- Aggregation Methods in Dynamical Systems and Applications in Population and Community Dynamics. *Physics of Life Reviews*, 5:79–105, 2008b.
- Pierre Auger, Jean-Christophe Poggiale, and Eva Sánchez. A Review on Spatial Aggregation Methods Involving Several Time Scales. *Ecological Complexity*, 2012.
- Carlos Bernstein, Pierre Auger, and Jean-Christophe Poggiale. Predator Migration Decisions, the Ideal Free Distribution and Predator-Prey Dynamics. *The American Naturalist*, 153:267–281, 1999.
- Jack Carr. *Applications of Centre Manifold Theory*. Number Vol. 35 in Applied Mathematical Sciences Series. Springer-Verlag, 1981.
- Hal Caswell and Ron J. Etter. Ecological Interactions in Patchy Environments: From Patch-Occupancy Models to Cellular Automata. In Simon Levin, Thomas Powell, and John Steele, editors, *Patch Dynamics*, volume 96 of *Lecture Notes in Biomathematics*, pages 93–109. Springer Berlin Heidelberg, 1993.
- Xu Changjin, Tang Xianhua, and Liao Maoxin. Stability and Bifurcation Analysis of a Delayed Predator-Prey Model of Prey Dispersal in Two-Patch Environments. *Applied Mathematics & Computation*, 216(10):2920 – 2936, 2010.
- Giovanna Chiorino, Pierre Auger, Jean-Luc Chass, and Sandrine Charles. Behavioral Choices Based on Patch Selection: A Model Using Aggregation Methods. *Mathematical Biosciences*, 157(1-2):189 – 216, 1999.
- Charles Conley. Isolated Invariant Sets and the Morse Index. In *CBMS Regional Conference Series in Math*, 38. AMS, Providence, Rhode Island, 1978.
- James T. Cronin. Movement and Spatial Population Structure of a Prairie Planthopper. *Ecology*, 84(5):1179–1188, 2003.
- Jane Cronin and Robert E. O’Malley. *Analyzing Multiscale Phenomena Using Singular Perturbation Methods*. American Mathematical Society short course. American Mathematical Society, Baltimore, Maryland, 1998.
- Jingan Cui. The Effect of Dispersal on Permanence in a Predator-Prey Population Growth Model. *Computers & Mathematics with Applications*, 44(89):1085 – 1097, 2002.

BIBLIOGRAPHY

- Eusebius J. Doedel, Alan R. Champneys, Yuri Kuznetsov, Björn Sandstede, Xianjun Wang, and Chenghai Zhang. *AUTO-07p: Continuation and Bifurcation Software for Ordinary Differential Equations, User's Guide*. Concordia University, Montreal, Canada, 2007.
- Peter John Dye. *Prediction of Variation in Grass Growth in Semi Arid Induced Grassland*. PhD thesis, University of Witwatersrand, Johannesburg, 1984.
- Abderrahim El Abdllaoui, Pierre Auger, Bob W. Kooi, Rafael Bravo de la Parra, and Rachid Mchich. Effects of Density-Dependent Migrations on Stability of a Two-Patch Predator-Prey Model. *Mathematical Biosciences*, 210(1):335–354, 2007.
- Lenore Fahrig and Gray Merriam. Habitat Patch Connectivity and Population Survival. *Ecology*, 66(6):1762–1768, 1985.
- Lenore Fahrig and Jyri Paloheimo. Effect of Spatial Arrangement of Habitat Patches on Local Population Size. *Ecology*, 69(2):468–475, 1988.
- Wei Feng and Jody Hinson. Stability and Pattern in Two-Patch Predator-Prey Population Dynamics. *Discrete and Continuous Dynamical Systems*, pages 268–279, 2005.
- Wei Feng, Brevin Rock, and Jody Hinson. On a New Model of Two-Patch Predator-Prey System with Migration of Both Species. *Journal of Applied Analysis and Computation*, 1(2):193–203, 2011.
- Nils Fenichel. Geometric Singular Perturbation Theory for Ordinary Differential Equations. *Journal of Differential Equations*, 31:53–98, 1979.
- Robert Franzosa. The Continuation Theory for Morse Decompositions and Connection Matrices. *Transactions of the American Mathematical Society*, 310(2):781–803, 1988.
- Robert Franzosa. The Connection Matrix Theory for Morse Decompositions. *Transactions of the American Mathematical Society*, 311(2):561–592, 1989.
- Robert Franzosa and Konstantin Mischaikow. The Connection Matrix Theory for Semiflows on (not Necessarily Locally Compact) Metric Spaces. *Journal of Differential Equations*, 71(2):270–287, 1988.
- Robert Franzosa and Konstantin Mischaikow. Algebraic Transition Matrices in the Conley Index Theory. *Transactions of the American Mathematical Society*, (350):889–912, 1998.

BIBLIOGRAPHY

- Stephen Dewitt Fretwell and HenryL Lucas. On Territorial Behavior and Other Factors Influencing Habitat Distribution in Birds. *Acta Biotheoretica*, 19:16–36, 1970.
- Wayne M. Getz. A Unified Approach to Multispecies Modelling. *Natural Resource Modelling*, 5: 393–421, 1991.
- Wayne M. Getz. Metaphysiological and Evolutionary Dynamics of Populations Exploiting Constant and Interactive Resources: R - K Selection revisited. *Evolutionary Ecology*, 7:287–305, 1993.
- Wayne M. Getz. A Metaphysiological Approach to Modeling Ecological Populations and Communities. In S. Levin, editor, *Frontiers in Mathematical Biology*, pages 411–442. Springer-Verlag, New York, USA, 1994.
- Wayne M. Getz and Norman Owen-Smith. A Metaphysiological Population Model of Storage in Variable Environments. *Natural Resource Modeling*, 12(2):197–230, 1999.
- Quaglia Giulia, Erica Re, Rinaldi Marco, and Venturino Ezio. A Two-Patch Predator-Prey Metapopulation Model. *East Asian Journal on Applied Mathematics*, 2(3):238–265, 2012.
- Mats Gyllenberg and Dmitrii Silvestrov. Quasi-Stationary Distributions of a Stochastic Metapopulation Model. *Journal of Mathematical Biology*, 33:35–70, 1994.
- Mats Gyllenberg, Gunnar Sderbacka, and Stefan Ericsson. Does Migration Stabilize Local Population Dynamics? Analysis of a Discrete Metapopulation Model. *Mathematical Biosciences*, 118(1):25 – 49, 1993.
- Ilkka Hanski. Single-Species Metapopulation Dynamics: Concepts, Models and Observations. *Biological Journal of the Linnean Society*, 42(1-2):17–38, 1991.
- Ilkka Hanski. A Practical Model of Metapopulation Dynamics. *Journal of Animal Ecology*, 63(1): 151–162, 1994a.
- Ilkka Hanski. Patch-Occupancy Dynamics in Fragmented Landscapes. *Trends in Ecology and Evolution*, 9(4):131–135, 1994b.
- Ilkka Hanski and M Gilpin. Metapopulation Dynamics: Brief History and Conceptual Domain. *Biological Journal of the Linnean Society*, 42(1-2):3–16, 1991.
- Ilkka Hanski and Daniel Simberloff. The Metapopulation Approach, Its History, Conceptual Domain, and Application to Conservation. In I. Hanski and M.E. Gilpin, editors, *Metapopulation Biology: Ecology, Genetics and Evolution*, pages 5–16. Academic Press/ New York, 1997.

BIBLIOGRAPHY

- Ilkka Hanski, Atte Moilanen, and Mats Gyllenberg. Minimum Viable Metapopulation Size. *The American Naturalist*, 147(4):527–541, 1996.
- Michael P. Hassell, Hugh N. Comins, and Robert M. May. Spatial Structure and Chaos in Insect Population Dynamics. *Nature*, 353:255 – 258, 1991.
- Alan Hastings. Spatial Heterogeneity and the Stability of Predator-Prey Systems. *Theoretical Population Biology*, 12(1):37 – 48, 1977.
- Alan Hastings. Dynamics of a Single Species in a Spatially Varying Environment: The Stabilizing Role of High Dispersal Rates. *Journal of Mathematical Biology*, 16:49–55, 1982.
- Alan Hastings and Carole L. Wolin. Within-Patch Dynamics in a Metapopulation. *Ecology*, 70(5): 1261–1266, 1989.
- Geertje Hek. Geometric Singular Perturbation Theory in Biological Practice. *Journal of Mathematical Biology*, 60:347–386, 2010.
- Robert Holt. Population Dynamics in Two-Patch Environments: Some Anomalous Consequences of an Optimal Habitat Distribution. *Theoretical Population Biology*, 28(2):181 – 208, 1985.
- Robert Holt. Prey Communities in Patchy Environments. *Oikos*, 50(3):276–290, 1987.
- Yoh Iwasa, Viggo Andreasen, and Simon Levin. Aggregation in model ecosystems. I. Perfect aggregation. *Ecological Modelling*, 37(3-4):287–302, 1987.
- Christopher K. R. T. Jones. *Geometric Singular Perturbation Theory*, pages 44–118. Lecture Notes in Mathematics. Berlin/ Heidelberg, 1994.
- Peter Kareiva, Ashley Mullen Mullen, and Richard Southwood. Population Dynamics in Spatially Complex Environments: Theory and Data [and Discussion]. *Philosophical Transactions: Biological Sciences*, 330(1257):175–190, 1990.
- Vlastimil Krivan. Dynamic Ideal Free Distribution: Effects of Optimal Patch Choice on Predator-Prey Dynamics. *The American Naturalist*, 149(1):164–178, 1997.
- Yang Kuang and Yasuhiro Takeuchi. Predator-Prey Dynamics in Models of Prey Dispersal in Two-Patch Environments. *Mathematical Biosciences*, 120(1):77 – 98, 1994.
- Simon A. Levin. Dispersion and Population Interactions. *The American Naturalist*, 108(960): 207–228, 1974.

BIBLIOGRAPHY

- Simon A. Levin and Stephen W. Pacala. Theories of Simplification and Scaling of Spatially Distributed Processes. *Spatial Ecology The Role of Space in Population Dynamics and Interspecific Interactions*, 30:271–295, 1997.
- Adam Lomnicki. Individual-Based Models and the Individual-Based Approach to Population Ecology. *Ecological Modelling*, 115(2-3):191 – 198, 1999.
- Stephen Lynch. *Dynamical Systems with Applications Using Maple*. Birkhäuser Boston, New York, 2009.
- Tian Ma and Shouhong Wang. *Bifurcation Theory and Applications*. Bifurcation Theory and Applications. World Scientific, 2005.
- Marcos Marva, Rafael Bravo de la Parra, and Jean-Christophe Poggiale. Approximate Aggregation of a Two Time Scales Periodic Multi-Strain SIS Epidemic Model: A Patchy Environment With Fast Migrations. *Ecological Complexity*, 10:34–41, 2012.
- William S. Massey. *Singular Homology Theory*. Graduate Texts in Mathematics. Springer-Verlag, 1980.
- Christopher McCord and Konstantin Mischaikow. Connected Simple Systems, Transition Matrices and Heteroclinic Bifurcations. *Transactions of the American Mathematical Society*, 333(1): 397–422, 1992.
- Rachid Mchich, Amal Bergam, and Nadia Raissi. Effects of Density Dependent Migrations on the Dynamics of a Predator Prey Model. *Acta Biotheoretica*, 53:331–340, 2005.
- Rachid Mchich, Pierre Auger, and Jean-Christophe Poggiale. Effect of Predator Density Dependent Dispersal of Prey on Stability of a Predator-Prey System. *Mathematical Biosciences*, 206:343–356, 2007.
- John Metz and Mats Gyllenberg. How Should we Define Fitness in Structured Metapopulation Models? Including an Application to the Calculation of Evolutionarily Stable Dispersal Strategies. *Proceeding of Royal Society*, 268:499–508, 2001.
- James D. Miess. *Differential Dynamical Systems*. SIAM, Philadelphia, 2007.
- Konstantin Mischaikow. Transition-Systems. *Proceeding of the Royal Society*, 112(Part 1-2):155–175, 1989.

BIBLIOGRAPHY

- Konstantin Mischaikow. *Dynamic Phase Transitions: A Connection Matrix Approach*, pages 164–180. Nonlinear Evolution Equations that Change Type. Springer-Verlag, New York, 1990.
- Konstantin Mischaikow. The Conley Index Theory: a Brief Introduction. In *Conley index theory (Warsaw, 1997)*, volume 47 of *Banach Center Publications*, pages 9–19. Polish Academy for Science, Warsaw, 1999.
- Konstantin Mischaikow and Marian Mrozek. Conley Index. volume 2 of *Handbook of Dynamical Systems*, chapter 9, pages 393–460. Elsevier Science, 2002.
- Todd Moeller. *Conley-Morse Chain Maps*. Phd, Georgia Institute of Technology, 2005.
- Michael G. Neubert, Petra Klepac, and P. van den Driessche. Stabilizing Dispersal Delays in Predator-Prey Metapopulation Models. *Theoretical Population Biology*, 61(3):339–347, 2002.
- R.M. Nisbet and W.S.C. Gurney. *Modelling fluctuating populations*. Wiley, 1982.
- Otso Ovaskainen and Ilkka Hanski. Spatially Structured Metapopulation Models: Global and Local Assessment of Metapopulation Capacity. *Theoretical Population Biology*, 60(4):281–302, 2001.
- Norman Owen-Smith. *Adaptive Herbivore Ecology. From Resource to Population in Variable Environment*. Cambridge Studies in Ecology. Cambridge University Press, Cambridge, UK, 2002a.
- Norman Owen-Smith. A Metaphysiological Modelling Approach to Stability in Herbivore-Vegetation Systems. *Ecological Modelling*, 149(1-2):153–178, 2002b.
- Norman Owen-Smith. Functional Heterogeneity in Resources within Landscapes and Herbivore Population Dynamics. *Landscape Ecology*, 19:761–771, 2004.
- Lawrence Perko. *Differential Equations and Dynamical Systems*. Texts in Applied Mathematics (7). Springer-Verlag, 1993.
- Steward Pickett and Mary Cadenasso. Landscape Ecology: Spatial Heterogeneity In Ecological Systems. *Science*, 269:331–334, 1995.
- Jean-Christophe Poggiale. Predator-Prey Models in Heterogeneous Environment: Emergence of Functional Response. *Mathematical and Computer Modelling*, 27(4):63–71, 1998.

BIBLIOGRAPHY

- Jean-Christophe Poggiale, Pierre Auger, Flora Cordoleani, and Thai Huu Nguyen. Study of a Virus-Bacteria Interaction Model in a Chemostat: Application of Geometrical Singular Perturbation Theory. *Philosophical Transactions of Royal Society*, 367:4685–4697, 2009.
- Rodrigo Ramos-Jiliberto, Eduardo Gonzalez-Olivares, and Francisco Bozinovic. Population-Level Consequences of Antipredator Behavior: A Metaphysiological Model Based on the Functional Ecology of the Leaf-Eared Mouse. *Theoretical Population Biology*, 62(1):63 – 80, 2002.
- David Richardson and Brian Hahn. A Short-Term Mechanistic Model of Forage and Livestock in the Semi-Arid Succulent Karoo: 1. Description of the Model and Sensitivity Analyses. *Agricultural Systems*, 95(1-3):49 – 61, 2007.
- Manojit Roy, Karin Harding, and Robert Holt. Generalizing Levins Metapopulation Model in Explicit Space: Models of Intermediate Complexity. *Journal of Theoretical Biology*, 255(1): 152 – 161, 2008.
- Bernt-Erik Saether, Steinar Engen, and Russell Lande. Finite Metapopulation Models with Density-Dependent Migration and Stochastic Local Dynamics. *Proceedings: Biological Sciences*, 266 (1415):113–118, 1999.
- Hans Schneider and George Phillip Barker. *Matrices and Linear Algebra*. Dover Books on Advanced Mathematics. Dover Publications, 1973.
- Hall Smith and Paul Waltman. *The Theory of the Chemostat: Dynamics of Microbial Competition*. Cambridge Studies in Mathematical Biology. Cambridge University Press, 1995.
- Joseph W.-H. So, Jianhong Wu, and Xingfu Zou. Structured Population on Two Patches: Modeling Dispersal and Delay. *Journal of Mathematical Biology*, 43(1):37–51, 2001.
- Monica Goigel Turner. Landscape Ecology: The Effect of Pattern on Process. *Annual Review of Ecology and Systematics*, 20:171–197, 1989.
- Grimm Volker. Ten Years of Individual- Based Modelling in Ecology. what Have we Learned and what Could We Learn In the Future? *Ecological Modelling*, 115:129–148, 1999.
- Stephen Wiggins. *Introduction to Applied Nonlinear Dynamical Systems and Chaos*. Springer-Verlag, New York, second edition, 2003.
- Rui Xu and Lansun Chen. Persistence and Stability for a Two-Species Ratio-Dependent Predator-Prey System with Time Delay in a Two-Patch Environment. *Computers & Mathematics with Applications*, 40(4-5):577–588, 2000.

BIBLIOGRAPHY

Rui Xu, Mark A.J. Chaplain, and Fordyce A. Davidson. Periodic Solutions for a Delayed Predator-Prey Model of Prey Dispersal in Two-Patch Environments. *Nonlinear Analysis: Real World Applications*, 5(1):183 – 206, 2004.

Appendix A. Stability of the reduced two-patch model on \mathcal{M}_0

The Jacobian matrix for the reduced two-patch model (4.10) evaluated at an arbitrary equilibrium point $E = (v_1^*, v_2^*, H^*)$ is given by

$$D(f|_E) = \begin{bmatrix} J_{1,1} & J_{2,1} & J_{3,1} \\ J_{2,1} & J_{2,2} & J_{2,3} \\ J_{3,1} & J_{3,2} & J_{3,3} \end{bmatrix}, \quad (1)$$

where

$$J_{1,1} = 1 - 2v_1^* - \frac{\eta_1 \alpha_2 \zeta_2 H^*}{(1 + \beta_2 v_2^*) \left(\frac{\alpha_2 \zeta_2}{1 + \beta_2 v_2^*} + \frac{\alpha_1}{1 + \beta_1 v_1^*} \right) (1 + \gamma_1 (v_1^* - \rho_1))} - \frac{\eta_1 (v_1^* - \rho_1) \alpha_2 \zeta_2 \alpha_1 \beta_1 H^*}{(1 + \beta_2 v_2^*) \left(\frac{\alpha_2 \zeta_2}{1 + \beta_2 v_2^*} + \frac{\alpha_1}{1 + \beta_1 v_1^*} \right)^2 (1 + \gamma_1 (v_1^* - \rho_1)) (1 + \beta_1 v_1^*)^2} + \frac{\eta_1 (v_1^* - \rho_1) \alpha_2 \zeta_2 \gamma_1 H^*}{(1 + \beta_2 v_2^*)^2 \left(\frac{\alpha_2 \zeta_2}{1 + \beta_2 v_2^*} + \frac{\alpha_1}{1 + \beta_1 v_1^*} \right) (1 + \gamma_1 (v_1^* - \rho_1))},$$

$$J_{1,2} = \frac{\eta_1 (v_1^* - \rho_1) \alpha_2 \zeta_2 \beta_2 H^*}{(1 + \beta_2 v_2^*) \left(\frac{\alpha_2 \zeta_2}{1 + \beta_2 v_2^*} + \frac{\alpha_1}{1 + \beta_1 v_1^*} \right) (1 + \gamma_1 (v_1^* - \rho_1))} - \frac{\eta_1 (v_1^* - \rho_1) \alpha_2^2 \zeta_2^2 \beta_2 H^*}{(1 + \beta_2 v_2^*)^3 \left(\frac{\alpha_2 \zeta_2}{1 + \beta_2 v_2^*} + \frac{\alpha_1}{1 + \beta_1 v_1^*} \right)^2 (1 + \gamma_1 (v_1^* - \rho_1))},$$

$$J_{1,3} = - \frac{\eta_1 (v_1^* - \rho_1) \alpha_2 \zeta_2}{(1 + \beta_2 v_2^*) \left(\frac{\alpha_2 \zeta_2}{1 + \beta_2 v_2^*} + \frac{\alpha_1}{1 + \beta_1 v_1^*} \right) (1 + \gamma_1 (v_1^* - \rho_1))},$$

$$J_{2,1} = \frac{\eta_2 (v_2^* - \rho_2) \alpha_1 \zeta_1 \beta_1 H^*}{(1 + \beta_1 v_1^*)^2 \left(\frac{\alpha_2}{1 + \beta_2 v_2^*} + \frac{\alpha_1 \zeta_1}{1 + \beta_1 v_1^*} \right) (1 + \gamma_2 (v_2^* - \rho_2))} - \frac{\eta_2 (v_2^* - \rho_2) \alpha_1^2 \zeta_1^2 \beta_1 H^*}{(1 + \beta_1 v_1^*)^3 \left(\frac{\alpha_2}{1 + \beta_2 v_2^*} + \frac{\alpha_1 \zeta_1}{1 + \beta_1 v_1^*} \right)^2 (1 + \gamma_2 (v_2^* - \rho_2))},$$

$$J_{2,2} = 1 - 2v_2^* - \frac{\eta_2 \alpha_1 \zeta_1 H^*}{(1 + \beta_1 v_1^*) \left(\frac{\alpha_2}{1 + \beta_2 v_2^*} + \frac{\alpha_1 \zeta_1}{1 + \beta_1 v_1^*} \right) (1 + \gamma_2 (v_2^* - \rho_2))} - \frac{\eta_2 (v_2^* - \rho_2) \alpha_1 \zeta_1 \alpha_2 \beta_2 H^*}{(1 + \beta_1 v_1^*) \left(\frac{\alpha_2}{1 + \beta_2 v_2^*} + \frac{\alpha_1 \zeta_1}{1 + \beta_1 v_1^*} \right)^2 (1 + \gamma_2 (v_2^* - \rho_2)) (1 + \beta_2 v_2^*)^2} + \frac{\eta_2 (v_2^* - \rho_2) \alpha_1 \zeta_1 \gamma_2}{(1 + \beta_1 v_1^*) \left(\frac{\alpha_2}{1 + \beta_2 v_2^*} + \frac{\alpha_1 \zeta_1}{1 + \beta_1 v_1^*} \right) (1 + \gamma_2 (v_2^* - \rho_2))^2},$$

$$J_{2,3} = - \frac{\eta_2 (v_2^* - \rho_2) \alpha_1 \zeta_1}{(1 + \beta_1 v_1^*) \left(\frac{\alpha_2}{1 + \beta_2 v_2^*} + \frac{\alpha_1 \zeta_1}{1 + \beta_1 v_1^*} \right) (1 + \gamma_2 (v_2^* - \rho_2))},$$

$$\begin{aligned}
 J_{3,1} = & \left[\frac{\xi_1 \alpha_2 \zeta_2}{(1 + \bar{\gamma}1 (v_1^* - \rho_1)) (1 + \beta_2 v_2^*) \left(\frac{\alpha_2 \zeta_2}{1 + \beta_2 v_2^*} + \frac{\alpha_1}{1 + \beta_1 v_1^*} \right)} \right. \\
 & - \frac{\xi_1 (v_1^* - \rho_1) \alpha_2 \zeta_2 \bar{\gamma}1}{(1 + \bar{\gamma}1 (v_1^* - \rho_1))^2 (1 + \beta_2 v_2^*) \left(\frac{\alpha_2 \zeta_2}{1 + \beta_2 v_2^*} + \frac{\alpha_1}{1 + \beta_1 v_1^*} \right)} \\
 & + \frac{\xi_1 (v_1^* - \rho_1) \alpha_2 \zeta_2 \alpha_1 \beta_1}{(1 + \bar{\gamma}1 (v_1^* - \rho_1)) (1 + \beta_2 v_2^*) \left(\frac{\alpha_2 \zeta_2}{1 + \beta_2 v_2^*} + \frac{\alpha_1}{1 + \beta_1 v_1^*} \right)^2 (1 + \beta_1 v_1^*)^2} \\
 & - \frac{\xi_2 (v_2^* - \rho_2) \alpha_1 \zeta_1 \beta_1}{(1 + \bar{\gamma}2 (v_2^* - \rho_2)) (1 + \beta_1 v_1^*)^2 \left(\frac{\alpha_2}{1 + \beta_2 v_2^*} + \frac{\alpha_1 \zeta_1}{1 + \beta_1 v_1^*} \right)} \\
 & + \frac{\xi_2 (v_2^* - \rho_2) \alpha_1^2 \zeta_1^2 \beta_1}{(1 + \bar{\gamma}2 (v_2^* - \rho_2)) (1 + \beta_1 v_1^*)^3 \left(\frac{\alpha_2}{1 + \beta_2 v_2^*} + \frac{\alpha_1 \zeta_1}{1 + \beta_1 v_1^*} \right)^2} \\
 & - \frac{\mu_1 \bar{\gamma}1 \alpha_2 \zeta_2}{(1 + \beta_2 v_2^*) \left(\frac{\alpha_2 \zeta_2}{1 + \beta_2 v_2^*} + \frac{\alpha_1}{1 + \beta_1 v_1^*} \right) (v_1^* - \rho_1)} \\
 & - \frac{\mu_1 (1 + \bar{\gamma}1 (v_1^* - \rho_1)) \alpha_2 \zeta_2 \alpha_1 \beta_1}{(1 + \beta_2 v_2^*) \left(\frac{\alpha_2 \zeta_2}{1 + \beta_2 v_2^*} + \frac{\alpha_1}{1 + \beta_1 v_1^*} \right)^2 (v_1^* - \rho_1) (1 + \beta_1 v_1^*)^2} \\
 & + \frac{\mu_1 (1 + \bar{\gamma}1 (v_1^* - \rho_1)) \alpha_2 \zeta_2}{(1 + \beta_2 v_2^*) \left(\frac{\alpha_2 \zeta_2}{1 + \beta_2 v_2^*} + \frac{\alpha_1}{1 + \beta_1 v_1^*} \right) (v_1^* - \rho_1)^2} \\
 & + \frac{\mu_2 (1 + \bar{\gamma}2 (v_2^* - \rho_2)) \alpha_1 \zeta_1 \beta_1}{(1 + \beta_1 v_1^*)^2 \left(\frac{\alpha_2}{1 + \beta_2 v_2^*} + \frac{\alpha_1 \zeta_1}{1 + \beta_1 v_1^*} \right) (v_2^* - \rho_2)} \\
 & - \left. \frac{\mu_2 (1 + \bar{\gamma}2 (v_2^* - \rho_2)) \alpha_1^2 \zeta_1^2 \beta_1}{(1 + \beta_1 v_1^*)^3 \left(\frac{\alpha_2}{1 + \beta_2 v_2^*} + \frac{\alpha_1 \zeta_1}{1 + \beta_1 v_1^*} \right)^2 (v_2^* - \rho_2)^{-1}} \right] H^*,
 \end{aligned}$$

$$\begin{aligned}
 J_{3,2} = & \left[- \frac{\xi_1 (v_1^* - \rho_1) \alpha_2 \zeta_2 \beta_2}{(1 + \bar{\gamma}1 (v_1^* - \rho_1)) (1 + \beta_2 v_2^*)^2 \left(\frac{\alpha_2 \zeta_2}{1 + \beta_2 v_2^*} + \frac{\alpha_1}{1 + \beta_1 v_1^*} \right)} \right. \\
 & + \frac{\xi_1 (v_1^* - \rho_1) \alpha_2^2 \zeta_2^2 \beta_2}{(1 + \bar{\gamma}1 (v_1^* - \rho_1)) (1 + \beta_2 v_2^*)^3 \left(\frac{\alpha_2 \zeta_2}{1 + \beta_2 v_2^*} + \frac{\alpha_1}{1 + \beta_1 v_1^*} \right)^2} \\
 & + \frac{\xi_2 \alpha_1 \zeta_1}{(1 + \bar{\gamma}2 (v_2^* - \rho_2)) (1 + \beta_1 v_1^*) \left(\frac{\alpha_2}{1 + \beta_2 v_2^*} + \frac{\alpha_1 \zeta_1}{1 + \beta_1 v_1^*} \right)} \\
 & - \frac{\xi_2 (v_2^* - \rho_2) \alpha_1 \zeta_1 \bar{\gamma}2}{(1 + \bar{\gamma}2 (v_2^* - \rho_2))^2 (1 + \beta_1 v_1^*) \left(\frac{\alpha_2}{1 + \beta_2 v_2^*} + \frac{\alpha_1 \zeta_1}{1 + \beta_1 v_1^*} \right)} \\
 & + \frac{\xi_2 (v_2^* - \rho_2) \alpha_1 \zeta_1 \alpha_2 \beta_2}{(1 + \bar{\gamma}2 (v_2^* - \rho_2)) (1 + \beta_1 v_1^*) \left(\frac{\alpha_2}{1 + \beta_2 v_2^*} + \frac{\alpha_1 \zeta_1}{1 + \beta_1 v_1^*} \right)^2 (1 + \beta_2 v_2^*)^2} \\
 & + \frac{\mu_1 (1 + \bar{\gamma}1 (v_1^* - \rho_1)) \alpha_2 \zeta_2 \beta_2}{(1 + \beta_2 v_2^*)^2 \left(\frac{\alpha_2 \zeta_2}{1 + \beta_2 v_2^*} + \frac{\alpha_1}{1 + \beta_1 v_1^*} \right) (v_1^* - \rho_1)} \\
 & - \frac{\mu_1 (1 + \bar{\gamma}1 (v_1^* - \rho_1)) \alpha_2^2 \zeta_2^2 \beta_2}{(1 + \beta_2 v_2^*)^3 \left(\frac{\alpha_2 \zeta_2}{1 + \beta_2 v_2^*} + \frac{\alpha_1}{1 + \beta_1 v_1^*} \right)^2 (v_1^* - \rho_1)} \\
 & - \frac{\mu_2 \bar{\gamma}2 \alpha_1 \zeta_1}{(1 + \beta_1 v_1^*) \left(\frac{\alpha_2}{1 + \beta_2 v_2^*} + \frac{\alpha_1 \zeta_1}{1 + \beta_1 v_1^*} \right) (v_2^* - \rho_2)} \\
 & - \frac{\mu_2 (1 + \bar{\gamma}2 (v_2^* - \rho_2)) \alpha_1 \zeta_1 \alpha_2 \beta_2}{(1 + \beta_1 v_1^*) \left(\frac{\alpha_2}{1 + \beta_2 v_2^*} + \frac{\alpha_1 \zeta_1}{1 + \beta_1 v_1^*} \right)^2 (v_2^* - \rho_2) (1 + \beta_2 v_2^*)^2} \\
 & \left. + \frac{\mu_2 (1 + C2 (v_2^* - \rho_2)) \alpha_1 \zeta_1}{(1 + \beta_1 v_1^*) \left(\frac{\alpha_2}{1 + \beta_2 v_2^*} + \frac{\alpha_1 \zeta_1}{1 + \beta_1 v_1^*} \right) (v_2^* - \rho_2)^2} \right] H^*,
 \end{aligned}$$

and

$$\begin{aligned}
 J_{3,3} = & \frac{\xi_1 (v_1^* - \rho_1) \alpha_2 \zeta_2}{(1 + \bar{\gamma}1 (v_1^* - \rho_1)) (1 + \beta_2 v_2^*) \left(\frac{\alpha_2 \zeta_2}{1 + \beta_2 v_2^*} + \frac{\alpha_1}{1 + \beta_1 v_1^*} \right)} \\
 & + \frac{\xi_2 (v_2^* - \rho_2) \alpha_1 \zeta_1}{(1 + \bar{\gamma}2 (v_2^* - \rho_2)) (1 + \beta_1 v_1^*) \left(\frac{\alpha_2}{1 + \beta_2 v_2^*} + \frac{\alpha_1 \zeta_1}{1 + \beta_1 v_1^*} \right)} \\
 & - \frac{\mu_1 (1 + \bar{\gamma}1 (v_1^* - \rho_1)) \alpha_2 \zeta_2}{(1 + \beta_2 v_2^*) \left(\frac{\alpha_2 \zeta_2}{1 + \beta_2 v_2^*} + \frac{\alpha_1}{1 + \beta_1 v_1^*} \right) (v_1^* - \rho_1)} \\
 & - \frac{\mu_2 (1 + \bar{\gamma}2 (v_2^* - \rho_2)) \alpha_1 \zeta_1}{(1 + \beta_1 v_1^*) \left(\frac{\alpha_2}{1 + \beta_2 v_2^*} + \frac{\alpha_1 \zeta_1}{1 + \beta_1 v_1^*} \right) (v_2^* - \rho_2)^{-1}} - \mu.
 \end{aligned}$$

Appendix A. Stability of the reduced two-patch model on \mathcal{M}_0

The Jacobian matrix for each of the fixed points E_1, E_2, E_3 and E_4 , when $\alpha_1 = 5.0$ and $\alpha_2 = 9.5$ is given by the following

$$D(f|_{E_1}) = \begin{bmatrix} 1 & 0 & 0.1688 \\ 0 & 1 & 0.4146 \\ 0 & 0 & -0.2065 \end{bmatrix}, \quad (2)$$

The eigenvalues are the solution of the following equation

$$\lambda^3 - 1.7935\lambda^2 + 0.5871\lambda + 0.2065 = 0,$$

and hence we have

$$\lambda_1 = -0.2065, \lambda_2 = \lambda_3 = 1.$$

For the fixed point E_2 we have

$$D(f|_{E_2}) = \begin{bmatrix} -1 & 0 & -0.2358 \\ 0 & -1 & -0.5276 \\ 0 & 0 & 0.2665 \end{bmatrix}, \quad (3)$$

with

$$\lambda_1 = 0.2665, \lambda_2 = \lambda_3 = 1.$$

For E_3 we have

$$D(f|_{E_3}) = \begin{bmatrix} -1 & 0 & -0.3658 \\ 0 & 1 & 0.3216 \\ 0 & 0 & 0.0421 \end{bmatrix}, \quad (4)$$

$$\lambda^3 - 0.0421\lambda^2 - \lambda + 0.0421 = 0$$

and hence the eigenvalues are

$$\lambda_1 = 1, \lambda_2 = 0.0421, \lambda_3 = -1.$$

For the fixed point E_4 we have

$$D(f|_{E_4}) = \begin{bmatrix} 1 & 0 & 0.0987 \\ 0 & -1 & -0.6169 \\ 0 & 0 & 0.1591 \end{bmatrix}, \quad (5)$$

$$\lambda^3 - 0.1591\lambda^2 - \lambda + 0.1591$$

$$\lambda_1 = 1, \lambda_2 = 0.1591, \lambda_3 = -1.$$

For the fixed point $(0.46, 0.1388, 1.4774)$ the Jacobian matrix and its eigenvalues are given by

$$D(f|_{(0.46, 0.1388, 1.4774)}) = \begin{bmatrix} -0.2164 & 0.2195 & -0.2575 \\ 0.0603 & -1.8373 & -0.1737 \\ 0.2745 & 1.8734 & -0.0351 \end{bmatrix}, \quad (6)$$

$$\lambda^3 + 2.0888\lambda^2 + 0.8525\lambda + 0.2533 = 0,$$

$$\lambda_1 = -0.2099 + 0.3282i, \lambda_2 = -0.2099 - 0.3282i, \lambda_3 = -1.669.$$

For the fixed point $(0.966, 0.2544, 0.1846)$ we have

$$D(f|_{(0.966, 0.2544, 0.1846)}) = \begin{bmatrix} 0.9546 & 0.0285 & -0.3167 \\ 0.0104 & 0.3441 & -0.283 \\ 0.0163 & 0.0824 & 0.1107 \end{bmatrix}, \quad (7)$$

$$\lambda^3 + 0.4998\lambda^2 - 0.3679\lambda + 0.0573 = 0$$

$$\lambda_1 = 0.2253 + 0.0976i, \lambda_2 = 0.2253 - 0.0976i, \lambda_3 = -0.9503.$$

For the fixed point $(0.828, 0.1681, 0.8668)$ we have

$$D(f|_{(0.828, 0.1681, 0.8668)}) = \begin{bmatrix} -0.7743 & 0.1417 & -0.3126 \\ 0.0373 & -0.4688 & -0.2022 \\ 0.0990 & 0.6822 & 0.0469 \end{bmatrix}, \quad (8)$$

$$\lambda^3 + 1.1963\lambda^2 + 0.4684\lambda + 0.1154 = 0$$

Appendix A. Stability of the reduced two-patch model on \mathcal{M}_0

$$\lambda_1 = -0.2044 + 0.3236i, \lambda_2 = -0.2044 - 0.3236i, \lambda_3 = -0.7876$$

For the fixed point (0.989, 0.1539, 0.0653) the Jacobian matrix and the eigenvalues are given by

$$D(f|_{(0.989, 0.1539, 0.0653)}) = \begin{bmatrix} -0.9861 & 0.0112 & -0.3359 \\ 0.0024 & 0.6013 & -0.1767 \\ 0.0068 & 0.0574 & 0.0526 \end{bmatrix}, \quad (9)$$

$$\lambda^3 + 0.3322\lambda^2 - 0.6008\lambda + 0.0399 = 0,$$

and hence the eigenvalues are given by

$$\lambda_1 = 0.0696, \lambda_2 = 0.5821, \lambda_3 = -0.9839.$$

For the Jacobian

$$D(f|_{(0.414, 0.1452, 0.8764)}) = \begin{bmatrix} -0.0515 & 0.1381 & -0.3141 \\ 0.0425 & -0.564 & -0.161 \\ 0.2118 & 0.8679 & -0.00004 \end{bmatrix}, \quad (10)$$

the eigenvalues are determined by the solution of the following equation

$$\lambda^3 + 0.6155\lambda^2 + 0.2295\lambda + 0.061 = 0$$

and hence we have

$$\lambda_1 = -0.0996 + 0.3696i, \lambda_2 = -0.0996 - 0.3696i, \lambda_3 = -0.4163.$$

For

$$D(f|_{(0.989, 0.09146, 0.356)}) = \begin{bmatrix} -1.0253 & 0.0663 & -0.4254 \\ 0.0051 & 0.1313 & -0.0541 \\ 0.0518 & 1.6637 & -0.00001 \end{bmatrix}, \quad (11)$$

the eigenvalues determined by the solution of the following equation

$$\lambda^3 + 0.894\lambda^2 - 0.0229\lambda + 0.0932 = 0$$

and hence we have

$$\lambda_1 = 0.0572 + 0.2986i, \lambda_2 = 0.0572 - 0.2986i, \lambda_3 = -1.0083.$$

For the reduced system (4.20), the Jacobian matrices for the fixed points $E_1 = (0, 0, 0)$, $E_2 = (1, 1, 0)$, $E_3 = (1, 0, 0)$ and $E_4 = (0, 1, 0)$ are given by the following

$$D(f|_{E_1}) = \begin{bmatrix} 1 & 0 & 0.0215 \\ 0 & 1 & 0.5618 \\ 0 & 0 & -0.2065 \end{bmatrix}, \quad (12)$$

$$\lambda^3 - 1.7935\lambda^2 + 0.5871\lambda + 0.2065 = 0,$$

with $\lambda_1 = -0.20651$ and $\lambda_2 = \lambda_3 = 1$.

$$D(f|_{E_2}) = \begin{bmatrix} -1 & 0 & -0.0301 \\ 0 & -1 & -0.7151 \\ 0 & 0 & 0.2377 \end{bmatrix}, \quad (13)$$

$$\lambda^3 + 1.7623\lambda^2 + 0.5246\lambda - 0.2377 = 0$$

with $\lambda_1 = 0.2377$ and $\lambda_2 = \lambda_3 = -1$.

$$D(f|_{E_3}) = \begin{bmatrix} -1 & 0 & -0.058 \\ 0 & 1 & 0.5419 \\ 0 & 0 & -0.1671 \end{bmatrix}, \quad (14)$$

$$\lambda^3 + 0.1678\lambda^2 - \lambda - 0.1678 = 0$$

with $\lambda_1 = 1$, $\lambda_2 = -0.1678$, and $\lambda_3 = -1$. For the Jacobian

$$D(f|_{E_4}) = \begin{bmatrix} 1 & 0 & 0.011 \\ 0 & -1 & -0.7285 \\ 0 & 0 & 0.2253 \end{bmatrix}, \quad (15)$$

$$\lambda^3 - 0.2253\lambda^2 - \lambda + 0.2253 = 0$$

Appendix A. Stability of the reduced two-patch model on \mathcal{M}_0

and hence $\lambda_1 = 1$, $\lambda_2 = 0.2253$, and $\lambda_3 = -1$.

Appendix B. Soil moisture equations

The lost in water in the layer a is given by w_{da}

$$w_{da} = \begin{cases} 0, & w_a + w_{in} \leq w_{amax} \\ w_a + w_{in} - w_{amax}, & w_a + w_{in} > w_{amax}. \end{cases}$$

The amount of water drained from the layer b is w_{db}

$$w_{db} = \begin{cases} 0, & w_b + w_{da} \leq w_{bmax} \\ w_b + w_{da} - w_{bmax}, & w_b + w_{da} > w_{bmax}. \end{cases} \quad (16)$$

The fraction of potential evaporation can be estimated as the following

$$w_{Efr} = \begin{cases} 0, & w_a \leq 16 \\ 0.0375 w_a - 0.6, & 16 < w_a \leq 24 \\ 0.4667 w_a - 10.9, & w_a > 24. \end{cases} \quad (17)$$

The potential evaporation rate (w_{Epot}) from the soil decreases as the above ground biomass increases (both green vegetation biomass and dry vegetation biomass) (Dye [1984]). Hence the potential evaporation can be estimated by the following

$$w_{Epot} = \begin{cases} w_{Emax}, & \text{Shoots} = 0 \\ [1.0 - (0.0422 + 0.1537 \text{Shoots})] w_{Emax}, & \text{Shoots} > 0 \end{cases} \quad (18)$$

where w_{Emax} is the maximum rate of water evaporation per day and Shoots is the density (g/m^2) of the above ground vegetation biomass.

Let w_{tot} be the total amount of water stored in the layers A and B

$$w_{tot} = w_a + w_b. \quad (19)$$

Appendix B. Soil moisture equations

The soil moisture index w_m estimated as the following

$$w_m = 0.043 w_{tot} - 3.73. \quad (20)$$

(Richardson and Hahn [2007]). The potential transpiration rate w_{pTr} is given by the following

$$w_{pTr} = \begin{cases} 0.018 - 1.728 \times 10^{-4} V_g & V_g \leq 90 \\ 0.00483 - 4.2243 \times 10^{-6} V_g & V_g > 90. \end{cases} \quad (21)$$

$$w_{fsi} = 100 \frac{w_i}{Sd_i} \quad i = a, b$$

and Sd_i is the soil depth of the layer i .

The transpiration coefficient, k_s is the efficiency of synthesis of forage and it is given by

$$k_s = \begin{cases} 1 & \text{Days}_{gr} \leq 175, \\ 2.75 - 0.01 \text{Days}_{gra} & \text{Days}_{gr} > 175. \end{cases} \quad (22)$$

r_v is an adjusted fraction allocated the green vegetation and it is given by the following

$$r_v = Fr_{vdry} fr_v \quad (23)$$

where fr_v is a relative growth rate of green vegetation, and it estimated by

$$fr_v = \begin{cases} 0.22 & \text{Days}_{gr} < 133 \\ 0.16 & 133 \leq \text{Days}_{gr} < 140 \\ 0.1 & 140 \leq \text{Days}_{gr} < 175 \\ 0.08 & 175 \leq \text{Days}_{gr}. \end{cases} \quad (24)$$

Fr_{vdry} is the proportion of new vegetation growth. This factor increases as the soil moisture increases and decreases as soil moisture decreases,

$$Fr_{vdry} = \begin{cases} 0, & w_{tot} < 95 \\ 1 - \exp(-0.183(w_{tot} - 95)), & w_{tot} \geq 95 \end{cases}$$

V_μ is the green vegetation death rate, which increases as the total water decreases below 110 mm (Richardson and Hahn [2007])

$$V_{\mu g} = v_{gdie} v_{die} \quad (25)$$

where

$$v_{\text{gdie}} = \begin{cases} 1, & w_{\text{tot}} \geq 110 \\ 10.57 - 0.087 w_{\text{tot}}, & w_{\text{tot}} < 110 \end{cases}$$

v_{die} is the green vegetation deaths rate which influences by the total amount of water accessible by roots and the age of vegetation

$$v_{\text{die}} = \begin{cases} 0 & \text{Shoots} \leq 20 \\ 0.00171 & \text{Shoots} > 20 \text{ and } \text{Days}_{\text{gr}} \leq 126 \\ 0.000015714 \text{Days}_{\text{gr}} - 0.000286 & \text{Shoots} > 20 \text{ and } 126 < \text{Days}_{\text{gr}} \leq 182 \\ 0.02 & \text{Shoots} > 20 \text{ and } \text{Days}_{\text{gr}} > 182 \end{cases}$$